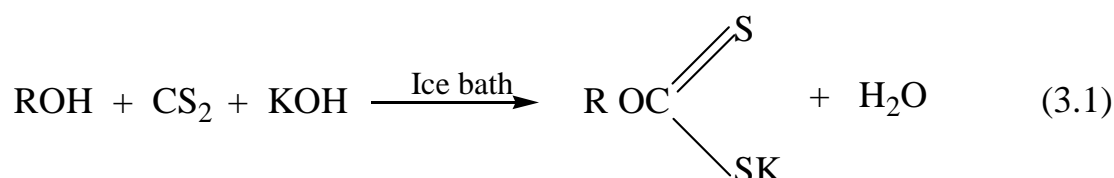


Chapter Three

Results & Discussion

3.1 Preparation of ligands

Potassium methyl xanthate, potassium ethyl xanthate, potassium isopropyl xanthate, potassium butyl xanthate, and potassium hexyl xanthate ligands were prepared according to the chemical reaction as shown in equation (3.1)

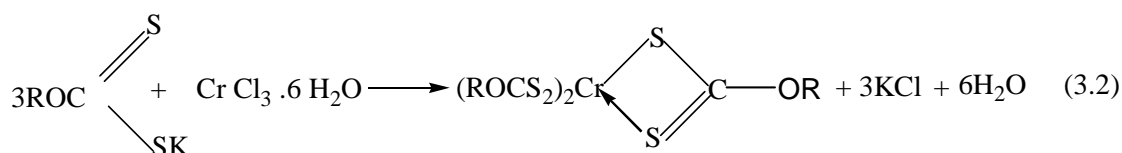


Where: R = CH₃-, C₂H₅-, C₃H₇-, C₄H₉-, or C₆H₁₃-

The reaction was one to one (1:1) stoichiometry. An excess of KOH solution was added to ensure complete reaction.

3.2 Preparation of complexes

Tris(methylxanthato)chromium(III), tris(ethylxanthato)chromium(III), tris(isopropylxanthato)chromium(III), tris(butylxanthato)chromium(III), and tris(hexylxanthato)chromium(III) complexes were prepared according to the chemical reaction as shown in equation (3.2)



The stoichiometry of the above reaction was 3: 1 with respect to ligand and metal salt, respectively

3.3 Physical properties of prepared ligands and complexes

Table (3.1) lists some of the physical properties of ligands and their complexes.

Table (3.1): Some physical properties of the prepared ligands and complexes

Compound	Color	Melting point ⁰C	M calc. %	M found %
PMX	Yellow	215-218	-	-
Cr(mex)₃	Deep green	>300*	2.53	3.84
PEX	Light brown	108-110	-	-
Cr(ety)₃	Greenish blue	>300	3.27	4.20
PPX	Yellowish white	208-210	-	-
Cr(prx)₃	Light blue	>300	6.51	7.32
PBX	Yellowish white	198-200	-	-
Cr(bux)₃	Light blue	>300	5.34	6.13
PHX	Yellowish white	210-212	-	-
Cr(hex)₃	Light grey	>300	4.88	5.10

* didn't melts below 300 ⁰C

The color of these ligands was all yellow but with different levels. The color of the prepared complexes has ranged from deep green to light grey. The melting points of the ligands were ranged from 108 to 218. However, the melting points of the complexes have be not recorded because they did not melt below 300 ⁰C. The data of metal were obtained

using flame atomic absorption technique. The calculation values were in a good agreement with the experimental values.

3.4 Magnetic susceptibility and molar conductivity measurements

The Experimental magnetic moment for each complex is listed in Table (3.2). Magnetic measurements are commonly used in studying transition metal complexes ⁽¹⁰⁰⁾. The magnetic properties are due to the presence of unpaired electrons in the partially filled d-orbital in the outer shell of that element. These magnetic measurements give an idea about the electronic state of the metal ion in the complex.

The resultant magnetic moment of an ion is due to both orbital and spin motion ⁽¹⁰¹⁾. The magnetic moment is given by the following equation ⁽¹⁰²⁾:

$$\mu_{S+L} = \sqrt{4S(S+1) + L(L+1)} \text{ B.M}$$

μ = Magnetic moment

S = Spin quantum number

L = Orbital quantum number

B.M. = $9.27 \times 10^{-24} \text{ J. T}^{-1}$

Although detailed determination of the electronic structure requires consideration of the orbital moment. However, for most complexes of the first transition series the spin – only moment is sufficient, if the orbital contribution is small ⁽¹⁰³⁾, therefore:

$$\mu_S = \sqrt{4S(S+1)} \text{ B.M.},$$

or

$$\mu_S = \sqrt{n(n+2)} \text{ B.M.}$$

$$S = n (1/2)$$

S = Spin multiplicity

n = Number of unpaired electrons.

The value of magnetic susceptibility of the prepared complexes at room temperatures was calculated using the following equation:

$$\mu_S = \sqrt{X_A \times T}$$

$$X_A = X_m + D$$

$$X_m = X_g \cdot \text{Mwt}$$

Where:

X_A = Atomic Susceptibility

X_m = Molar Susceptibility (corrected)

X_g = Mass Susceptibility

Mwt = Molecular weight of complex

D = Diamagnetic correction factor $\times 10^{-6}$

T = Temperature in Kelvin ($^{\circ}\text{C} + 273$)

B. M = Magnetic moment unit (Bohr magneton)

The observed magnetic moments for the prepared Cr(III) complexes is shown in Table (3.2). These values are typical of high spin octahedral complexes of Cr(III)⁽¹⁰⁴⁾. These values were in a good agreement with that given by Kazzer et al. for the Cr(etx)₃ which has been reported to be 4.18 B.M. However, the value for Cr(mex)₃ was reported to be 3.89 B.M.⁽¹⁰⁵⁾ compared to our value of 4.20. The values of the molar conductivity measurements in DMSO solvent at 25⁰C in Table (3.2)

showed, that tris(alkylxanthato)chromium (III) complexes were non-electrolyte

Table (3.2): Magnetic Moment and molar conductivity Measurements of complexes

<i>complex</i>	<i>Magnetic Moment (B.M)</i>	<i>Molar conductivity $\text{Ohm}^{-1}\text{cm}^2\text{mol}^{-1}$</i>	<i>Suggested Structure</i>
Cr(mex) ₃	4.20	18	octahedral
Cr(etx) ₃	4.18	17	octahedral
Cr(prx) ₃	4.15	10	octahedral
Cr(bux) ₃	4.12	16	octahedral
Cr(hex) ₃	4.16	13	octahedral

3.5 FTIR Spectra for ligands and their complexes

The FTIR spectra of the prepared potassium alkyl ligands and their chromium complexes are shown in Figures (3.1-3.10) for comparison. The FTIR spectra of the chromium complexes were run on both KBr and CsI discs. This is because the absorption bands below 500cm^{-1} were weak with CsI disc due to high absorption bands above 500cm^{-1} as shown in Figures 3.2, 3.4, 3.6, 3.8, and 3.10, (a) and (b) for KBr and CsI discs, respectively.

The main absorption bands for both ligands and their complexes are listed in Table (3.3).

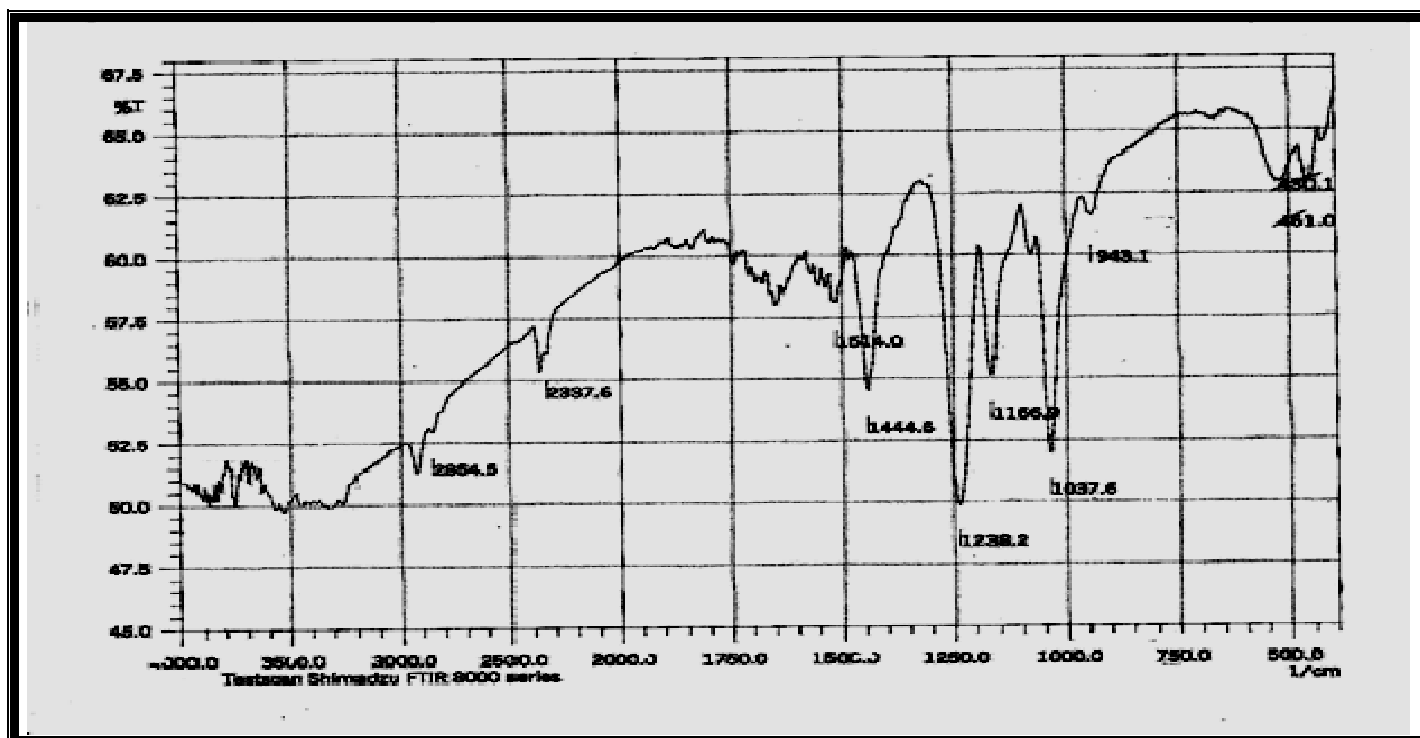
The absorption bands observed at ($1155\text{-}1188\text{ cm}^{-1}$) in the spectra of free xanthate ligands were may be assigned to $\nu(\text{O-C-O})$. This bands have shifted to higher values of ($1226\text{-}1250\text{ cm}^{-1}$) for chromium (III)

complexes which range from (44-81 cm⁻¹), indicating some involvement of oxygen of (C-O-C) in bonding with metals⁽¹⁰⁶⁾.

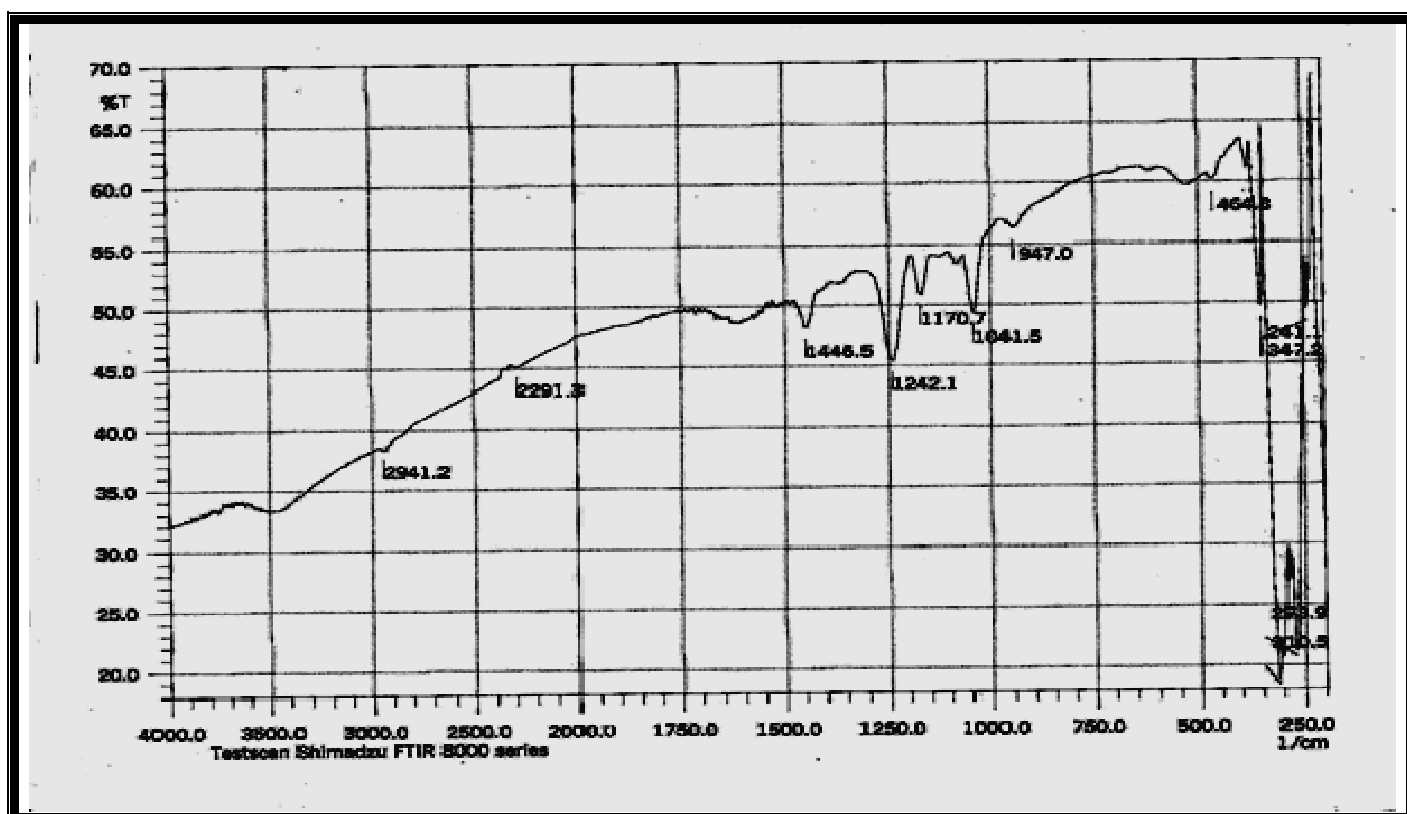
The bands at (1042-1065 cm⁻¹) in the spectra of xanthate ligands can be assigned to (C-S) stretching frequencies. In the spectra of all complexes, these bands shifted to lower frequencies ranged from (7-24 cm⁻¹) to give absorption bands for the complexes in the range (1032-1050 cm⁻¹) suggesting that sulphur is involved in bonding to the metal ion, this is in agreement with previous earlier assignment⁽¹⁰⁶⁾. Furthermore, the occurrence of this single band due to $\nu(\text{C-S})$ in all xanthate complexes showed the uninegative bidentate behavior of the xanthate ligands⁽¹⁰⁷⁾.

The bands at (1105-1145 cm⁻¹) in the spectra of xanthate ligands can be assigned to $\nu(\text{C=S})$. The absorption bands of the $\nu(\text{C=S})$ for the PMX was 1105 cm⁻¹ compared to 1145 cm⁻¹ for PHX which indicated a large shift from methyl to hexyl group in the ligands. This is in agreement with that reported previously⁽¹⁰⁸⁾. This has been attributed to the greater electron-releasing tendency of the hexyl compared to the methyl group⁽¹⁰⁸⁾. In the spectra of all complexes, these bands shifted to higher frequency of (1117-1190 cm⁻¹), which represented a shift to longer frequency of as much as 62 cm⁻¹.

The FTIR spectra of the complexes have shown new bands in the range of (347-352 cm⁻¹) for all complexes as listed in Table (3.3). These bands were assigned to (Cr-S) stretching vibration^(109,110).

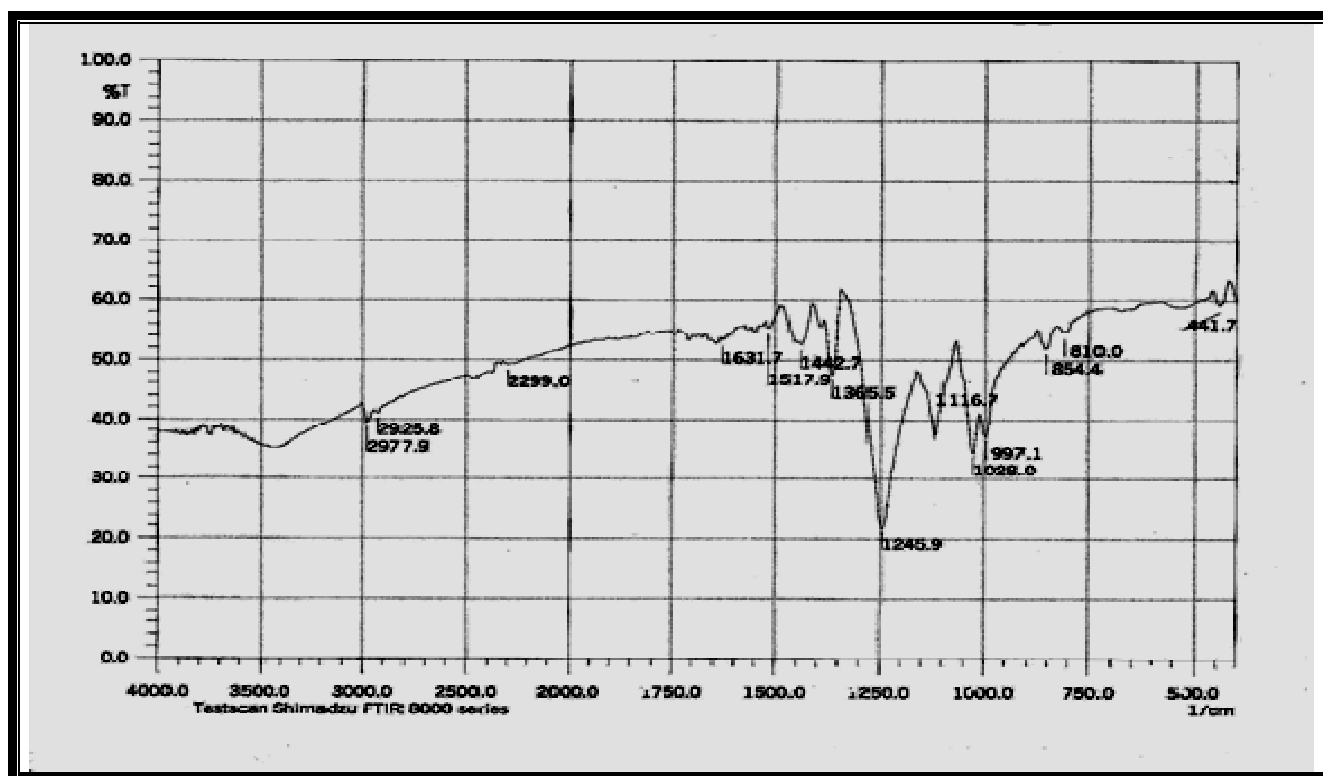


(a)

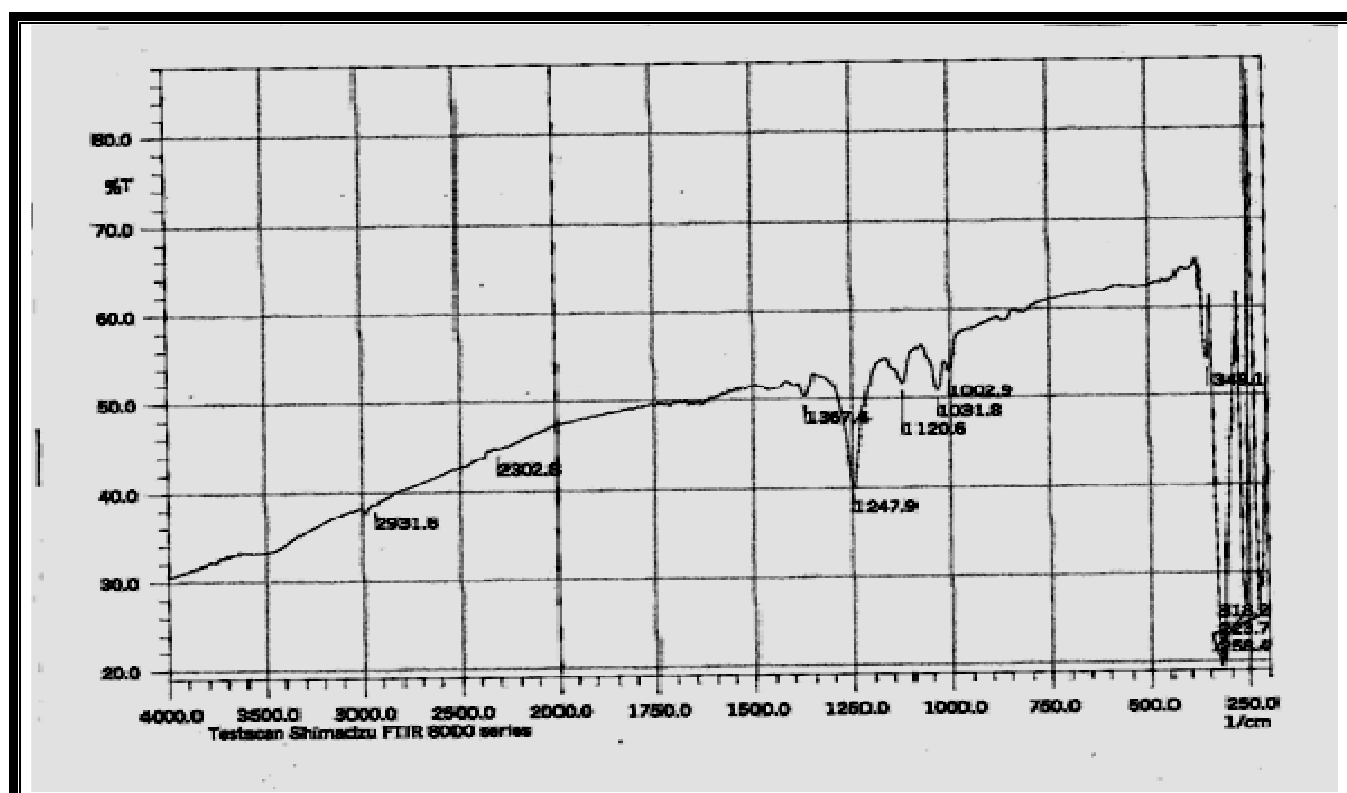


(b)

Figure (3.2): FTIR spectrum for tris (methylxanthato) chromium (III) complex using (a) KBr (b) CsI discs.

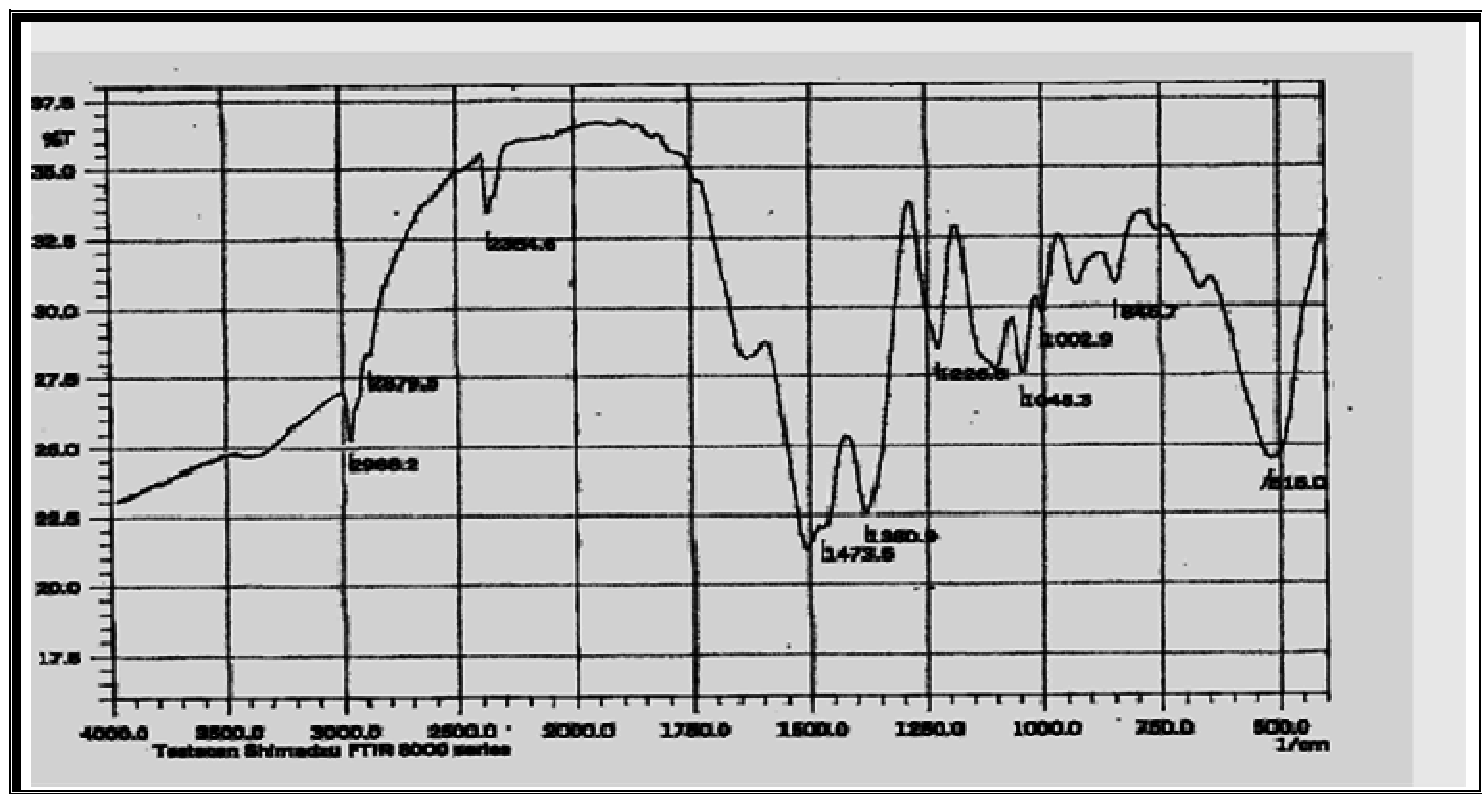


(a)

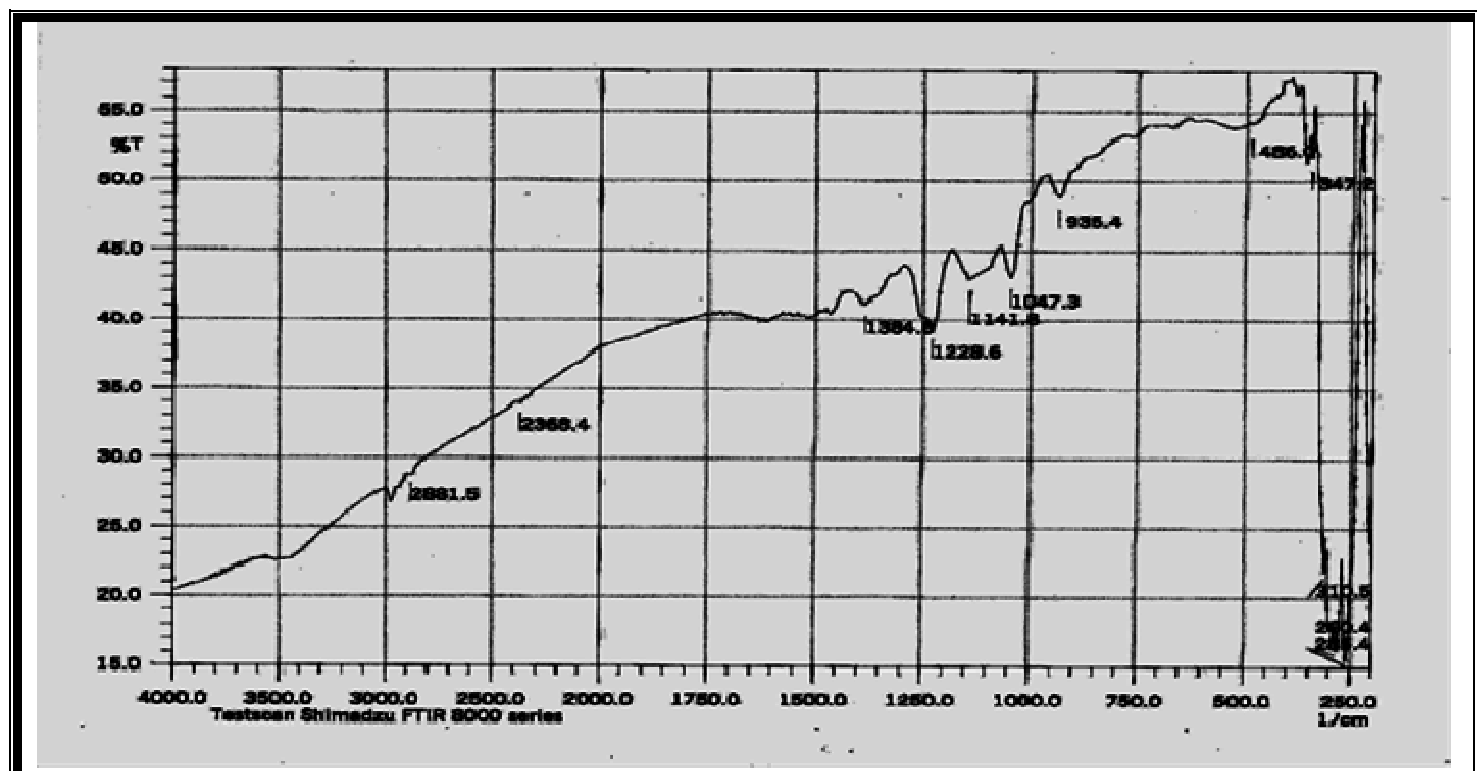


(b)

Figure (3.4): FTIR spectrum for tris(ethylxanthato)chromium(III) complex using (a) KBr (b) CsI discs.

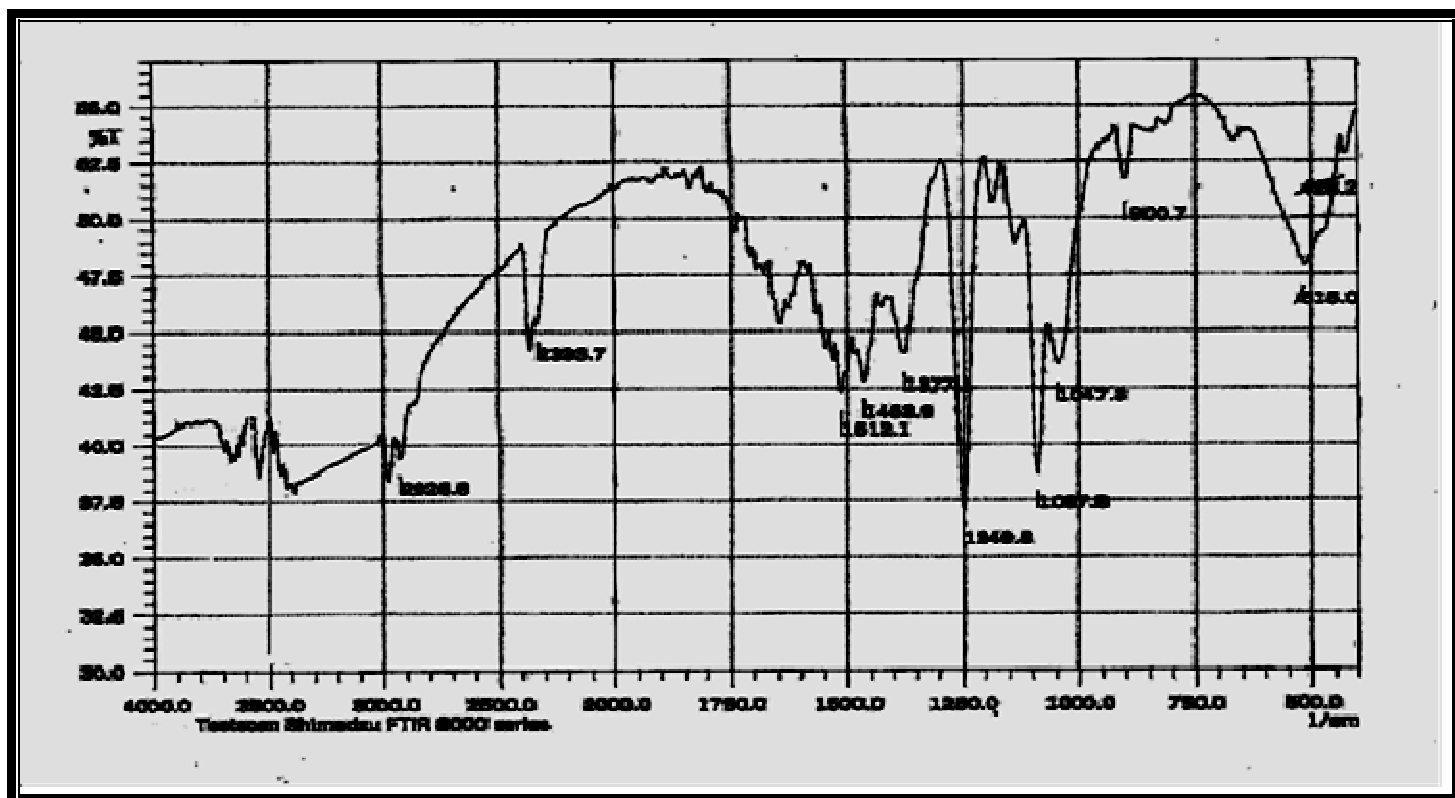


(a)

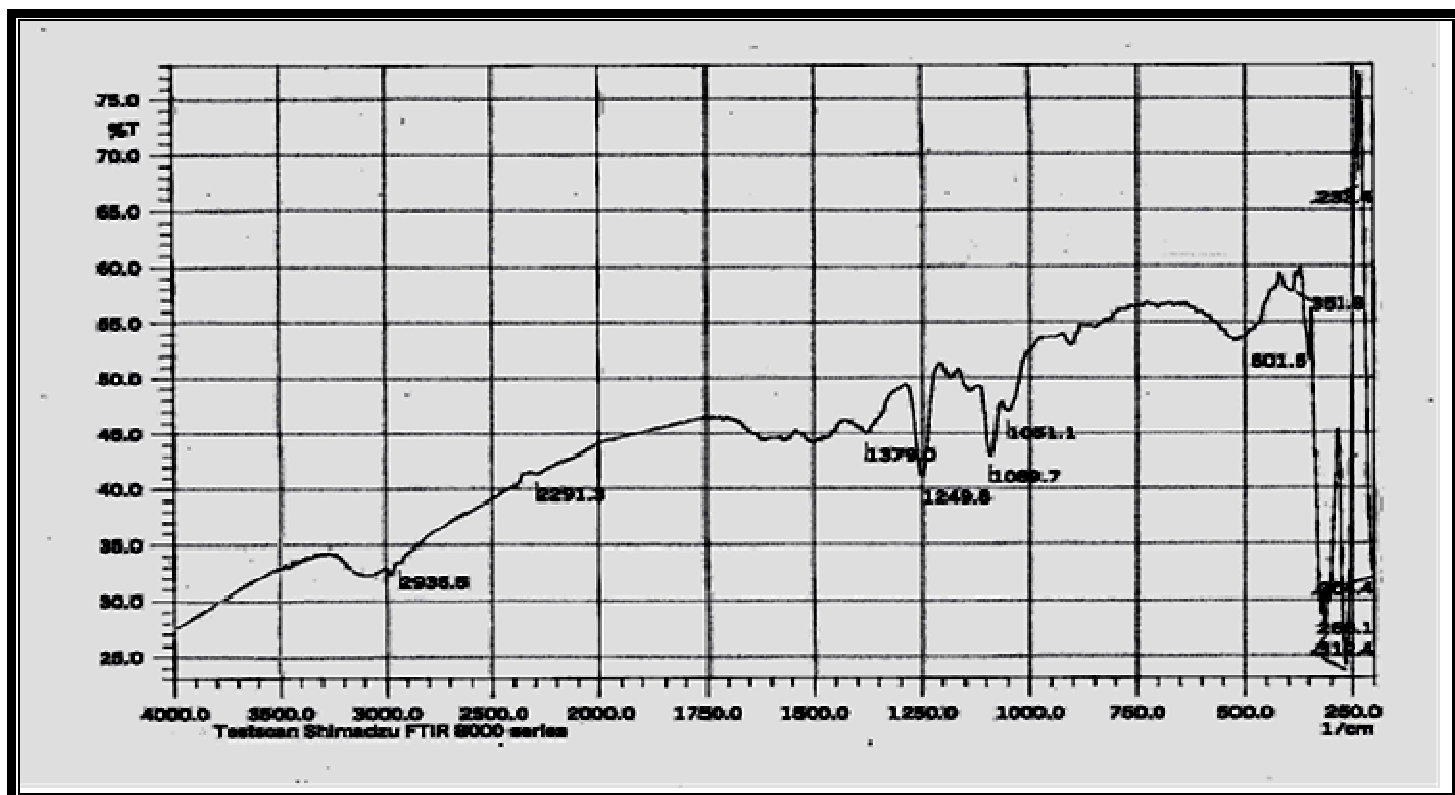


(b)

Figure (3.6): FTIR spectrum for tris(isopropylxanthato)chromium(III) complex using (a) KBr (b) CsI discs.

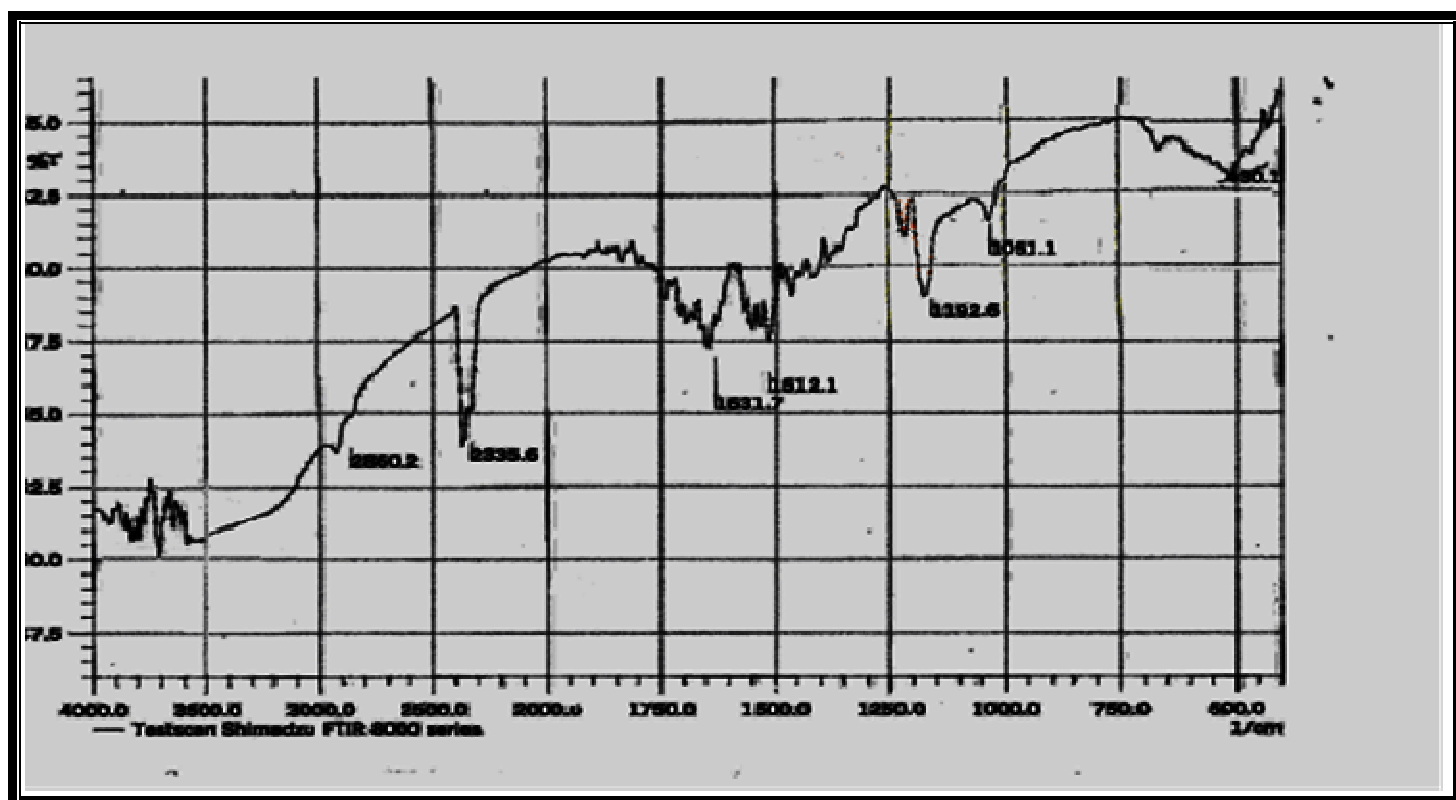


(a)

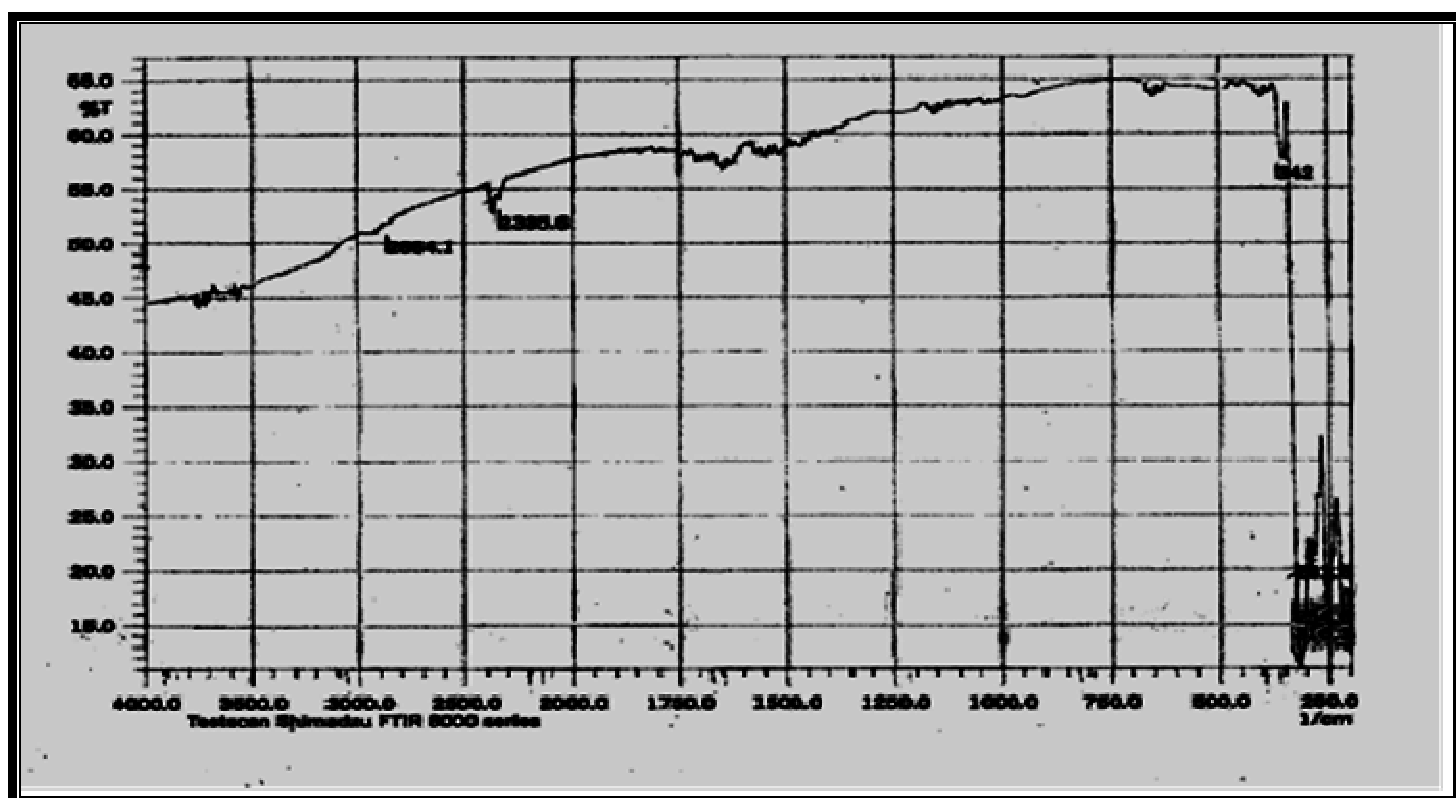


(b)

Figure (3.8): FTIR spectrum for tris(butylxanthato)chromium(III) complex using (a) KBr (b) CsI discs.



(a)



(b)

Figure (3.10): FTIR spectrum for tris(hexylxanthato)chromium(III) complex using (a) KBr (b) CsI discs.

Table (3.3): Infrared bands of xanthate ligands and their complexes

Compounds	$\nu(\text{C-O-C})\text{cm}^{-1}$	$\nu(\text{C-S})\text{cm}^{-1}$	$\nu(\text{C=S})\text{cm}^{-1}$	$\nu(\text{Cr-S})\text{cm}^{-1}$
<i>PMX</i>	1188	1045	1105	*
<i>Cr(mex)₃</i>	1238	1038	1167	347
<i>PEX</i>	1165	1042	1113	*
<i>Cr(etx)₃</i>	1246	1032	1117	349
<i>PPX</i>	1155	1065	1123	*
<i>Cr(prx)₃</i>	1227	1041	1141	347
<i>PBX</i>	1184	1055	1136	*
<i>Cr(bux)₃</i>	1250	1047	1180	352
<i>PHX</i>	1182	1062	1145	*
<i>Cr(hex)₃</i>	1226	1050	1190	347

* Not found

3.6 Ultraviolet – Visible Spectroscopy

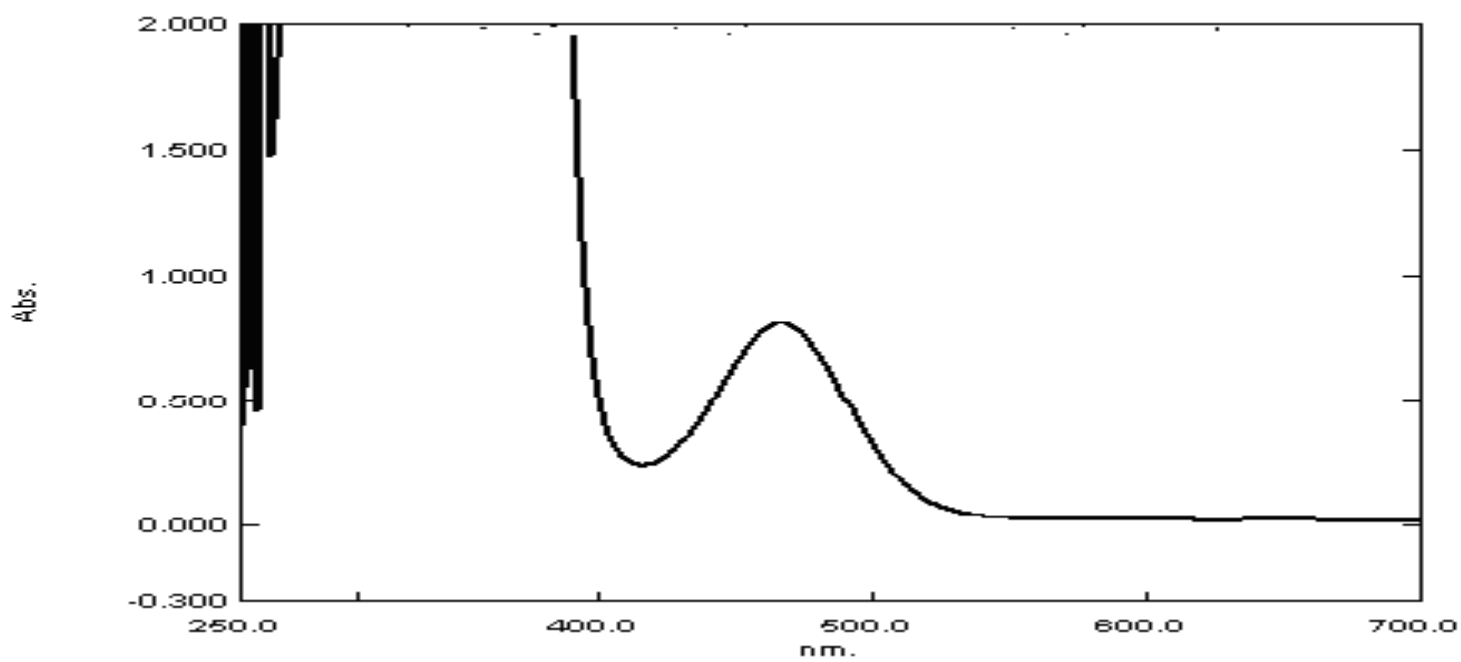
The ultraviolet-visible absorption spectra of potassium alkyl xanthate (PAX) ligands in DMSO were recorded and shown in Figures (3.11a-3.16a). A maximum absorption wavelengths were observed at (450-486nm) of moderate absorbance and off-scale high absorbance reading below 400nm. These transitions may be attributed to $n \rightarrow \pi^*$, and $\pi \rightarrow \pi^*$ electronic transition respectively. The absorbencies of these transitions were employed to follow the decomposition of the complex. Although, the $\pi \rightarrow \pi^*$ transition which occur at shorter wavelength, below 400nm, with very high absorbance reading, for this reason it was

difficult to follow any decrease in the absorbance. Therefore, the decomposition reaction was followed using $n \rightarrow \pi^*$ electronic transitions.

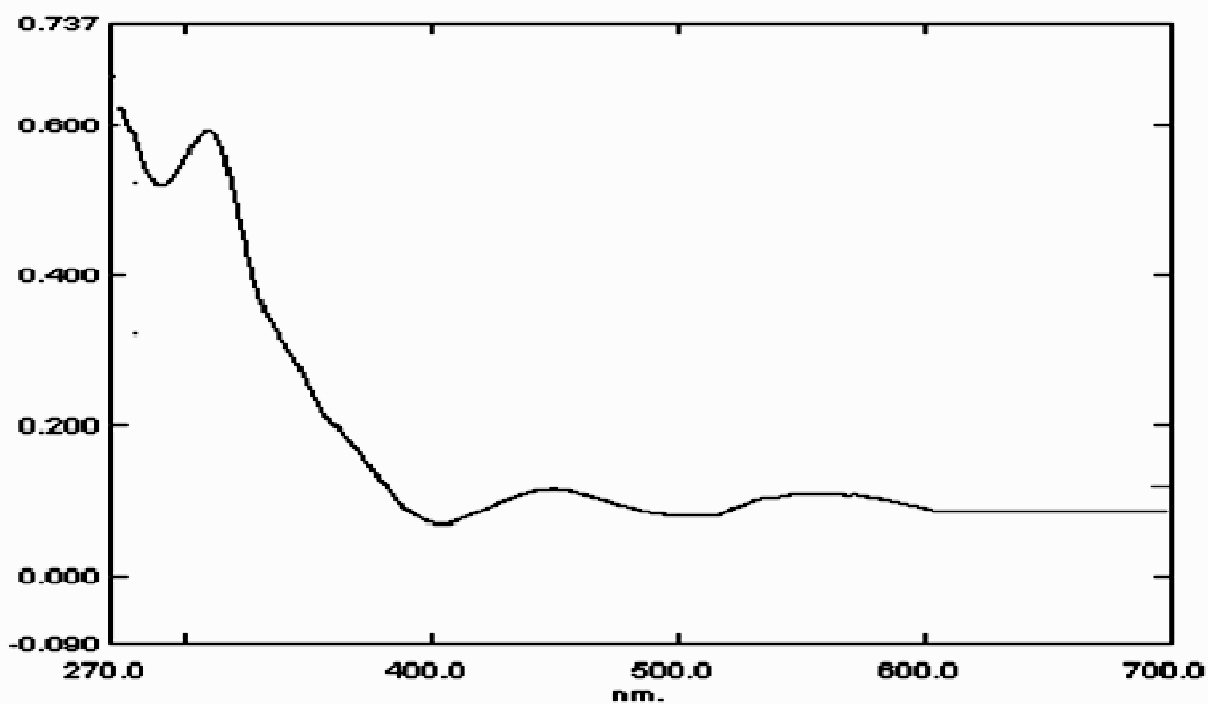
The absorption spectra of tris(alkylxanthato) chromium (III) complexes have shown different absorption wavelength from that of the free ligand as shown in Figures (3.1b-3.16b). These complexes absorbance wavelengths were shifted to different wavelengths than the corresponding bonds in their ligands, which appears in the wavelength range between 310 to 620nm. These values are listed in Table (3.4).

These blue shift may be attributed to the formation of chromium(III) complex which was in agreement with the color of the resultant prepared complexes as shown in Table (3.3) and their FTIR spectra.

The ligand field electronic transitions between the metal d orbitals appear in Cr(III) bands located in the visible region for tris(alkylxanthato)chromium(III) complexes at (576-620nm) assigned to the transition ${}^4A_{2g}(F) \rightarrow {}^4T_{1g}(F)$ and (442-460 nm) assigned to the transition ${}^4A_{2g}(F) \rightarrow {}^4T_{1g}(F)$ and (310-312nm) ${}^4A_{2g}(F) \rightarrow {}^4T_{2g}(P)$. These transitions are showed in Table (3.4).

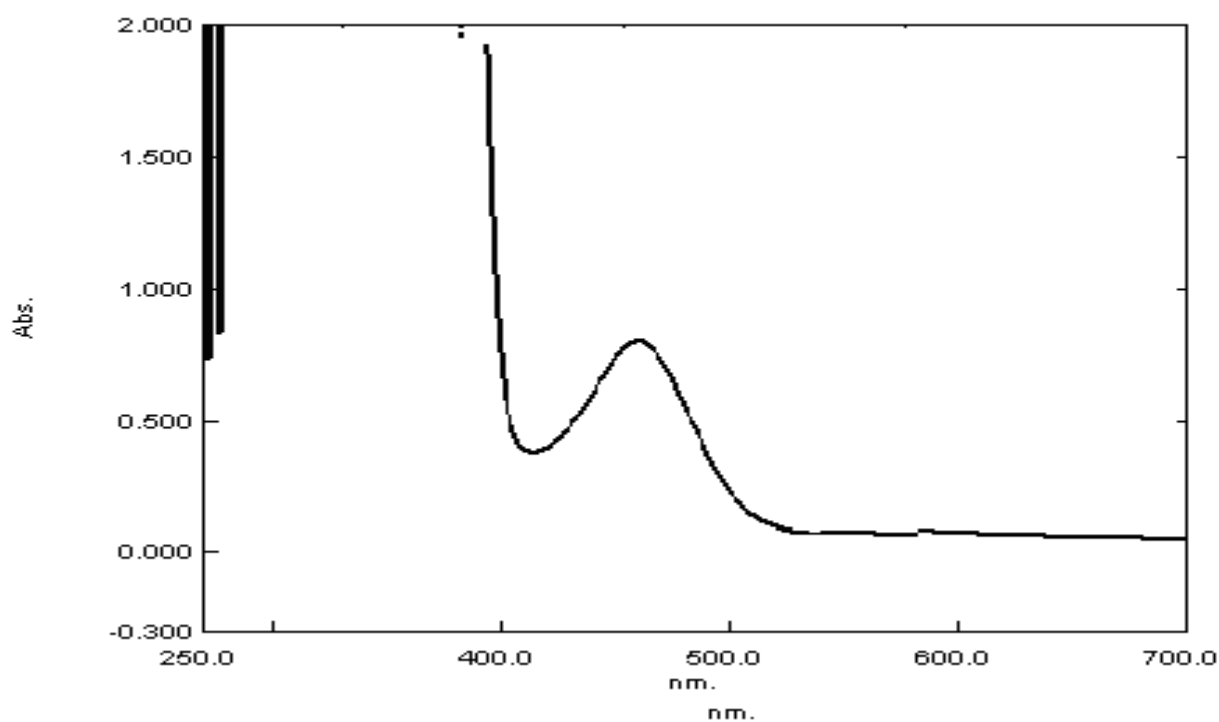


(a)

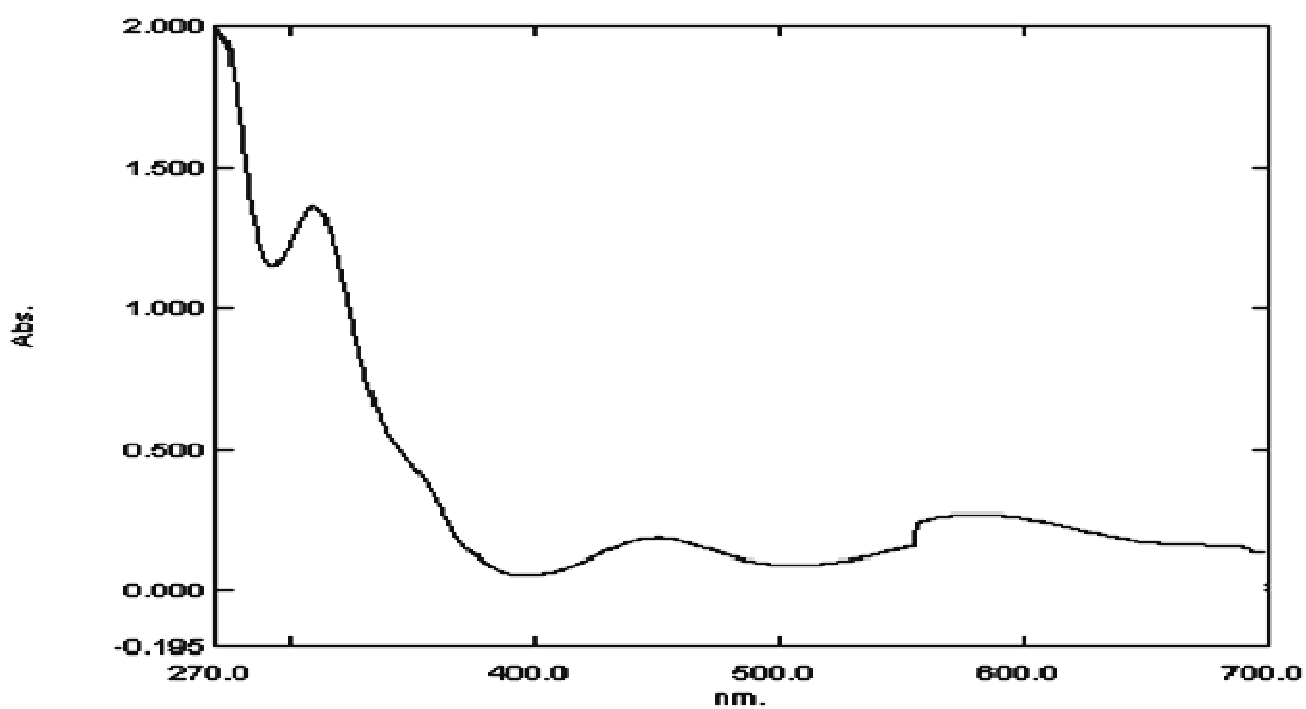


(b)

Figure (3. 11): The ultraviolet visible spectrum for a) potassium methyl xanthate and b) tris(methylxanthato)Chromium (III) complex.



(a)



(b)

Figure (3. 12): The ultraviolet visible spectrum for a) potassium ethyl xanthate and b) tris(ethylxanthato)Chromium (III) complex.

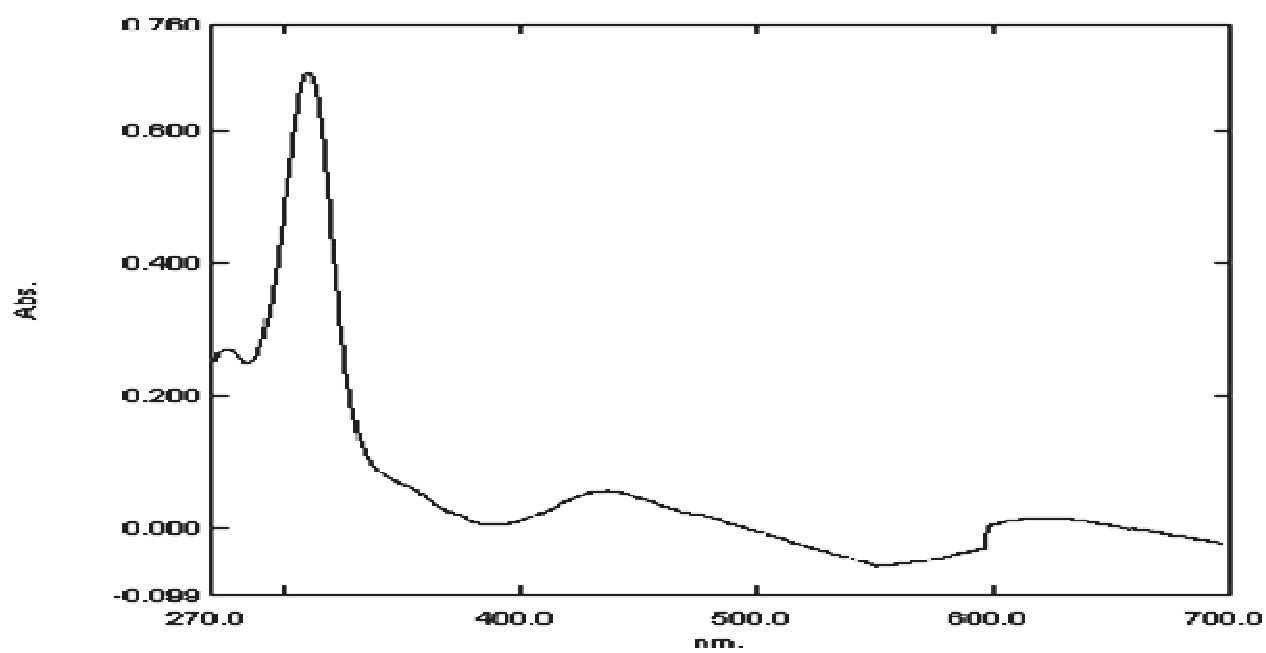
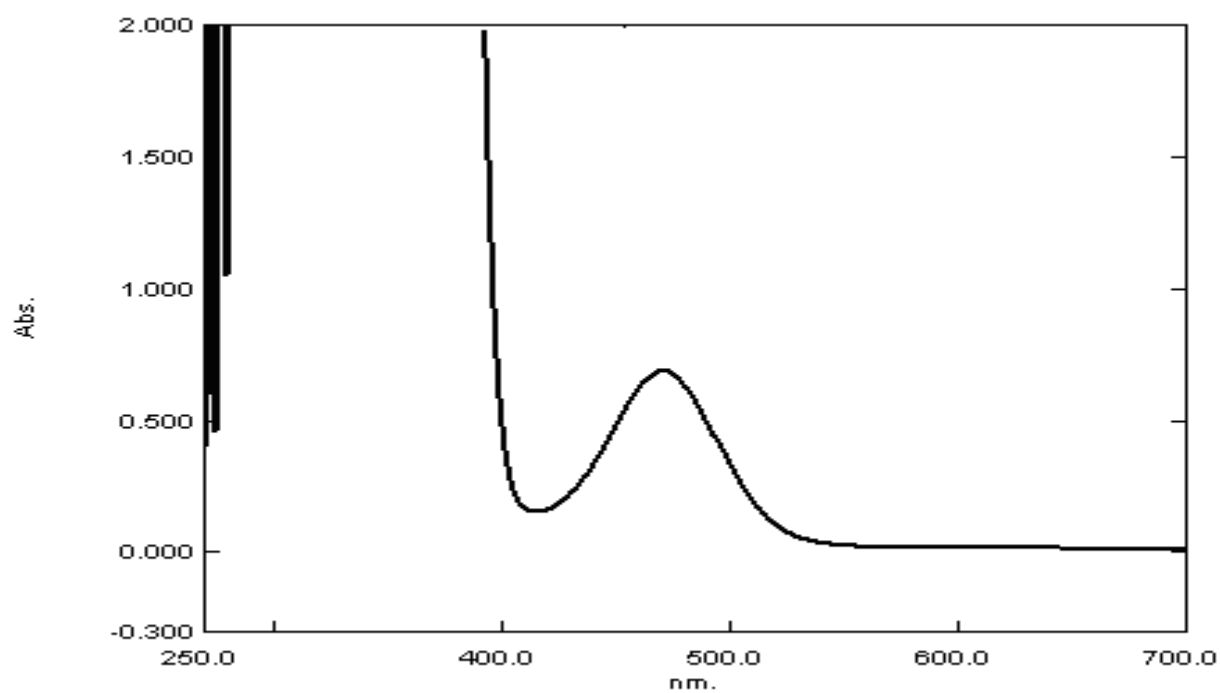
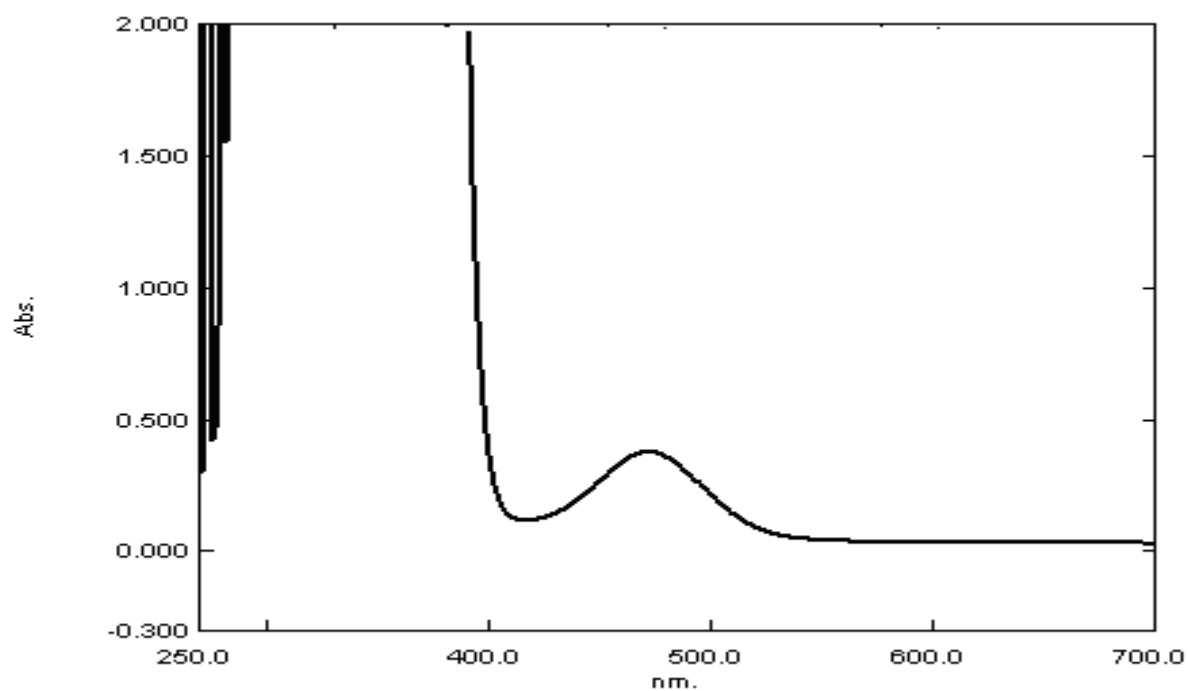
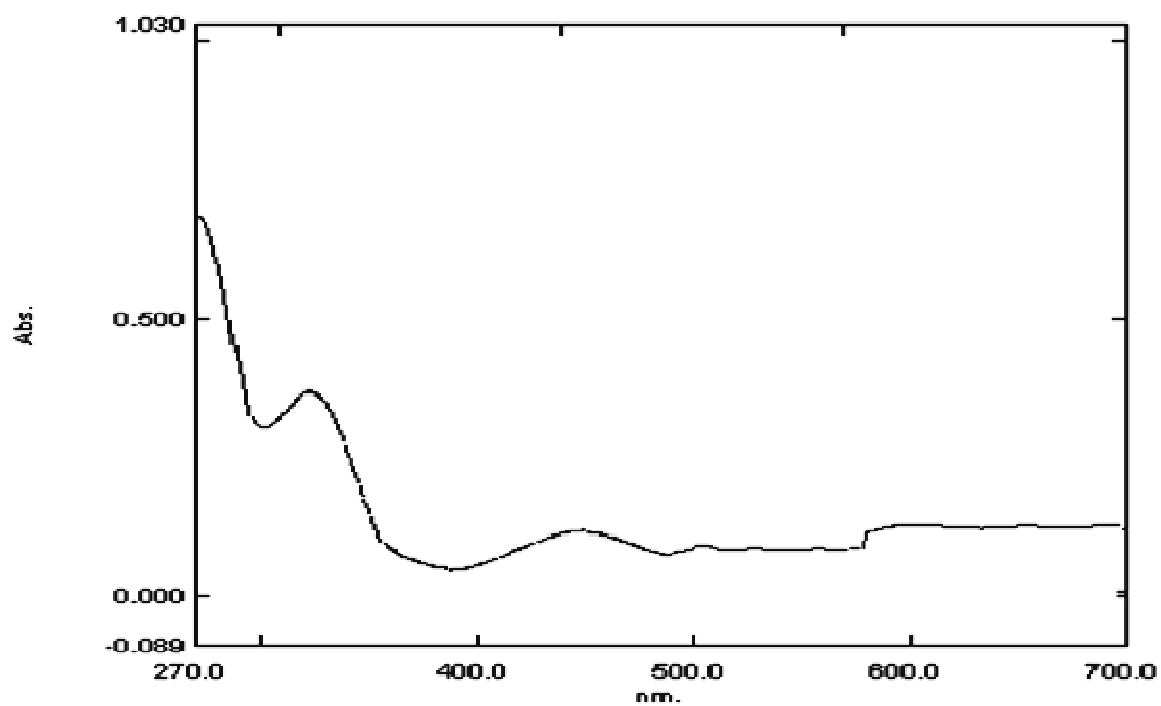


Figure (3. 13): The ultraviolet visible spectrum for a) potassium propyl xanthate and b) tris(isopropylxanthato)Chromium (III) complex.

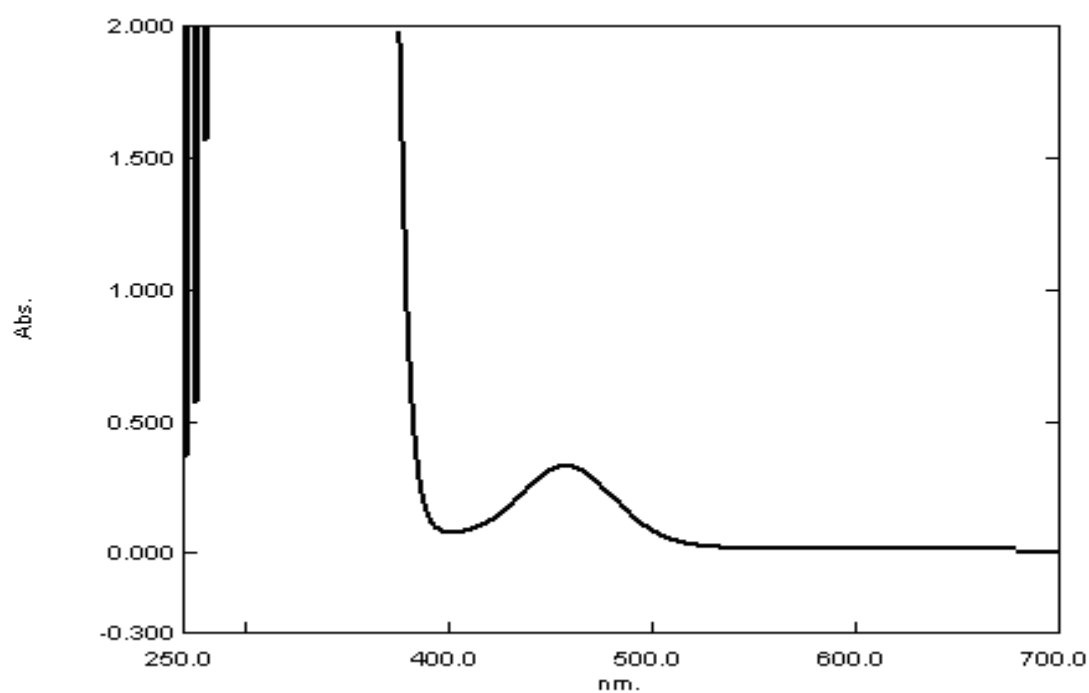


(a)

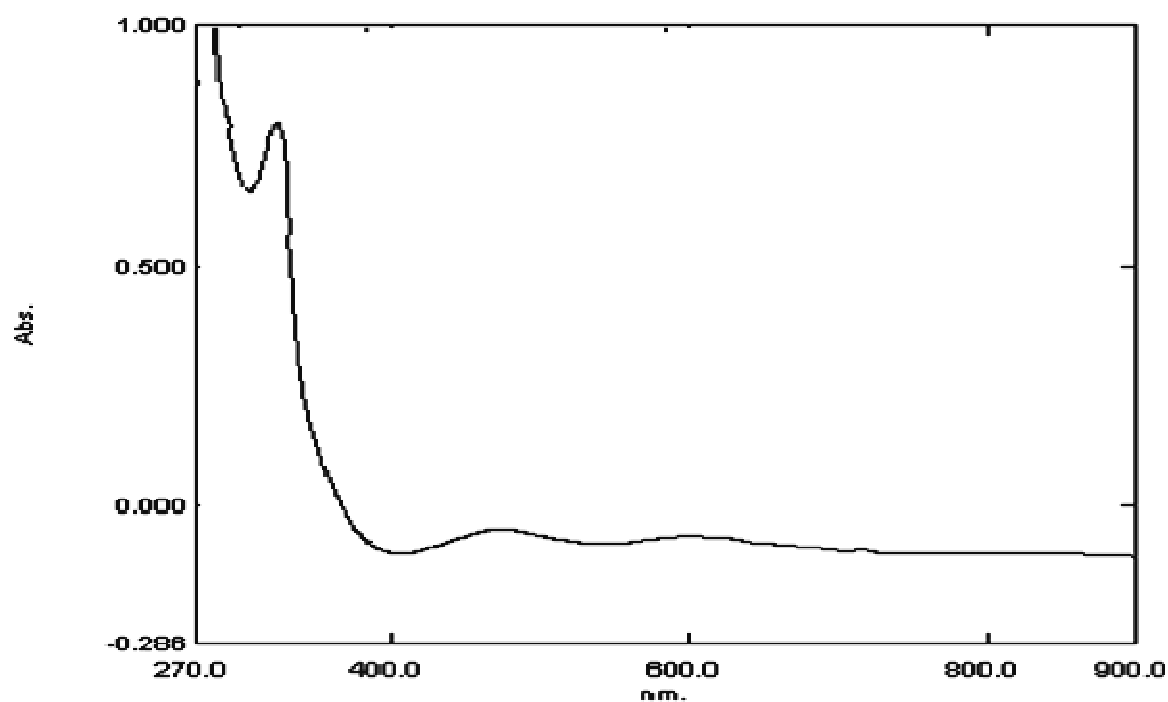


(b)

Figure (3. 14): The ultraviolet visible spectrum for a) potassium butyl xanthate and b) tris(butylxanthato)Chromium (III) complex.



(a)



(b)

Figure (3. 15): The ultraviolet visible spectrum for a) potassium hexyl xanthate and b) tris(hexylxanthato)Chromium (III) complex.

Table (3.4): Absorption wavelengths of the prepared ligands and their complexes

Ligand complex	wavelength nm(cm^{-1})	Assigned transition
PMX	472(21186)	$n \rightarrow \pi^*$
Cr(mex)₃	590(16949)	${}^4A_{2g}(F) \rightarrow {}^4T_{1g}(F)$
	455(21978)	${}^4A_{2g}(F) \rightarrow {}^4T_{1g}(F)$
	311(32154)	${}^4A_{2g}(F) \rightarrow {}^4T_{2g}(P)$
PEX	478(20921)	$n \rightarrow \pi^*$
Cr(etx)₃	576(17361)	${}^4A_{2g}(F) \rightarrow {}^4T_{1g}(F)$
	450(22222)	${}^4A_{2g}(F) \rightarrow {}^4T_{1g}(F)$
	312(32051)	${}^4A_{2g}(F) \rightarrow {}^4T_{2g}(P)$
PPX	486(20576)	$n \rightarrow \pi^*$
Cr(prx)₃	615(16260)	${}^4A_{2g}(F) \rightarrow {}^4T_{1g}(F)$
	445(22472)	${}^4A_{2g}(F) \rightarrow {}^4T_{1g}(F)$
	310(32258)	${}^4A_{2g}(F) \rightarrow {}^4T_{2g}(P)$
PBX	481(20790)	$n \rightarrow \pi^*$
Cr(bux)₃	603(16584)	${}^4A_{2g}(F) \rightarrow {}^4T_{1g}(F)$
	460(21739)	${}^4A_{2g}(F) \rightarrow {}^4T_{1g}(F)$
	312(32051)	${}^4A_{2g}(F) \rightarrow {}^4T_{2g}(P)$
PHX	465(21505)	$n \rightarrow \pi^*$
Cr(hex)₃	620(16129)	${}^4A_{2g}(F) \rightarrow {}^4T_{1g}(F)$
	442(22624)	${}^4A_{2g}(F) \rightarrow {}^4T_{1g}(F)$
	310(32258)	${}^4A_{2g}(F) \rightarrow {}^4T_{2g}(P)$

3.7 Photodecomposition of tris(alkylxanthato)chromium

(III) complexes

The primary concern was to follow the spectral changes which occurred on irradiation of Cr(Ax)₃chelate complex in DMSO. UV-visible spectral techniques and FTIR identification methods were used to follow the photodecomposition reaction. The uv-visible spectral technique was also used to determine the rate of photodecomposition of the chelate complexes.

3.8 Spectrophotometric measurements

On irradiation of 5×10^{-5} mol/l Cr(Ax)₃ in DMSO at room temperature, the complex absorption spectrum changes with the irradiation time. A decrease in the absorbance intensity was observed at wavelength of its maximum absorbencies as shown in Figures (3.16-3.20) for ($n \rightarrow \pi^*$) transitions in all prepared complexes. Table (3.5) lists the changes in absorbance (A_t) values with the irradiation time. From these changes in absorbance values during irradiation, one could say that the intra oxidation-reduction reaction occurs with homolytic scission of Cr-S bond and $\overset{\text{II}}{\text{Cr}}(\text{Ax})_2$ was formed.

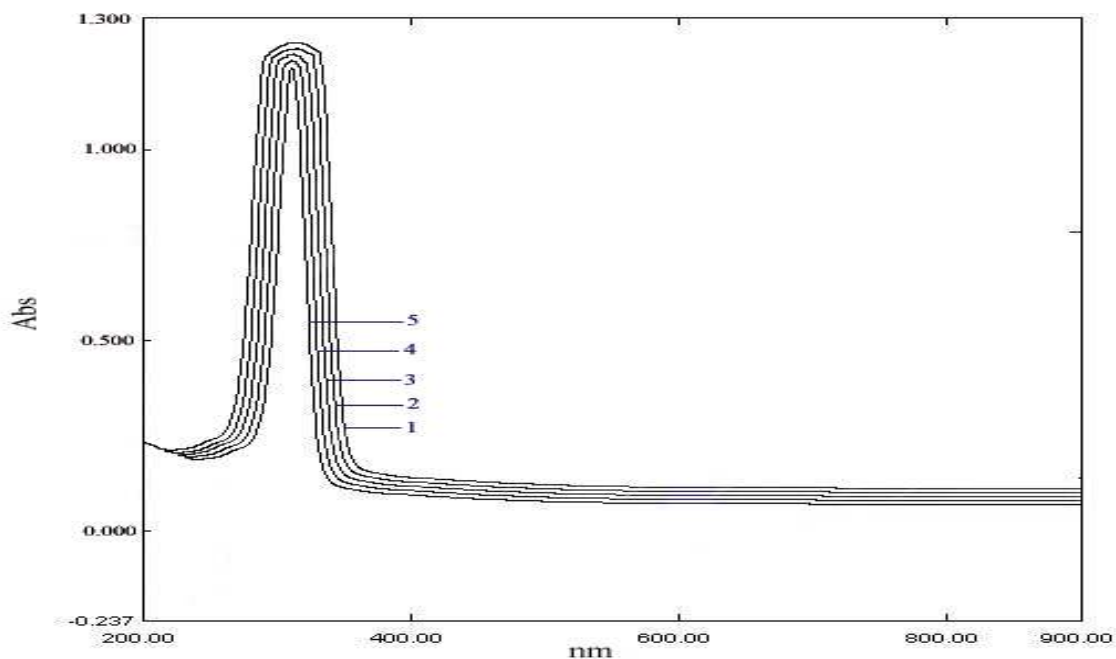
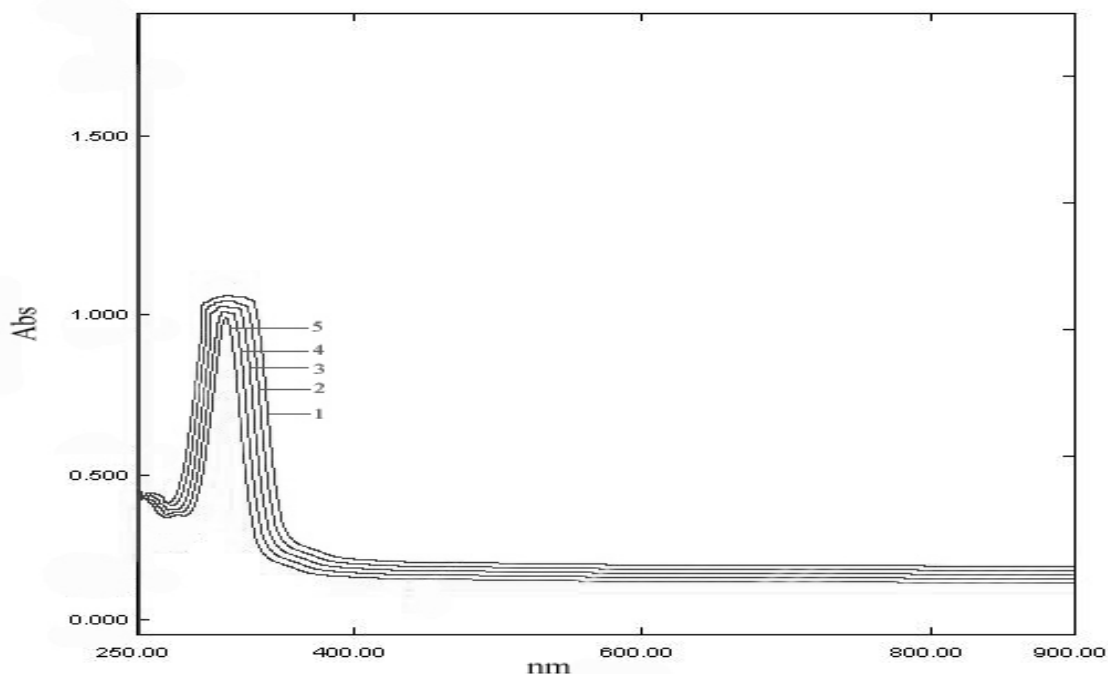


Figure (3.16): Uv-visible spectral changes in the absorbance of $\text{Cr}(\text{mex})_3$ during irradiation; (1) Before irradiation (zero time) (2) After 15 min. (3) After 30 min. (4) After 45 min. (5) After 60 min. irradiation, measured at $\lambda_{\text{irr.}} = 311\text{nm}$, at room temperature.



Figure(3.17): Uv-visible spectral changes in the absorbance of $\text{Cr}(\text{etx})_3$ during irradiation; (1) Before irradiation (zero time) (2) After 15 min. (3) After 30 min. (4) After 45 min. (5) After 60 min. irradiation, measured at $\lambda_{\text{irr.}} = 311\text{nm}$, at room temperature.

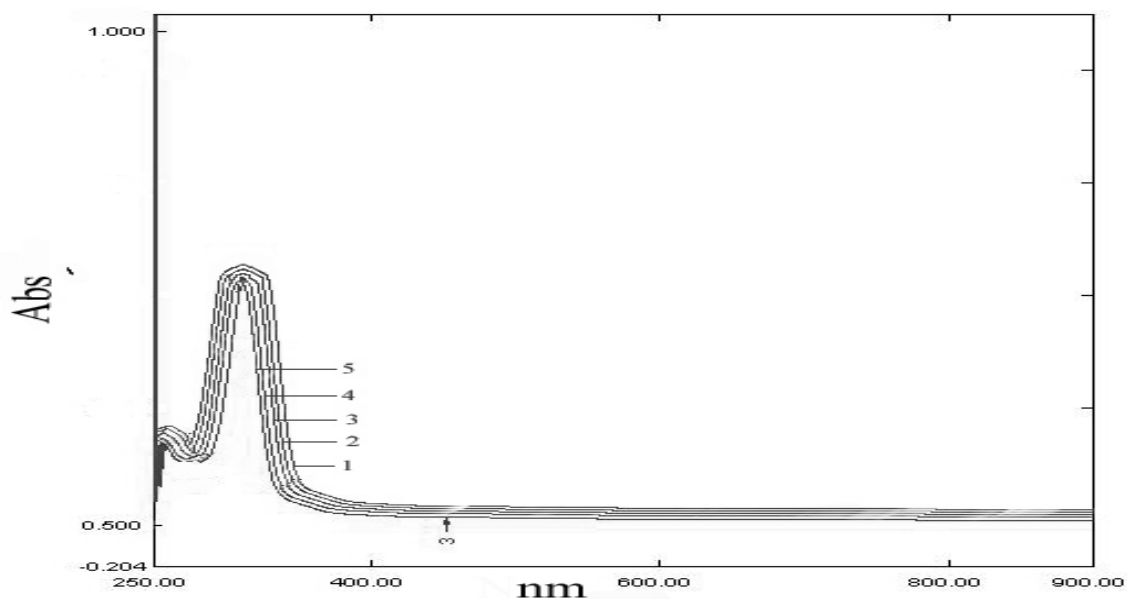


Fig.(3.18): *Uv-visible spectral changes in the absorbance of Cr(prx)₃ during irradiation; (1) Before irradiation (zero time) (2) After 15 min. (3) After 30 min. (4) After 45 min. (5) After 60 min. irradiation measured at $\lambda_{irr.} = 311\text{nm}$. at room temperature.*

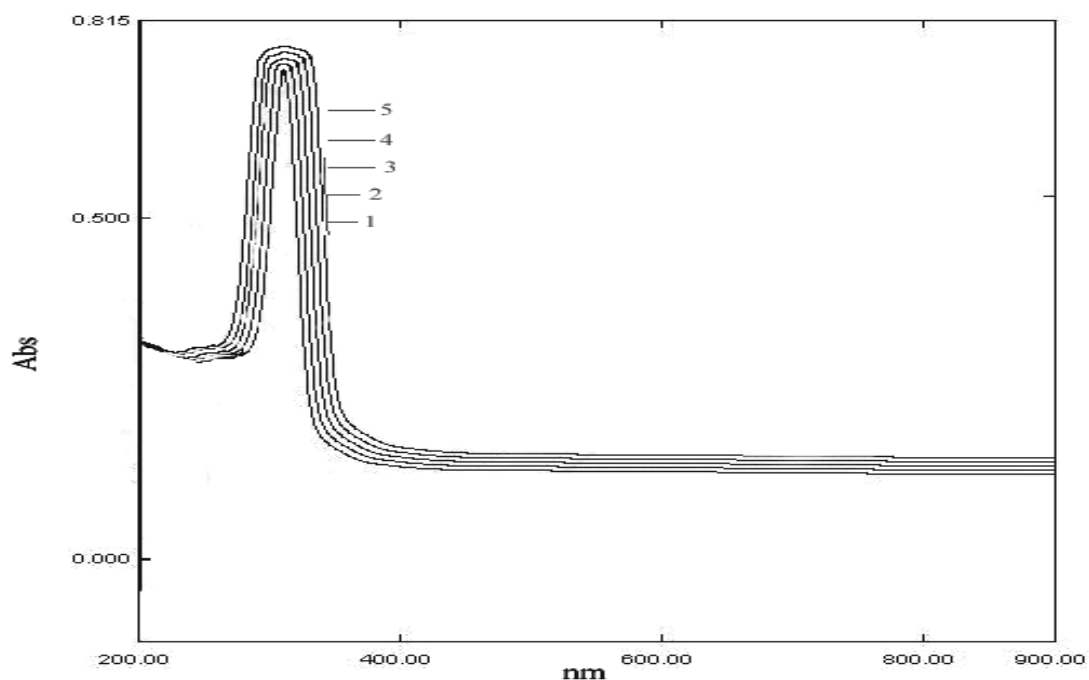


Figure (3.19): *Uv-visible spectral changes in the absorbance of Cr(bux)₃ during irradiation; (1) Before irradiation (zero time) (2) After 15 min. (3) After 30 min. (4) After 45 min. (5) After 60 min. irradiation measured at $\lambda_{irr.} = 311\text{nm}$. at room temperature.*

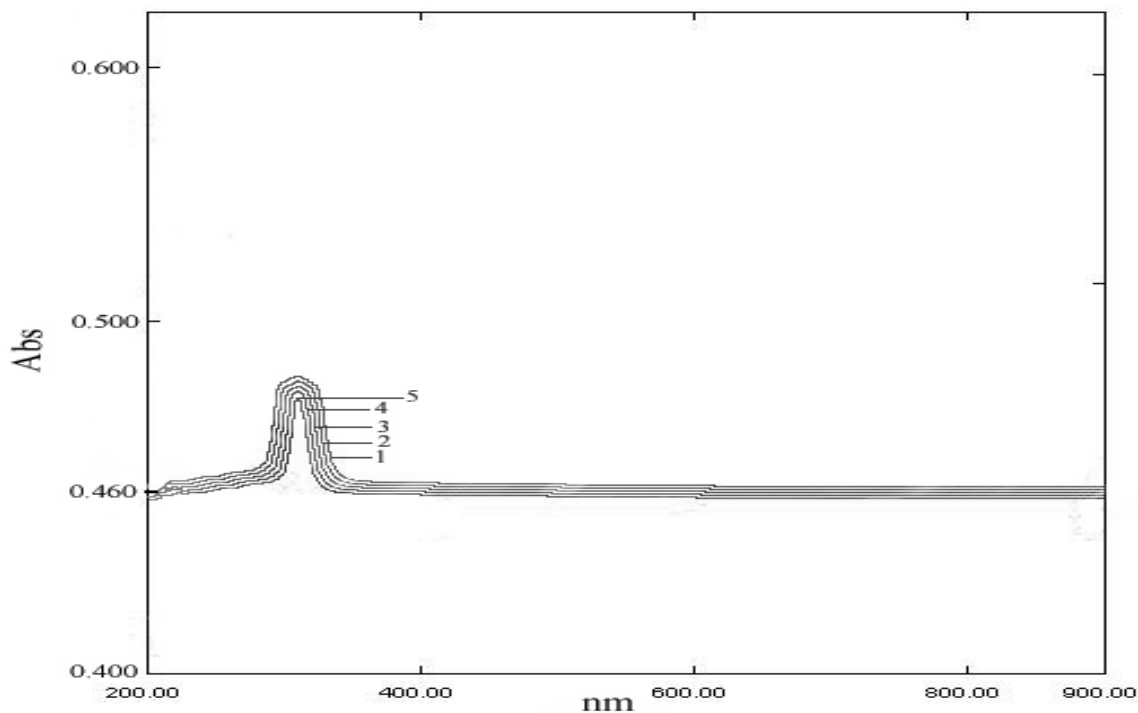


Figure (3.20): Uv-visible spectral changes in the absorbance of $\text{Cr}(\text{hex})_3$ during irradiation; (1) Before irradiation (zero time) (2) After 15 min. (3) After 30 min. (4) After 45 min. (5) After 60 min. irradiation, measured at $\lambda_{\text{irr.}} = 311\text{nm}$, at room temperature.

Table (3.5): Variation of absorbance with irradiation time of the complexes

Irradiation time (sec.)	Absorbance at $\lambda_{\text{irr.}} = 311 \pm 1\text{nm}$ for				
	$\text{Cr}(\text{mex})_3$	$\text{Cr}(\text{etx})_3$	$\text{Cr}(\text{prx})_3$	$\text{Cr}(\text{bux})_3$	$\text{Cr}(\text{hex})_3$
0	1.205	1.037	0.814	0.632	0.459
900	1.134	0.978	0.786	0.616	0.449
1800	1.060	0.930	0.741	0.601	0.441
2700	1.011	0.897	0.717	0.589	0.433
3600	0.959	0.854	0.687	0.580	0.425
4500	0.913	0.818	0.657	0.569	0.418
5400	0.868	0.783	0.630	0.558	0.412

The absorbencies at infinite irradiation (A_{∞}) of each compound were measured after a period of more than 50 hours. Each absorbance was subtracted from (A_{∞}) as listed in Tables (3.6 - 3.10). The natural logarithm of each value was taken. To convert the negative values of the resulting logarithm, one was added to each value.

Table (3.6): Natural logarithm of absorbance with irradiation time of $Cr(mex)_3$

Irradiation time(sec.)	A_t	$(A_t - A_{\infty})$	$\ln(A_t - A_{\infty})$	$1 + \ln(A_t - A_{\infty})$
0	1.205	0.897	-0.109	0.891
900	1.134	0.828	-0.191	0.809
1800	1.060	0.752	-0.285	0.715
2700	1.011	0.703	-0.352	0.648
3600	0.959	0.651	-0.429	0.570
4500	0.913	0.605	-0.503	0.497
5400	0.868	0.560	-0.579	0.420
$A_{\infty} = \text{Absorbance at infinite time} = 0.308$				

Table (3.7): Natural logarithm of absorbance with irradiation time of $Cr(etx)_3$

Irradiation time(sec.)	A_t	$(A_t - A_{\infty})$	$\ln(A_t - A_{\infty})$	$1 + \ln(A_t - A_{\infty})$
0	1.037	0.771	-0.260	0.740
900	0.978	0.712	-0.339	0.660
1800	0.930	0.664	-0.409	0.590
2700	0.897	0.631	-0.460	0.540
3600	0.854	0.588	-0.531	0.469
4500	0.818	0.552	-0.594	0.406
5400	0.783	0.517	-0.659	0.340
$A_{\infty} = \text{Absorbance at infinite time} = 0.266$				

Table (3.8): Natural logarithm of absorbance with irradiation time of $Cr(prx)_3$

<i>Irradiation time(sec.)</i>	A_t	$(A_t - A_\infty)$	$\ln(A_t - A_\infty)$	$1 + \ln(A_t - A_\infty)$
0	0.814	0.604	-0.540	0.496
900	0.786	0.576	-0.551	0.448
1800	0.741	0.531	-0.633	0.367
2700	0.717	0.507	-0.679	0.320
3600	0.687	0.477	-0.740	0.260
4500	0.657	0.447	-0.805	0.195
5400	0.630	0.460	-0.867	0.133
$A_\infty = \text{Absorbance at infinite time} = 0.210$				

Table (3.9): Natural logarithm of absorbance with irradiation time of $Cr(bux)_3$

<i>Irradiation time(sec.)</i>	A_t	$(A_t - A_\infty)$	$\ln(A_t - A_\infty)$	$1 + \ln(A_t - A_\infty)$
0	0.632	0.480	-0.734	0.266
900	0.616	0.464	-0.768	0.233
1800	0.601	0.449	-0.800	0.200
2700	0.589	0.437	-0.828	0.172
3600	0.580	0.426	-0.849	0.151
4500	0.569	0.417	-0.875	0.125
5400	0.558	0.406	-0.901	0.098
$A_\infty = \text{Absorbance at infinite time} = 0.152$				

Table (3.10): Natural logarithm of absorbance with irradiation time of $\text{Cr}(\text{hex})_3$

<i>Irradiation time(sec.)</i>	A_t	$(A_t - A_\infty)$	$\ln(A_t - A_\infty)$	$1 + \ln(A_t - A_\infty)$
0	0.459	0.425	-0.855	0.144
900	0.449	0.415	-0.879	0.120
1800	0.441	0.407	-0.898	0.101
2700	0.433	0.399	-0.919	0.081
3600	0.425	0.391	-0.939	0.061
4500	0.418	0.384	-0.957	0.043
5400	0.412	0.376	-0.973	0.027

$A_\infty = \text{Absorbance at infinite time} = 0.034$

These values were then plotted against irradiation time, as shown in Figures (3.21-3.25). The slopes of these plots represent the inverse photodecomposition rate constant (K_d) of each complex.

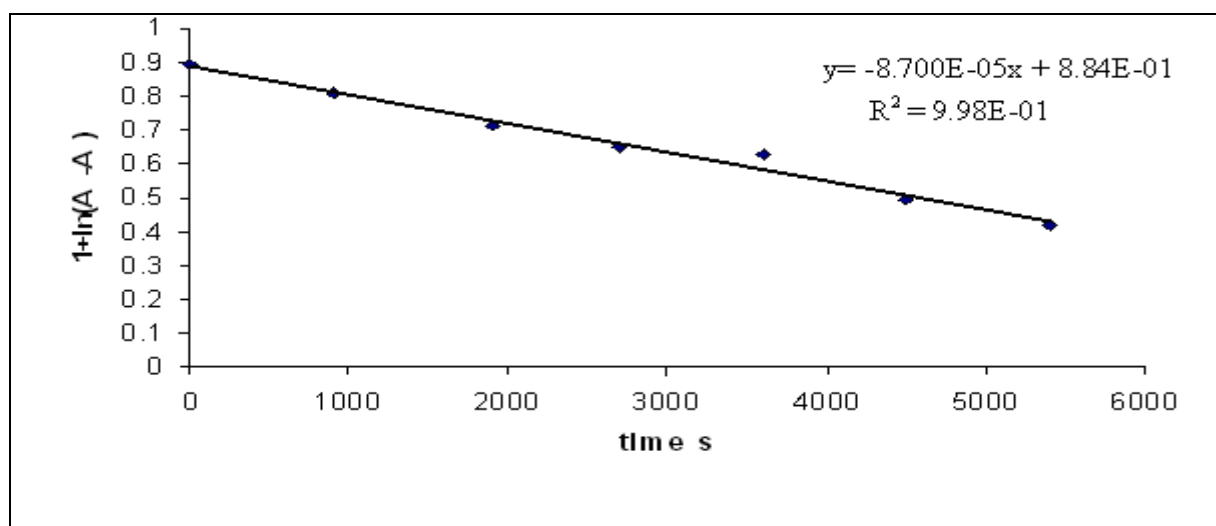


Figure (3.21): Plot of natural logarithm of absorbance against irradiation time for $\text{Cr}(\text{hex})_3$

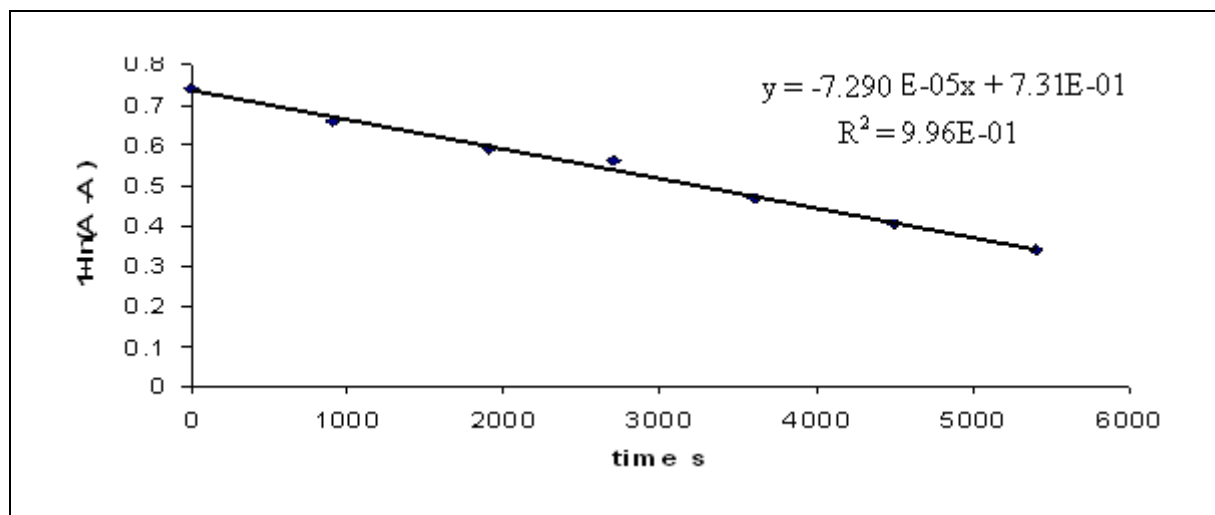


Figure (3.22:) Plot of natural logarithm of absorbance against irradiation time for Cr(etx)_3 .

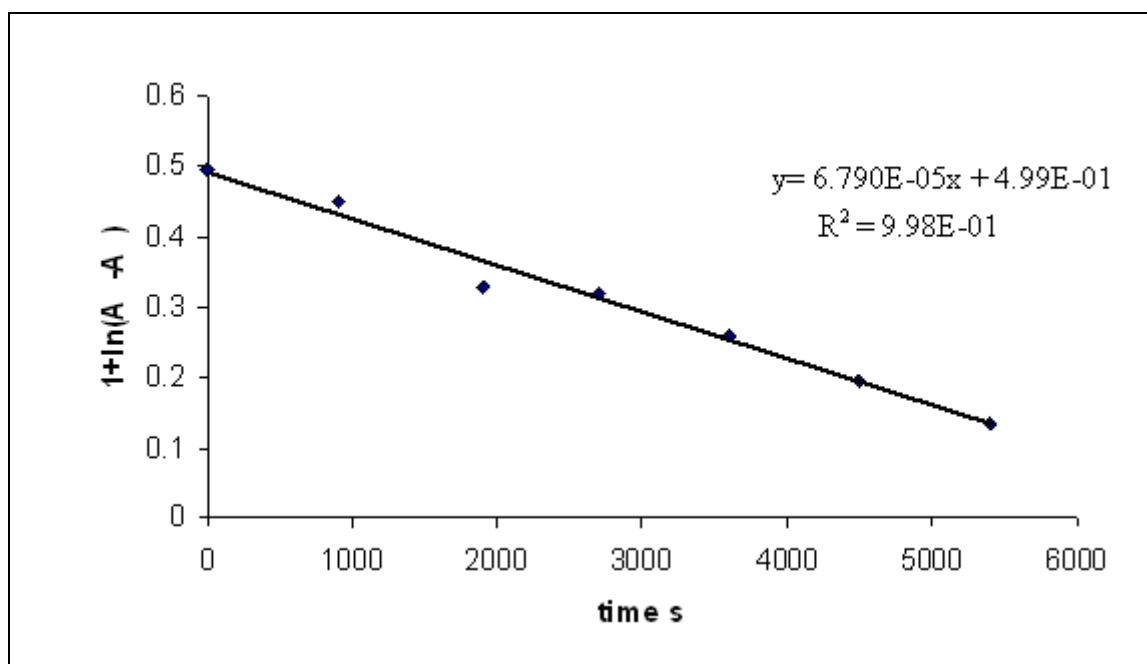


Figure (3.23): Plot of natural logarithm of absorbance against irradiation time for Cr(prx)_3 .

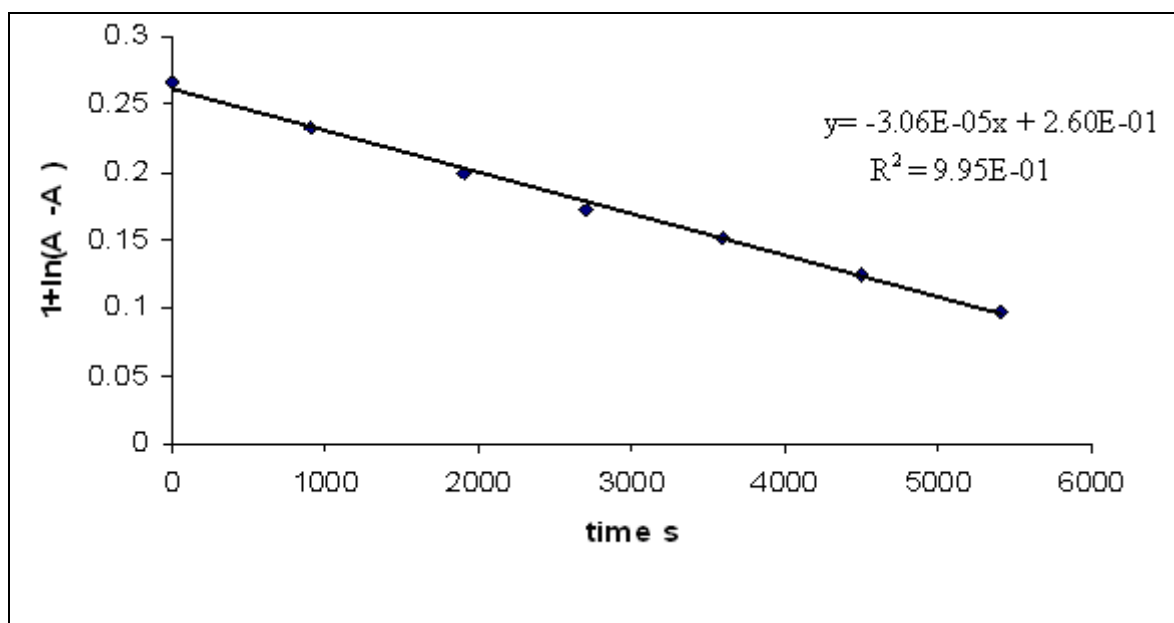


Figure (3.24:) Plot of natural logarithm of absorbance against irradiation time for $Cr(bux)_3$.

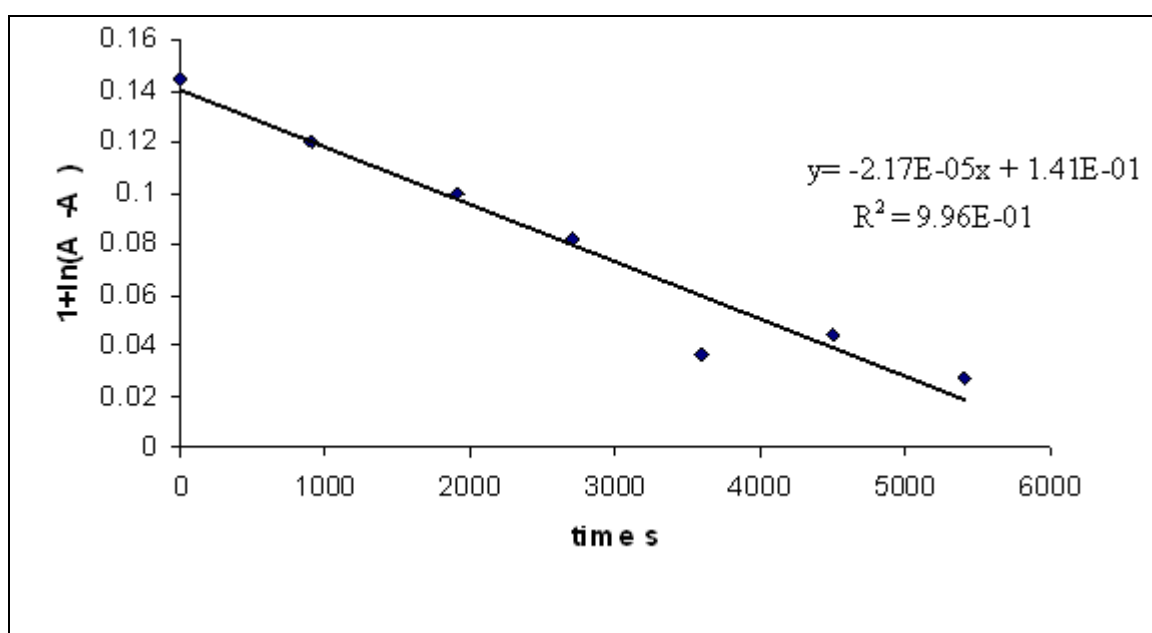


Figure (3.25): Plot of natural logarithm of absorbance against irradiation time for $Cr(hex)_3$.

3.9 Kinetic of the photodecomposition reactions using uv-visible spectrophotometric measurements

The change in the uv-visible absorptions spectra during irradiation were monitored through the photolysis experiments. The decay of tris(alkylxanthato)chromium(III) complexes during the irradiation at 311 ± 1 nm, was followed by the change in the chelate concentration spectrophotometrically. In order to determine the rate of photodecomposition of $\text{Cr}(\text{Ax})_3$ complexes. From this change, it was found that the value of $(A_t - A_\infty)$ decreased exponentially with irradiation time corresponding to the first order chelate decomposition and was consistent with first order reaction.

At wavelength 311 ± 1 nm, the value of $|A_t - A_\infty|$ decreased exponentially with irradiation time as summarized in Figure(3.26) for the variation of $1 + \ln(A_t - A_\infty)$ with irradiation time (t) of $\text{Cr}(\text{Ax})_3$ complexes. The straight lines are consistent with the first order chelate decomposition processes. Therefore, from the slopes of these straight lines, the values of specific rate constants (K_d) were evaluated. Using the value of (K_d), the rate of photodecomposition were calculated ($\text{Rate} = K_d [\text{Concentration of } \text{Cr}(\text{Ax})_3]$) and the quantum yield of this process is deduced.

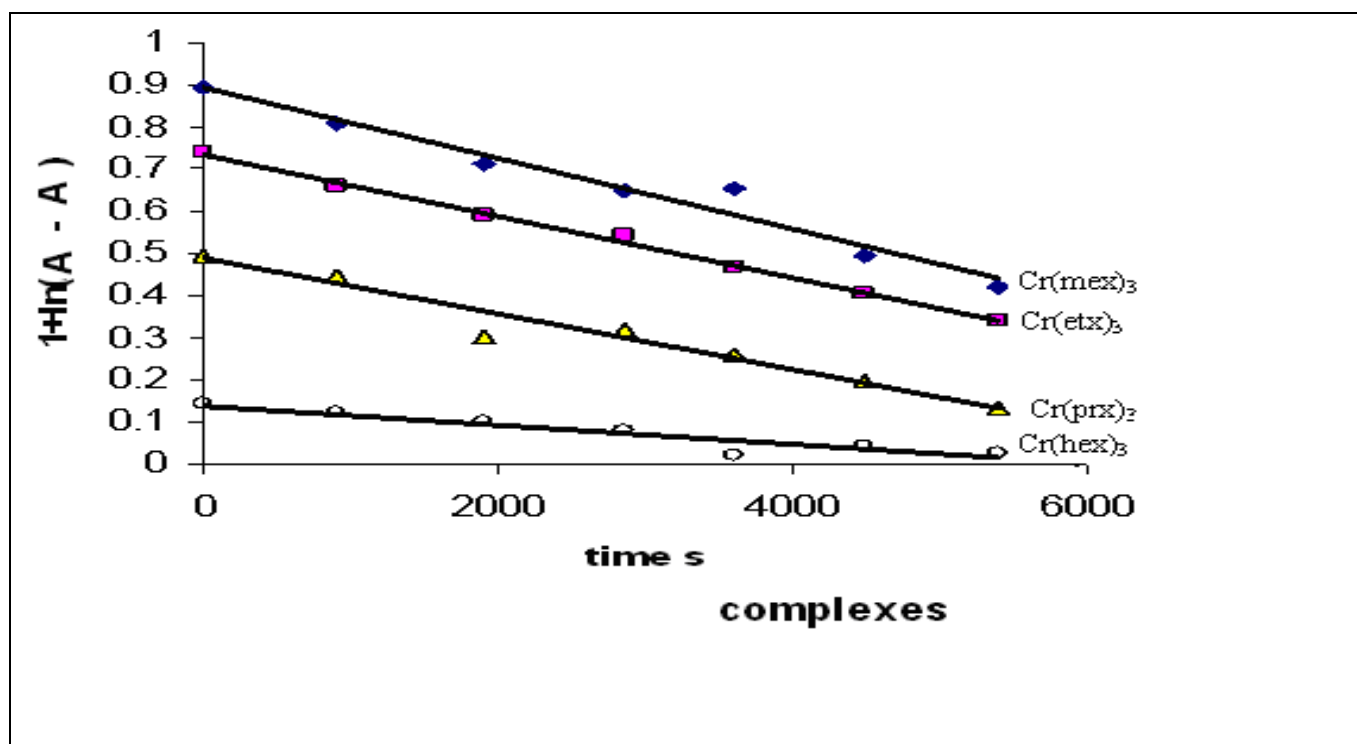


Figure (3.26): Variation of natural plot logarithm of absorbance with irradiation time of the $\text{Cr}(\text{Ax})_3$ complexes in DMSO ($\lambda_{\text{irr}} = 311 \pm 1 \text{ nm}$. at room temperature).

The following kinetic equilibria⁽⁷⁵⁾ might be followed for the reactions in equation (3.1) of scheme (3.1) :

$$-\frac{d[\text{Cr}(\text{Rx})_3]^*}{dt} = I_{\text{abs}} - K_{-1} [\text{Cr}(\text{Rx})_3]^* \quad (3.3)$$

Where I_{abs} is absorbed intensity radiation. I_0 and I_{abs} of DMSO were calculated using equation (2.1) and found to be equal to $1.3891 \times 10^{-5} \text{ Ein.l}^{-1}.\text{S}^{-1}$ and $5.114 \times 10^{-7} \text{ Ein.l}^{-1}.\text{S}^{-1}$, respectively. These values were used in the calculation of the quantum yield according to equation (3.4):

$$Q_d = \text{rate of photodecomposition} / I_{\text{abs}} \quad (3.4)$$

Since the rate of excited state decomposition can be expressed as in equation (3.5) is:

$$-\frac{d[\text{Cr}(\text{Rx})_3]^*}{dt} = I_{\text{abs}} - K_2 [\text{Cr}(\text{Rx})_3]^* - K_{-1} [\text{Cr}(\text{Rx})_3]^* \quad (3.5)$$

Assuming that the $[\text{Cr}(\text{Rx})_3]^*$ excited state concentration is fixed, then:

$$[\text{Cr}(\text{Rx})_3]^* = \frac{I_{\text{abs}}}{K_{-1} + K_2} \quad (3.6)$$

The value of excited state concentration, $[\text{Cr}(\text{Rx})_3]^*$, in equation (3.6) is substituted in equation (3.3), one can get:

$$\begin{aligned} -\frac{d[\text{Cr}(\text{Rx})_3]}{dt} &= I_{\text{abs}} - \frac{I_{\text{abs}} K_{-1}}{K_{-1} + K_2} \\ &= I_{\text{abs}} \left(1 - \frac{K_{-1}}{K_{-1} + K_2} \right) \end{aligned} \quad (3.7)$$

Then equation (3.4) can take the form:

$$Q_d = \frac{\text{Rate of photodecomposition}}{I_{\text{abs}}} = -\frac{d[\text{Cr}(\text{Rx})_3]}{dt} / I_{\text{abs}} \quad (3.8)$$

The value of quantum yield of photodecomposition (Q_d) can then be given by equation (3.9):

$$Q_d = 1 - \frac{K_{-1}}{K_{-1} + K_2} \quad (3.9)$$

or

$$Q_d = \frac{K_2}{K_{-1} + K_2} \quad (3.10)$$

By rearranging equation (3.9) and equation (3.10), we can obtain equation (3.11) for the value of reactivity ratio (K_2 / K_{-1}).

$$\frac{K_2}{K_{-1}} = \frac{Q_d}{1 - Q_d} \quad (3.11)$$

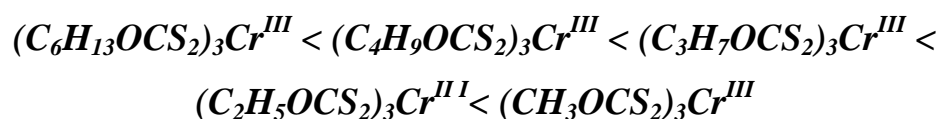
Equation (3.11) was used to calculate the reactivity ratio of the photodecomposition of $\text{Cr}(\text{Ax})_3$ in DMSO. These values are listed in Table (3.11). The results of Table (3.11) for the reactivity ratio indicated that these values decreased as the number of CH_3 -group in complexes increased and that should be expected since the value of Q_d decreased in the same manner. This also may be explained as the number of methyl group in complexes decreased, the excitation of the complex become much easier, i.e., the probability of excitation (ϵ) became larger compared to longer saturated alkyl chain⁽¹¹¹⁾. However, the small difference in the above values between the ethyl and the isopropyl group ligands may be due to the similarity in the spacial configuration of the two-alkyl group. Therefore, the concentration of the populated excited state will be larger for the small alkyl containing complexes (equation 3.1 in mechanism Scheme (3.1)). Consequently, the photodecomposition step (K_2) which dependent on the concentration of excited state will be larger for the less number alkyl group containing complexes.

Table (3.11): Specific rate constant (K_d), photodecomposition constant (R_d), the quantum yield (Q_d) and the reactivity ratio (K_r) for different complexes in DMSO (Irradiation wavelength 311 ± 1).

Complexes	Concentration $10^{-5}M$	K_d $10^{-5} s^{-1}$	R_d $10^{-9} s^{-1}M$	Q_d 10^{-3}	K_r 10^{-3}
$Cr(mex)_3$	5.000	8.700	4.350	7.702	7.762
$Cr(etx)_3$	5.000	7.290	3.645	6.454	6.496
$Cr(prx)_3$	5.000	6.790	3.395	6.011	6.047
$Cr(bux)_3$	5.000	3.060	1.530	2.709	2.716
$Cr(hex)_3$	5.000	2.170	1.080	1.921	1.925

From the results shown in Table (3.11), one could notice that K_d and Q_d values were dependent on the number of CH_3 - group in the complexes.

The photodecomposition increased as the number of CH_3 - group in the complexes decrease. Also the rate constant and quantum yield decrease from the higher number of CH_3 - group as in hexane complex (1.925×10^{-3}) compared to the lower number of CH_3 - as in methyl complex (7.762×10^{-3}) following the order:



The effect of the number of CH_3 - group in the complexes on the rate of photodecomposition process is, therefore, correlated with the value of quantum yield. The relationship of the Q_d values for the complexes in DMSO were plotted against the type of complex. The results shown

schematically in Figure(3.27), which indicated that Q_d increases as the number of CH_3 - group in complex decrease.

This shape of Figure (3.27) could be explained by considering that -OR group is electron-withdrawing group that would cause less electron density on the metal ion. The presence of the highly positive center, Cr(III), made the dissociation of this weak adduct that produce a higher quantum yield. This may be explain the observation of higher Q_d of $\text{Cr}(\text{Ax})_3$ complexes in DMSO.

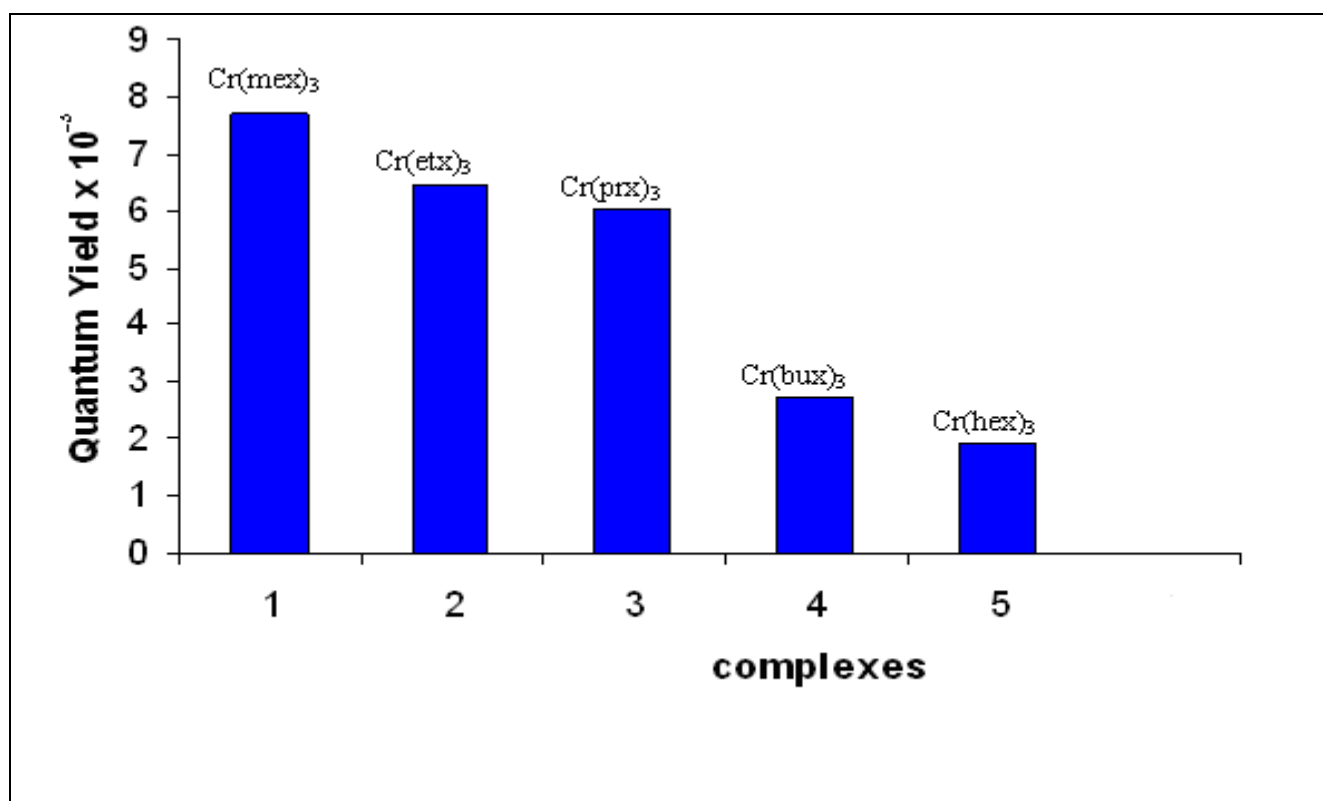
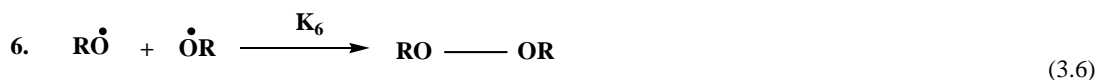
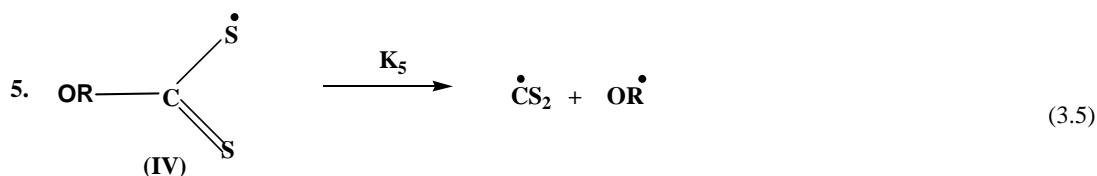
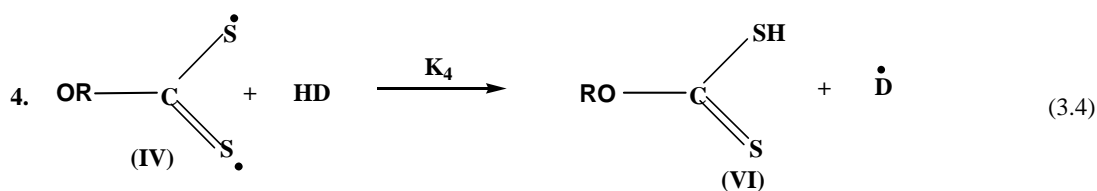
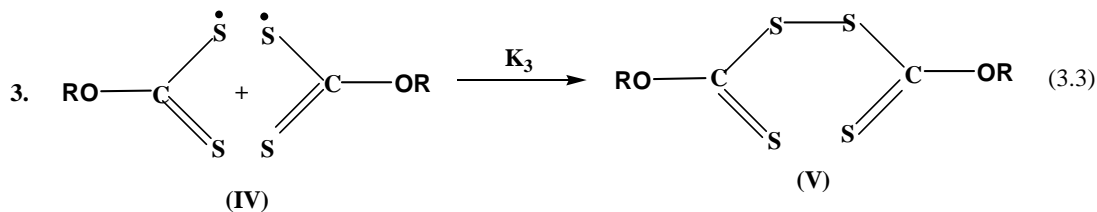
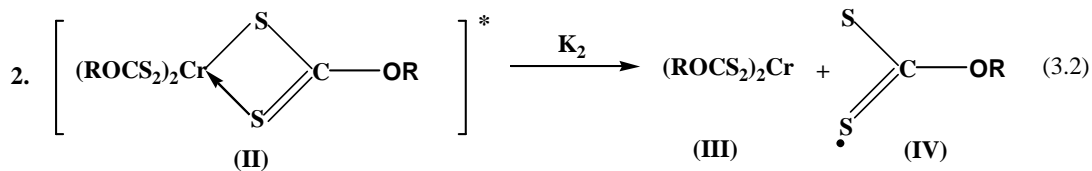
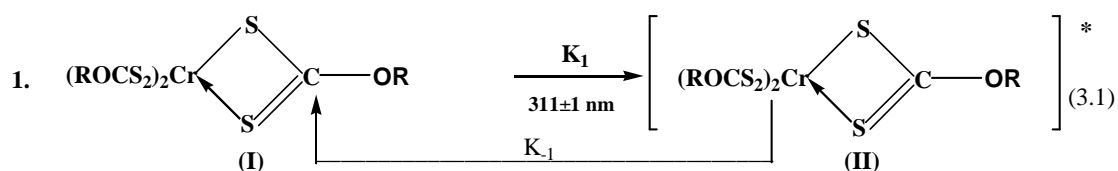


Figure (3.27): Variation in quantum yields (Q_d) with the number of methyl group in complexes for the photodecomposition of $\text{Cr}(\text{Ax})_3$ complex DMSO

3.10 Photolytic Reaction mechanism for the prepared tris(alkylxanthato) chromium (III) Complexes

The mechanism that may be suggested for the photodecomposition processes is shown in Scheme (3.1). The uv-visible spectra of the photolytic products indicated that the primary photolysis step might be the hemolytic scission of a Cr-S bond as shown in equation (3.2). After that, the obtained xanthate radical was rapidly decomposed to CS₂ and R[•] radicals, which were then expected to abstract hydrogen from the solvent (HD) forming alcohol.



Where: $K_{-1}, K_1, K_2, K_3, K_4, \dots$, etc. are the rate constants for the above reactions.

Scheme (3.1): The suggested reaction mechanism for the prepared complexes⁽⁷⁵⁾

The compound (I) has been excited to compound (II) by uv-radiation at $311 \pm 1 \text{ nm}$. The bonds between the chromium atom and the two sulphur atoms in the excited state of this compound break to yield compounds (III) and radical (IV) as shown in equation (3.2). The radical compound (IV) may undergo different radical reactions. It may either recombine to yield the dimer (V), or abstract hydrogen from the solvent (HD) as in equations (3.3) and (3.4), respectively. The bond between the oxygen and carbon may break to yield carbon disulphide and alkoxy radical (equation 3.5). The alkoxy radicals may be combined to yield peroxy as in equation (3.6) or abstract hydrogen from the solvent to yield alcohol (equation 3.7). The solvent radicals produce from equations (3.4) and (3.7) may finally recombine as in equation (3.8). However, these suggestions need further investigation using modern instrumentation such as ESR, mass spectrometry and other spectroscopic and separation techniques to validate the above reactions scheme. The reaction rate constant K_3 , K_4 , K_5 , K_6 , K_7 , and K_8 in equations (3.3-3.8) were very large, since, they involved very reactive radical reactions. However, excitation irradiation reaction in equation (3.1) was assumed to be the slowest step followed by the decomposition reaction in equation (3.2). Consequently, this reaction was considered as the rate-determining step.

Therefore, the dissociation reaction was followed by uv-visible spectrophotometry by measuring the decrease in the absorbance of the prepared tris(alkylxanthato)chromium(III) complexes as will be described thereafter.

3.11 Conclusion Remarks

In the work described in this thesis, the photochemistry of tris(alkylxanthato) chromium (III) complexes in DMSO was studied. The results have suggested that these complexes were photosensitive when irradiated with uv radiation of wavelength 311 ± 1 nm. and decomposed through the scission of the Cr-S bond. The $\text{Cr}(\text{Ax})_3$ complexes after irradiation produced $\text{Cr}^{\text{II}}(\text{Ax})_2$ and $[(\text{CS}_2)\text{OR}]^\cdot$ radical which ultimately decomposed to CS_2 and R^\cdot radical. The latter abstracted hydrogen from solvent molecular to produce alcohol as suggested by the propose mechanism. It was also found that the photochemical reaction is first order accordingly. The specific rate constants (K_d) at room temperature, were evaluated by monitoring the spectral changes during irradiation process.

The quantum yield of photodecomposition process is generally low and is greatly affected by the type of ligands in Cr(III) chelate complexes and the number of CH_3 - group. The value of quantum yield of photodecomposition in these complexes increases as the number of CH_3 -group decreased in the order, from $(\text{C}_6\text{H}_{13}\text{OCS}_2)_3\text{Cr}^{\text{III}}$, $(\text{C}_4\text{H}_9\text{OCS}_2)_3\text{Cr}^{\text{III}}$, $(\text{C}_3\text{H}_7\text{OCS}_2)_3\text{Cr}^{\text{III}}$, $(\text{C}_2\text{H}_5\text{OCS}_2)_3\text{Cr}^{\text{III}}$, to $(\text{CH}_3\text{OCS}_2)_3\text{Cr}^{\text{III}}$

It is well established that transition metal chelate are photochemically active in polymer photochemistry. These complexes might be useful in many applications. Moreover, as mentioned earlier, metal chelate with metals at high oxidation state is active in the enhancement of photodegradation of plastic and therefore, might serve as photocatalyst to treat the plastic waste pollution problem.

3.12 Suggestion for future work

- 1- It is recommended to study the photodecomposition reactions of these and other complexes using modern instrumentation as mentioned above.
- 2- The use of different metal complexes to compare the photodecomposition of these metals.
- 3- The use of unsaturated, phenyl and other aromatic compounds instead of alkyl group to compare their photodecomposition constants and other values.
- 4- Study the effect of polar and nonpolar solvent on the photodecomposition reactions.
- 5- Using these complexes as photoinitiator for polymerization process might be good extension of the present work.

ACKNOWLEDGMENTS

First and foremost I would like to thank my advisor, Dr. Shahbaz A. Maki, for his guidance, suggestions, criticism and support he has provided throughout the course of my studies and research.

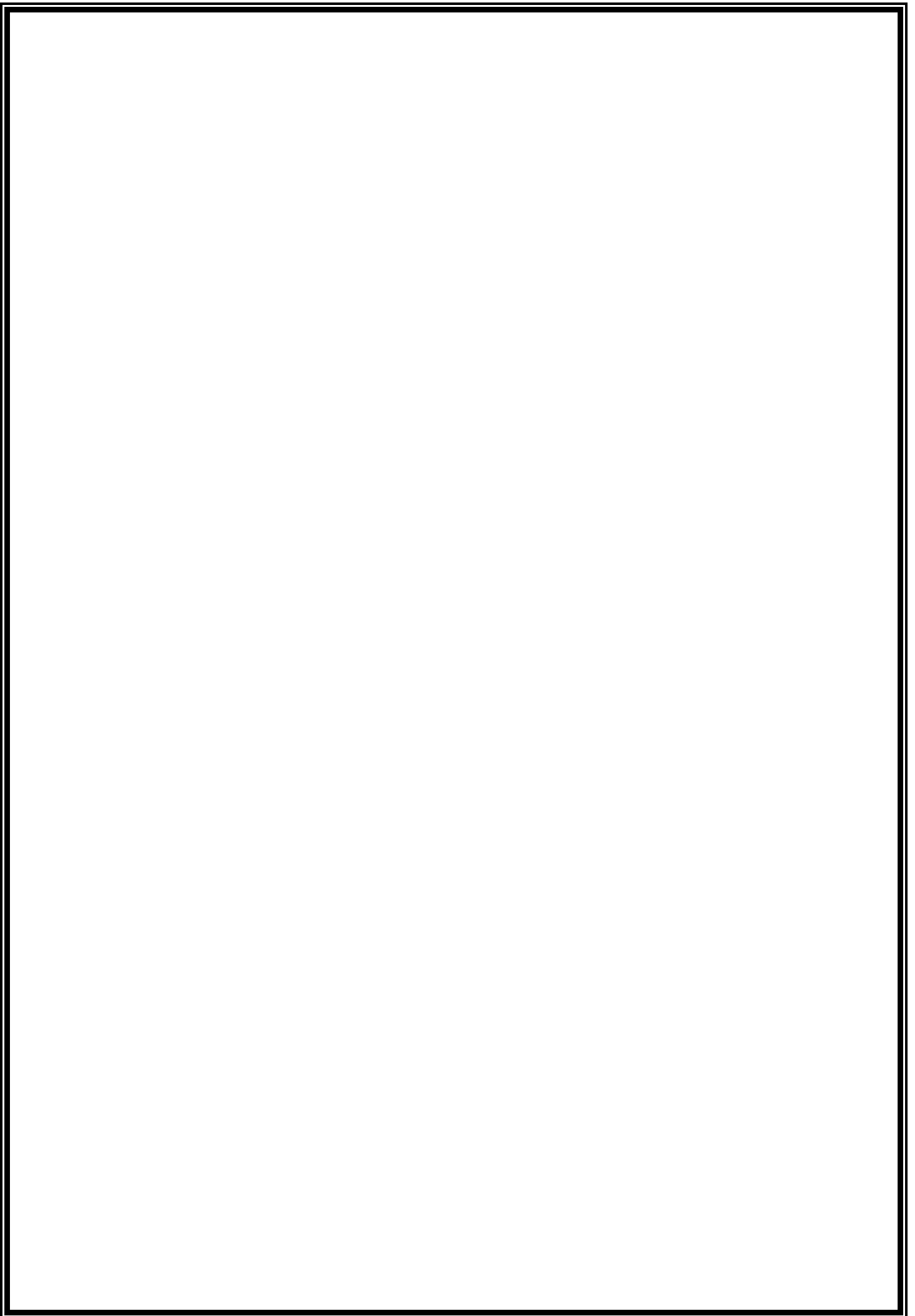
I would like to express my deep gratitude to Dr. Emad A. Yousif for introducing me to the field of photochemistry. Thanks are due to the other chemistry faculty members for their continuous support and feedback. My thanks are also extended to staff member of the Department of Chemistry, Dean of College of Science, Al-Nahrain University. I would like to express my sincere appreciation especially Khalida , Belal and all others my dear friends for their encouragement and assistance during the experimental work. Thanks are also due to all the people who helped me during the period of this work.

Let GOD Bless Them All

Eklas
2008

List of abbreviation

<i>Code</i>	<i>Name</i>
PAX	<i>Potassium alkyl xanthate</i>
PMX	<i>Potassium methyl xanthate</i>
PEX	<i>Potassium ethyl xanthate</i>
PPX	<i>Potassium isopropyl xanthate</i>
PBX	<i>Potassium butyl xanthate</i>
PHX	<i>Potassium hexyl xanthate</i>
Cr(AX) ₃	<i>Tris(alkylxanthato)chromium(III) complexes</i>
Cr(mex) ₃	<i>Tris(methylxanthato)chromium(III) complex</i>
Cr(etx) ₃	<i>Tris(ethylxanthato)chromium(III) complex</i>
Cr(prx) ₃	<i>Tris(isopropylxanthato)chromium(III) complex</i>
Cr(bux) ₃	<i>Tris(butylxanthato)chromium(III) complex</i>
Cr(hex) ₃	<i>Tris(hexylxanthato)chromium(III) complex</i>
[Ru(bpy) ₃] ⁺²	<i>Ruthenium tris bipyridine complex</i>
ET	<i>Electron transfer</i>
CT	<i>Charge transfer</i>
LF	<i>Ligand field</i>
IF	<i>Intraligand field</i>
MLCT	<i>Metal to ligand charge transfer</i>
LMCT	<i>Metal to ligand charge transfer</i>
IC	<i>Internal conversion</i>
ISC	<i>Intersystem crossing</i>
acac	<i>Acetyl acetonate</i>
en	<i>Ethylene diamine</i>
Niox	<i>Nickel oxime</i>
OAC	<i>Acetic acetate</i>
Co(etx) ₃	<i>Tris(cobaltxanthato)chromium (III) complex</i>
Co(dtc) ₃	<i>Tris(diethyldithcarbamate)Cobalt(III) Complex</i>
DMSO	<i>Dimethy soulfoxide</i>
Me	<i>methanol</i>
Ac	<i>Acetone</i>
Py	<i>pyridine</i>
Be	<i>benzene</i>
K _d	<i>Specific rate constant</i>
R _d	<i>Photodecomposition constant</i>
Q _d	<i>Quantum yield</i>
K _r	<i>Reactivity ratio</i>
O _h	<i>Octahedral</i>
FTIR	<i>Fourier transform spectroscopy</i>
UV	<i>Ultraviolet – visible spectroscopy</i>



List of Tables

<i>Table No.</i>	<i>Title</i>	<i>Page No.</i>
1.1	Photochemical processes	2
2.1	Chemicals and their suppliers	29
3.1	Some physical properties for the prepared ligands and their complexes	41
3.2	Magnetic moment measurement of complexes.	44
3.3	Infrared bands of xanthate ligands and their complexes	56
3.4	Absorption wavelength of the prepared ligands and their complexes	65
3.5	Variation of absorbance with irradiation time of the complexes	69
3.6	Natural logarithm of absorbance with irradiation time of Cr(mex) ₃	69
3.7	Natural logarithm of absorbance with irradiation time of Cr(etx) ₃	70
3.8	Natural logarithm of absorbance with irradiation time of Cr(prx) ₃	70
3.9	Natural logarithm of absorbance with irradiation time of Cr(bux) ₃	71
3.10	Natural logarithm of absorbance with irradiation time of Cr(hex) ₃	71
3.11	Specific rate constants , the quantum yield and the reactivity ratio for different complexes in DMSO	78

List of Figures

<i>Figure No.</i>	<i>Title</i>	<i>Page No.</i>
1.1	Orbital energy diagram of electronic transition in octahedral complexes	8
1.2	Deactivation process for an excited molecules	10
1.3	Absorption spectrum of Cr(III) complex having practically octahedral microsymmetry.	25
1.4	Energy levels for d^3 configuration in octahedral symmetry	25
2.1	(a) Photolysis apertures set up and (b) Filter transmittance	33
2.2	Calibration curve for Fe(II) complex at 510nm	
3.1	FTIR spectrum for potassium methyl xanthate ligand	46
3.2	FTIR spectrum for tris(methylxanthato)chromium(III) complex	47
3.3	FTIR spectrum for potassium ethyl xanthate ligand	48
3.4	FTIR spectrum for tris(ethylxanthato)chromium(III) complex	49
3.5	FTIR spectrum for potassium isopropyl xanthate ligand	50
3.6	FTIR spectrum for tris(isopropylxanthato)chromium(III) complex	51
3.7	FTIR spectrum for potassium butyl xanthate ligand	52
3.8	FTIR spectrum for tris(butylxanthato)chromium(III) complex	53
3.9	FTIR spectrum for potassium hexyl xanthate ligand	54
3.10	FTIR spectrum for tris(hexylxanthato)chromium(III) complex	55
3.11	The ultraviolet visible spectrum for a) potassium methyl xanthate and b) tris(methylxanthato)chromium(III) complex	57
3.12	The ultraviolet visible spectrum for a) potassium ethyl xanthate and b) tris(ethylxanthato)chromium(III) complex	58
3.13	The ultraviolet visible spectrum for a) potassium isopropyl xanthate and b) tris(isopropylxanthato)chromium(III) complex	59
3.14	The ultraviolet visible spectrum for a) potassium butyl xanthate and b) tris(butylxanthato)chromium(III) complex	60
3.15	The ultraviolet visible spectrum for a) potassium hexyl xanthate and b) tris(hexylxanthato)chromium(III) complex	61

3.16	UV. Visible spectra changes in the absorbance of Cr(mex) ₃ during irradiation	64
3.17	UV. Visible spectra changes in the absorbance of Cr(etx) ₃ during irradiation	64
3.18	UV. Visible spectra changes in the absorbance of Cr(prx) ₃ during irradiation	65
3.19	UV. Visible spectra changes in the absorbance of Cr(bux) ₃ during irradiation.	65
3.20	UV. Visible spectra changes in the absorbance of Cr(hex) ₃ during irradiation	66
3.21	Plot of Natural logarithm of absorbance against irradiation time for the Cr(mex) ₃	69
3.22	Plot of Natural logarithm of absorbance against irradiation time of the Cr(etx) ₃	70
3.23	Plot of Natural logarithm of absorbance against irradiation time of the Cr(prx) ₃	70
3.24	Plot of Natural logarithm of absorbance against irradiation time of the Cr(bux) ₃	71
3.25	Plot of Natural logarithm of absorbance against irradiation time of the Cr(hex) ₃	71
3.26	Variation of natural plot logarithm of absorbance with irradiation time of the xanthate complexes in DMSO	75
2.27	Variation in quantum yield(Q _a) with the number of methyl group in complexes for the photodecomposition of Cr(AX) ₃ complexes in DMSO	77

List of Schemes

<i>Scheme No.</i>	<i>Title</i>	<i>Page No.</i>
1.1	Photoinduced cyclotrimerization of acetylene in the presence of mixed ligand azido complexes (M: Ni, Pd, Pt; L: Mono-and diphosphane ligands)	14
1.2	Schematic representation of photoinduced catalyst (I) and photoassisted reaction(II)	16
3.1	Reaction mechanism for the prepared complexes	79

References

- 1- P. Atkins and J. de Paula, "Atkin`s" Physical Chemistry ", 7^{ed}, Oxford univ., New York (2002).
- 2- A. Boudebous, Ph.D. Thesis, Basel Univ., Belford (2006).
- 3- C. Jeannin, Chem. Phys. Lett. 51(2000)316.
- 4- M. O. Krause, J. of Phys. and Chem. Ref. Data 8(1979)307.
- 5- D. E. Sayers, E. A. Stern, and F. W. Lytle, Phys. Rev. Lett. 27(1971)1204.
- 6- E. A. Stern, Phys. Rev. B10 (1974)3027.
- 7- A. Vlcek, Coord. Chem. Rev. 1(1998)177.
- 8- A. Vlcek, Coord. Chem. Rev. 200(2000)933.
- 9- J. Ferguson, F. Herren, E. R. Krausz, M. Meader, and J. Vbancich, Coordination Chemistry Rev. 21(1985)64.
- 10- J. K. Mccusker, Acc. Chem. Res. 876(2003)36.
- 11- N. Serpona and M. A. Jamieson, Coord. Chem. Rev. 87(1998)93.
- 12- V. Balzani, A. Juris, M. Venturi, S. Campagna, and S. Serroni, Chem. Rev. 759(1996)96.
- 13- A. Juris, Coord. Chem. Rev. 85(1998)84.
- 14- V. Balzani, Electron Transfer in Chemistry, Wiley–Vett, Weinheim; New York 2001.
- 15- J. I Zink, J. Am. Chem. 12(1973)1018.
- 16- J. I Zink, Inorg. Chem. 12(1973)1018
- 17- J. I Zink, Mol. Photochem. 5(1973)151
- 18- L. G. Vanquikenborne, A. Ceulemans, J. Am. Chem. Soc. 99(1977)2208

- 19- M. Wrigton, H. B. Gray, G. S. Hammond, *Mol. Photochem.* 5(1973)165.
- 20- A. W. Adamson, *J. Phys. Chem.* 71(1967)798.
- 21- K. G. Al-Lamee, M.Sc. Thesis, Baghdad univ., Baghdad (1976).
- 22- C. K. Iorgensen, "Absorption spectra and bonding in complexes", Pergamon, London (1966).
- 23- T. M. Dunn, "Modern coordination chemistry", ed. J. Lewis and R.G. Wilkins, Interscience, London (1960).
- 24- G. S. Arnold, W. L. Klotz, W. Halper and M.K. Dearmond, *Chem. Phys. Lett.* 19 (1973) 546.
- 25- A. Volgler and A. Kern, *Angew. Chem.* 88 (1976) 688.
- 26- S. D. Hanna, J. I. Zink, *Inorg. Chem.* 35(1996)297.
- 27- J. Alvarellos, H. J. Metiu, *Chem. Phys.* 88(1988)4957.
- 28- R. A. Marcus, *Pure Appli. Chem.* 69(1997)13.
- 29- E. L. Wehry, *Chim. Soc., Qur. Rev.* 2 (21) (1967) 213.
- 30- C. Reber, J. I. Zink, *J. Chem. Phys.* 88(1988)5291.
- 31- A. Volgler, R. E. Wright and H. Kunkely, *Angew. Chem.* 926 (1980) 745.
- 32- A. W. Adamson and P. D. Fleischauer, "Concepts of inorganic photochemistry", John Wiley, New York (1975).
- 33- V. Balzani and V. Carassiti, "Photochemistry of coordination compounds", Academic Press, London 1970.
- 34- J. A. Allison and R. S. Becker, *Chem. Phys.* 32 (1960) 1413.
- 35- K. R. Mukherjee, "Fundamentals of photochemistry", Wiley eastern limited, New Delhi 1988.
- 36- A. W. Adamson and A. H. Soper, *J. Am. Chem. Soc.* 80 (1958) 3863.

- 37- S. Oishi and K. Nozaki. *Chem. Lett.* (1979) 549.
- 38- H. A. Abdulla, Ph.D. Thesis, Mustansiriah Univ., Baghdad (1997).
- 39- L. Moggi, F. Bolletta, V. Balzani and F. Scandola, *J. Inorg. Nucl. chem.* 28 (1966) 2589.
- 40- K. L. Sterenson, *J. Am. Chem. Soc.* 94 (1972) 6652.
- 41- Balzani, R. Ballardini, N. Sabbatini and L. Moggi, *Inorg. chem.* 7 (1968) 1398.
- 42- I. I. Cherngaev, L. S. Korabina and G. S. Nuvaveriskaya, *Russ. Inorg. Chem.* 10 (1965) 567.
- 43- H. Hennig, D. Rehoek and R. D. Archer, *Coord. Chem. Rev.* 61 (1985) 1.
- 44- M. J. Mirbach, *EPA News Lett.* 20 (1984) 16.
- 45- V. Carassiti, *EPA News Lett.* 20 (1983) 53.
- 46- W. Strochemicier, *Angew. Chem. Internat. Edn.* 3(1964)730.
- 47- H. Hennig and R. Billing, *Coord. Chem. Rev.* 125 (1993) 89.
- 48- R. A. Plane and J. P. Hunt, *J. Am. Chem. Soc.* 79(1957)3343.
- 49- H. Hennig, R. Stich, H. Konll and D. Rehorek, *Z. Inorg. Allg. Chem.* 576 (1989) 139.
- 50- H. Knoll, R. Stich, H. Hennig and D. J. Stufkens, *Inorg. Chem. Acta.* 178 (1990) 71.
- 51- H. Hennig, E. Hoyer, E. Lippman, E. Nagorsink, P. Thomas and M. Weissentels, *J. Sign. Chun.* 6(1978) 39.
- 52- T. Masuda, Y. Kuwane and T. Higashimura, *J. Polym., Chem. Ed.* 20 (1982) 1043.
- 53- T. Masuda, K. Yamamoto and T. Higashimura, *Polym. J.* 23 (1982) 1663
- 54- B. Palmer and C. Kutal, *Macromolecules* 28 (1995) 1328.

- 55- C. H. Bamford and A. N. Ferrar, *J. Chem. Soc., Faraday Trans. 1*, 68 (1972)1243.
- 56- S. M. Aliwi, C. H. Bamford and S. V. Muilik, *J. Polym. Sci., Polym. Sympo.* 50 (1975) 33.
- 57- S. M. Aliwi and C. H. Bamford. *J. Chem. Soc. Faraday Trans. 1*, 71 (1975) 1737.
- 58- S. M. Aliwi and C. H. Bamford, *Polym. J.* 18 (1977) 375.
- 59- S. M. Aliwi and S. M. Abdullah, *Polym. Interat.* 35 (1995) 309.
- 60- N. J. Saleh, Ph. D. Thesis, Mustansiriah Univ., Baghdad (1996).
- 61- H. Halmann and M. Gratzel, "Energy Resources through photochemistry and catalysis", Academic press, New York 1983.
- 62- P. G. Russel, N. Kovac, S. Srinvasan and M. Steinberg. *J. Electroanal. Chem.* 124 (1977) 1331.
- 63- J. O. Bokris, B. Dandopani, D. Cocks and J. Ghoroghchain, *Int. J. Hydrogen Energy*, 10 (1985) 79.
- 64- S. M. Aliwi, *J. Photochem. Photobiol., A*, 67 (1992) 329.
- 65- S. T. Hamdi and S. M. Aliwi, *Mon. Fur. Chemie.* 127 (1996) 339.
- 66- S. T. Hamdi and S. M. Aliwi, *Z. Phys. Chem* 174 (1991) 199.
- 67- S. M. Aliwi and E. M. Hanna, *J. Solar Energy Research* 5 (1989) 39.
- 68- S. M. Aliwi, *J. Photochem. Photobiol., A*, 67 (1992) 65.
- 69- R. P. R. Ranaweera and G. Scott, *J. Eur. Polym.* 12 (1976) 91.
- 70- A. Zweig and J. W. Henderson, *J. Polym. Sci., Polym. Chem. Ed.* 13 (1975) 717.
- 71- M. S. Wrighton, D. S. Ginley, M. A. Schroeder and D. L. Morse, *Pure Appl. Chem.* 41 (1975) 671.
- 72- R. G. Salomon, *Tetrahedron* 39 (1983) 1.

- 73- A. Cannizzo, *Angew. Chem. Internat. Edn.* 45(2006)3174.
- 74- Zikova, G. B. Shulpin and Lederer, *Collect. Czech. Chem. Commun.* 49 (1984) 2376.
- 75- E. A. Al-Sarraj, M.Sc.Thesis, Al-Nahrain Univ. Baghdad (1998).
- 76- P. Nasielski, P. Kirsch and Wilputt-Steinert, *L. J. Organometallics* 29(1971)269.
- 77- F. D. Canmassi and L. S. Fasteur, *Chem. Phys.* 50(1969)2603.
- 78- J. L. Laver and P. W. Chem. Commun. 769 (1968).
- 79- K. L. Slevenson and J. F. Verdick, *J. Amer. Chem. Soc.* 90(1968)2974.
- 80- J. M. Eder *J. Prakt. Chem.* 14(1979)294.
- 81- B. Y. Dain and E. A. Compt. Rend. Acad. Sci., Rus 28(1940)228.
- 82- G. L. Geoffroy, "Organometallic Photochemistry" Academic Press, London (1979).
- 83- M. Wrihion, H. B. Gray, and G. S. Hammond, *Mol. Photochem.* 5(1973)165.
- 84- P. Riccirri and E. Zinato, *Proceedings of the XIV inte. Conf. on Coordination Chem. Int, union of Pure and Appl. Chem., Toronto, Ganda, P. 252(1972).*
- 85- D. Valentine, *J. Adv. Photochem.* 6(1968)123.
- 86- A. W. Adamson, *J. Phys. Chem.* 69(1965)2201.
- 87- C. J. Ballhausen, "Introduction to ligand field theory", NCGeaw-Hill, New York (1962).
- 88- M. Linhard, M. Weigel, *Z. Inorg. Chem.* 49(1951)266.
- 89- J. R. Perumaddi, *Phys. Chem.* 71(1967)3155.
- 90- W. A. Baker and M. G. Phillips, *Inorg. Chem.* 5(1966)1042.

- 91- A. B. Lever, *Coord. Chem. Rev.* 31(1968)119.
- 92- J. Glerup and C. E. Schaffar in "Prograss in Coordination Chemistry", Amsterdam, P.500 (1968).
- 93- L. E. Orgel, In "report of the tenth solay Conference", Brusseeies, P.289 (1964).
- 94- C. K. Jogensen , *Eperienia, Suppl.* 9(1964)98.
- 95- W. U. Malik, R. Bembi and V. K. Bhardwaj, *J. Indian Chem.Soc.* 57(1980)35.
- 96- M. N. Ansari, M .C. Jain and W. U. Malik, *J. Indian Chem. Soc.* 57(1980)861.
- 97- I. A. Al-Kassar, M.Sc. Thesis, Mosul Univ. Mousl (1990).
- 98- C. G. Hatchard and C. A. Parker, *Proc. Roy. Soc. A*, 235 (1956) 518.
- 99- G. Ganqlitz and S. Hubiq, *Pure and Appl. Chem.* 61(1986)187.
- 100- D. nicholis, "Complex and first-row transition elements" by Dr. W. I. Azeez, pp.141(1984).
- 101- F. A. Cotton and G. W. Wilkinsom, "Advanced inorganic chemistry", pp.535 (1972).
- 102- K. S. Ayid , M.Sc. thesis , Al-Nahrain univ., Baghdad (2007).
- 103- L. G. Miessler and A. T. Donald, "Inorganic chemistry", Ed. Prentic Hall, Inc. 2nd (1999).
- 104- J. Podlaha and J. Podlahova, *Inorg. Chem. Acta.* 4(1970)521.
- 105- A. F. Kazzer , S. E. Al-Maukhtar and I. A. Mustafa , *Iraqi J. of Chem.* 14(1)1989, 34.
- 106- L. W. Poling and J. Leja, *Cand. J. Chem.* 39(1961)754.
- 107- B. B. Kual and K. B. Pandeya, *J. Inorg. Nucl. Chem.* 40(1978)1035.

- 108- M. L. Shankaranragana and C. C. Patel, *Cand. J. Chem.* 39(1961)1634.
- 109- G. W. Watta and B. J. Mecormic, *Spectrochim. Acta. Part A* 39(1965)753.
- 110- K. Nakamoto, "Infrared spectra of inorganic and Coordination Compound", Wiley Interscience, pp166-167(1970).
- 111- R. M. Silverstein, GC. Bassler, and T. C. Morrill, *Spectrometric identification of organic compounds*, 3rd, ed. New York : Wiley, pp. 241-255 (1974)

Supervisor certification

I certify that this thesis was prepared under my supervision at the Department of Chemistry, College of Science, at Al-Nahrain University as a partial requirement for the degree of M. Sc. in chemistry.

Signature
Assistant Professor
Dr. Shahbaz A. Maki

In view of the available recommendation, I forward this thesis for debate by the examining committee.

Assistant Professor
Dr. Salman A. Ali
Head
of the Department of chemistry
College of Science
Al- Nahrain University

Examining Committee`s certification

We the examining committee, certify that we read this thesis and examined the student *Ekhlas Abdul-Kuder Salman*, in its contents and that, according to our opinion, is accepted as thesis for the degree of M. Sc. In Chemistry

Signature:

Name:

Date:

(Chairman)

Signature:

Name:

Date:

(Member)

Signature

Name:

Date:

(Member)

Signature:

Name : *Dr. Shahbaz A. Maki*

Date:

(Member/Advisor)

Approved for the council of the College of Science.

Signature:

Name: Dr. Laith Abdul-aziz Al-Ani

Dean of the college of Science

Date:

اسم الطالبة: اخلاص عبد الخضر سلمان الزبيدي

الكلية / القسم : كلية العلوم / قسم الكيمياء

الجامعة : جامعة النهريين

الاختصاص : الكيمياء الفيزيائية اللاعضوية / الكيمياء الضوئية

اسم الاطروحة: دراسة ضوئية اشعاعية مع دراسة الحركيات لتفكك معقدات ثلاثي (الكيل زانثيتو)

كروم (III) في مذيب ثنائي مثيل سلفوكسايد

موعد المناقشة: الخميس ١٩/٦/٢٠٠٨

اسم المشرف : الاستاذ المساعد الدكتور شهباز احمد مكي / قسم الكيمياء / كلية العلوم / جامعة النهريين

اللجنة المناقشة:

- ١ - الاستاذ الدكتور علي سلمان الطائي/ قسم الكيمياء / كلية العلوم للبنات/ جامعة بغداد رئيسا
- ٢ - الاستاذ المساعد الدكتورة محاسن الياس/ قسم الكيمياء/ كلية العلوم للبنات / جامعة بغداد عضوا
- ٣ - المدرس الدكتور نسرين رحيم جبر / قسم الكيمياء / كلية العلوم / جامعة النهريين عضوا

الاهـداء

من شرفني بحمل اسمه
من افنى حياته لأجل تربيّتي وانشائي
المفارق عنا جسدا والباقي فينا ذكرا
روحه الطاهرة اسكنه الله فسيح جناته

الى

ابي
مصدر فخري

السراج الذي اضاء طريق نجاحي
الينبوع الذي ارتوي منه حبا وحنانا

الى

امي
حنان الدنيا كلها

الدم الذي يسري في عروقي
الذين لم يبخلوا علي بحنانهم

الى

اخوتي واخواتي
مصدر عزتي

كل نسيب لي في الروح
الذين احاطوني بحبهم و قدموا لي
الدعم المعنوي

الى

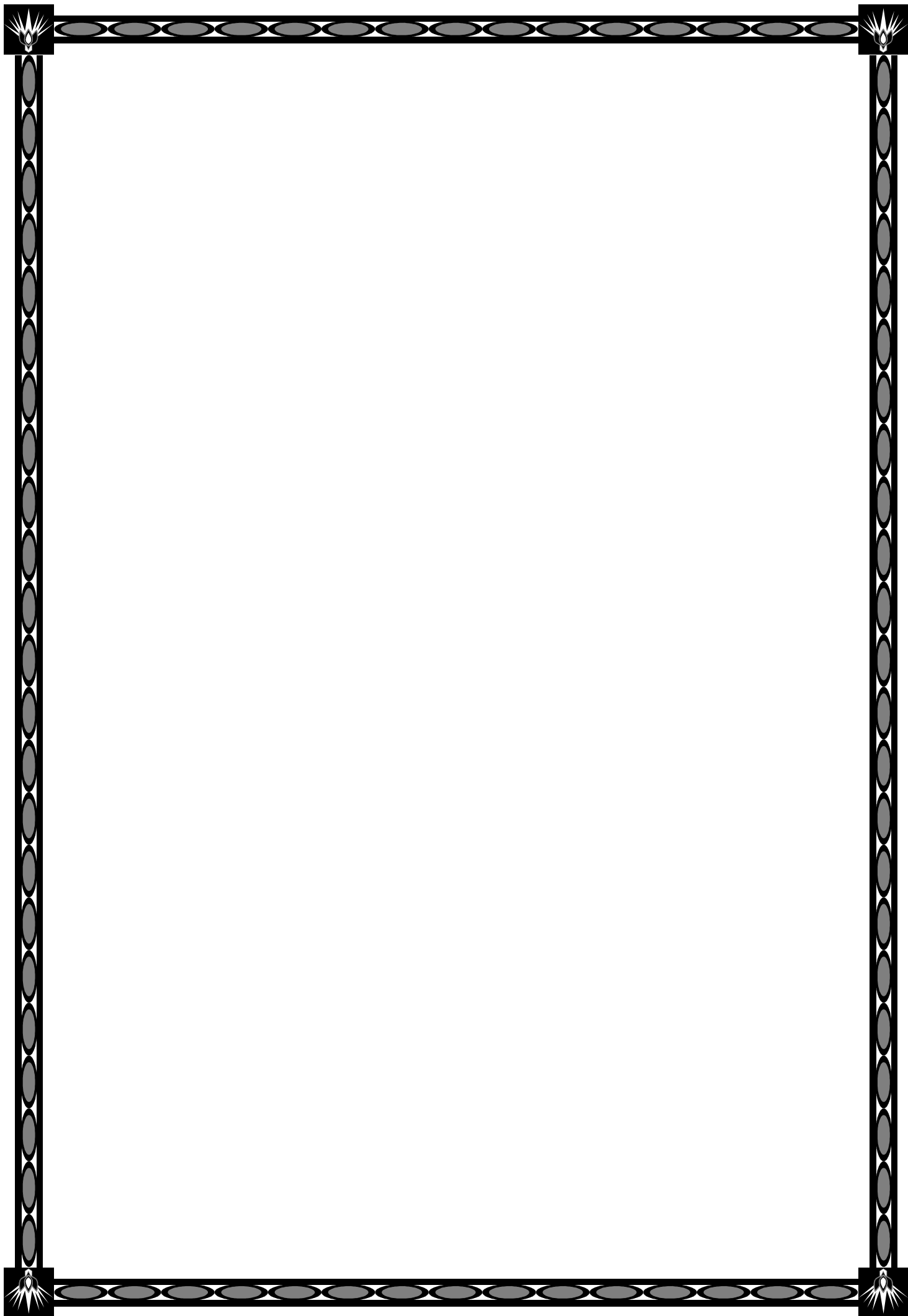
زملائي

كل من علمني حرفا
كل من اضاف الي قطرات علمي علما

الى

اساتذتي

واليكـم جميعا اهـدي ما وفقتي به ربي



الخلاصة

تم تحضير معقدات الكروم الثلاثي ثنائية السن والمشتقة من متصلات حاوية على الكبريت. وهذه المعقدات هي:

- ١- ثلاثي (مثيل زانثيتو) كروم (III) $Cr(mex)_3$
- ٢- ثلاثي (أثيل زانثيتو) كروم (III) $Cr(etx)_3$
- ٣- ثلاثي (ايزوبروبيل زانثيتو) كروم (III) $Cr(prx)_3$
- ٤- ثلاثي (بيوتيل زانثيتو) كروم (III) $Cr(bux)_3$
- ٥- ثلاثي (هكسيل زانثيتو) كروم (III) $Cr(hex)_3$

تم تشخيص هذه المعقدات من خلال مطيافية الاشعة تحت الحمراء (FTIR) والاشعة فوق البنفسجية والمرئية (UV.Vis) بالإضافة الى قياس بعض الخصائص الفيزيائية كدرجة الانصهار و الحساسية المغناطيسية.

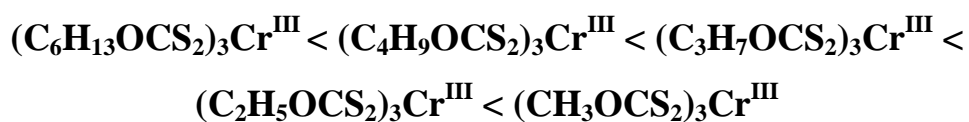
تم دراسة التفكك الضوئي لهذه المعقدات في مذيب ثنائي مثيل سلفوكسايد بعد التشعيع بواسطة ضوء احادي ذات طول موجي 1 ± 311 في درجة حرارة الغرفة . وجد ان ثابت التفكك الضوئي لهذه المعقدات تتبع ميكانيكية الدرجة الاولى لذلك فأن هذه الثوابت تعتمد على تركيز المعقد فقط.

تم قياس ثابت السرعة النوعية بأستعمال النقصان في قراءة الامتصاصية عند ذلك الطول الموجي بعد تشعيع المعقدات المحضرة. وجد ان سرعة ثابت التفكك (K_d) يعتمد بوضوح على عدد مجاميع الالكيل في تلك المعقدات . لوحظ ان سرعة تفكك المعقدات تزداد كلما قلت مجاميع الالكيل في المعقدات مثال على ذلك فأن K_d لمعقد ثلاثي (مثيل زانثيتو) كروم (III) يساوي $(8,700 \times 10^{-5} s^{-1})$ مقارنة بـ $(2,170 \times 10^{-5} s^{-1})$ لمعقد ثلاثي (هكسيل زانثيتو) كروم (III).

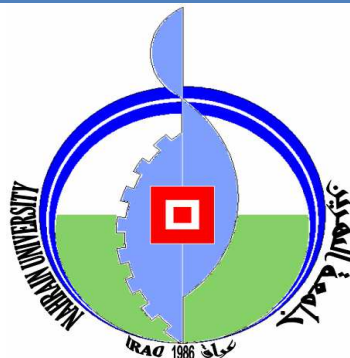
التغيير في قيمة الامتصاصية بعد تشعيع هذه المعقدات استعملت لدراسة ميكانيكية تفاعلات التفكك الضوئي . لقد اظهرت النتائج ان تشعيع هذه المعقدات هي الخطوة البطيئة الاولى .

يتبع هذه الخطوة مباشرة كسر الأصرة Cr-S (حيث يتجزأ معقد الزانثيت الثلاثي) وتفاعلات الجذور الحرة السريعة . وبناءا عليه فقد تم حساب السرعة النسبية لتفكك هذه المعقدات .

تم تعيين ناتج الكم لتفاعل التجزئة الضوئية للمعقدات الخمسة اعلاه وكانت تتراوح بين $(1.925 \times 10^{-3} - 7.762 \times 10^{-3})$. ومن خلال قيم ناتج الكم للمعقدات الخمسة اعلاه فإن هذه القيم للمعقدات المذكورة اعلاه اخذت الترتيب التالي:



Republic of Iraq
Ministry of Higher Education
and Scientific Research
AL-Nahrain University
College of Science
Department of Chemistry



*Photochemical Radiation and Kinetics
Studies of Tris (Alkylxanthato)
Chromium (III) Complexes in DMSO
Solvent*

*A Thesis
Submitted to the
College of Science Al-Nahrain University
as a Partial Fulfillment of the Requirements for the
Degree of M. Sc. in Chemistry*

*By
Ekhlās Abdul-Kudher Salman
(B. Sc. 1996)*

19-June-2008



جمهورية العراق
وزارة التعليم العالي و البحث العلمي
جامعة النهرين/كلية العلوم
قسم الكيمياء

**دراسة ضوئية اشعاعية مع دراسة الحركيات
لتفكك معقدات
ثلاثي (الكيل زانثيتو) كروم (III) في مذيب
ثنائي مثيل سلفوكسايد**

رسالة مقدمة الى
كلية العلوم – جامعة النهرين
وهي جزء من متطلبات نيل درجة الماجستير في الكيمياء

من قبل
إخلاص عبد الخضر سلمان
بكالوريوس علوم كيمياء (١٩٩٦)

حزيران ٢٠٠٨

بِسْمِ اللَّهِ الرَّحْمَنِ الرَّحِيمِ

فَفَقَّمْنَا مَا سُئِلْنَا مِنْهُ وَإِنَّا لَكُنَّا لَهُ سَمْعًا وَأَنبَاءً

مَقْرُونًا كَذَلِكَ يُبَيِّنُ اللَّهُ لَكَ آيَاتِهِ لِقَوْمٍ يُعْقِلُونَ

صَدَقَ اللَّهُ الْعَظِيمِ

الأنبياء (٧٩)

Chapter one

Introduction

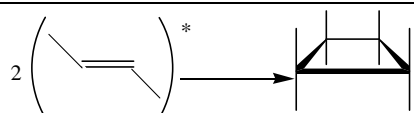
1.1 Photochemistry

Many reactions can be initiated by the absorption of electromagnetic radiation via different mechanisms. The most important of all are the photochemical processes that capture the radiant energy of these reactions lead to the heating of the atmosphere during the daytime. Other includes the absorption of visible radiation during photosynthesis processes in plants. Table (1.1) summarizes some types of common photochemical reactions⁽¹⁾.

Photochemistry is a natural phenomenon, which began at the origin of the universe world. Modern science describes the interaction between light and matter in several main sciences such as chemistry, physics and biology⁽²⁾. Photochemistry plays a fundamental role in life (photosynthesis, vision, photoaxis, etc....). The last 30 years of photochemistry have shown the fundamental role played in experimental and theoretical investigations⁽³⁾. It's used for the determination of molecular mechanisms, photocatalysis and electronic information of complex devices⁽²⁾. The photochemical and photophysical processes of thousands of organic and organometallic, coordination compounds complexes have been studied⁽⁴⁾. The major parts of photochemical investigations were focused on molecular species with simple process (i.e. molecular photochemistry)⁽²⁾.

Photochemical processes are initiated by the absorption of radiation by at least one component of a reaction mixture. In a **primary process**, products are formed directly from the excited state of the reactants. Products of a **secondary process** originated from intermediates that are formed directly from the excited of the reactants ⁽¹⁾.

Table (1.1): Photochemical processes⁽¹⁾

Process	General Form	Example
Ionization	$A^* \longrightarrow A^+ + e^-$	$NO^* \longrightarrow NO^+ + e^-$
Electron transfer	$A^* + B \longrightarrow A^+ + B^-$	$[Ru(bpy)_3]^{2+*} + Fe^{3+} \longrightarrow [Ru(bpy)_3]^{3+} + Fe^{2+}$
Dissociation	$A^* \longrightarrow B + C$ $A^* + B - C \longrightarrow A + B + C$	$O_3^* \longrightarrow O_2 + O$ $Hg^* + CH_4 \longrightarrow Hg + CH_3 + H$
Addition	$2A^* \longrightarrow B$	
Abstraction	$A^* + B - C \longrightarrow A - B + C$	$Hg^* + H_2 \longrightarrow HgH + H$

The excited state is denoted by an asterisk(*). In each example, the photochemical process is initiated by radiation.

1.2 Photochemistry of transition metal complexes

The photophysics and photochemistry of transition metal complexes has become an important branch of inorganic chemistry as well as photochemistry ⁽⁵⁾. On the contrary, a very little is known about the photophysics and photochemistry of coordination compounds of the main group metals ⁽⁶⁾. These compounds are kinetically labile and can exist with variable coordination numbers and structure in the solid state and in solution. In addition, the structures of many complexes deviate from highly symmetrical geometries. These properties complicate the spectroscopic identification and characterization of main group metal complexes. On the other hand, there are also features which facilitate the

investigation of these compounds. Since the valence shell includes only (s) and (p) orbitals, the (d) orbitals have not to be considered for low-energy electronic transitions. Compared to transition metals, the variation of stable oxidation states of main group metals is much smaller.

Chemical reactivity depends mainly on the excited state properties of a given molecular system and is relevant to all photochemical processes regardless of the origin and nature of the photoactive species⁽⁷⁻⁹⁾. Most of the photochemical reactions in transition metal complexes can be triggered with visible light, since their excitation energies are usually lower than that of most organic molecules. The visible excitation usually accesses the available low energy charge transfer states of mixed metal and ligand character, the so called metal-to-ligand charge (MLCT) states⁽¹⁰⁾. These states provide a rather unique gateway, through which the optical excitation energy can be very efficiently transferred into molecular excitation energy triggering a variety of possible relaxation involving electronic, magnetic and structural dynamics.

The photoinduced dynamics of transition metal complexes involved many different types of excited states, which may differ in their localization within the molecule, orbital parentage, energy, dynamics and thus chemical reactivity⁽¹¹⁾. In addition, the density of available excited states is much higher than in case of organic molecules, which means that several different excited states may be populated within the same narrow energy range. This, in turn, leads to an enhanced interaction between them, which makes the photochemical cycle rather complex with competing relaxation and reactivity pathways⁽¹²⁾. Many transition metal complexes are redox-active, already in their electronic ground state configuration⁽¹³⁾. Their corresponding electron transfer (ET) reaction can involve either an increase of the oxidation state of metal (MLCT reactions) or that of the Ligand-to-Metal Charge Transfer (LMCT)

reactions. This redox activity is often preserved in the excited states as well ⁽¹⁴⁾. Therefore, many of these complexes undergo photoinitiated ET (either intramolecular or intermolecular) ⁽¹⁵⁾, which may occur within the metal orbitals, ligand orbitals or within both simultaneously.

1.3 Ligand-field excited-state photochemistry ⁽¹⁶⁻²⁰⁾

Excited electronic states of transition metal complexes have bonding properties that are different from those of the ground state. These properties can be predicted in straight forward manner from ligand-field theory. This idea can be applied to metal complexes with any coordination number, but the most advanced theoretical development involved the ligand field or d-d excited states of six-coordinate complexes of metals with d^3 - d^6 – electron configurations. The development of the theory was spurred by the publication of Adamson's rules. The first rule states that the axis having the weakest average crystal field will be the one labialized. The second rule states that if the labialized axis contains two different ligands, then the ligand of grater field strength preferentially equates. The theoretical basis for these rules consists of two steps. Step one predicts which axis will be photolabilized. Step two predicts which ligand on the labialized axis will be preferentially labialized if the two ligands are different.

1.4 Quantum yields

The photochemical reactions are based on that each light quantum absorbed by molecules activated them.

Excited molecules are unstable and thus all of them may undergo chemical reaction and / or physical deactivation processes. Each process starting with absorption of a photon and ending with disappearance of the molecule or its deactivation to a non-reactive state is called primary process. The efficiency of photochemical and / or photophysical primary process (i.e. the primary quantum yield (Q) is defined as ⁽²¹⁾:

$$Q_d = \frac{\text{Number of molecule undergoing that process}}{\text{Number of photon absorbed by that reactant}} \text{ at same time}$$

The determination of the quantum yields obviously required the measurements of two quantities, namely, the change in the concentration of the reactant (or products) and the number of photons absorbed by the reactant at the same time.

1.5 Electronic Spectra and Excited States ^(22,23)

Generally, electronic absorption spectra of transition metal complexes are frequently complicated and spectral assignments are difficult to establish. Coordination compounds are characterized by absorption spectra rich in bands in the ultraviolet and visible region of the light spectrum.

Irradiation in this region will sometimes cause photoreactions which are more fascinating in inorganic photoreactions because of the possibility of generating a more divers number of electronic excited states of high density distribution.

There are three basic types of electronic transformations of excited states of metal complexes.

i- Ligand Field (LF(d-d))Transition:

These transitions arise from electronic transitions between the metal d orbitals perturbed by the ligand field. They are localized on the central metal atom and their properties depend on the number of d electrons, type of atomic term, local symmetry around the metal atom and the nature of the ligand field. The molar absorptivity coefficients ⁽²⁴⁾ (ϵ) for such transitions are in the range between 1-100 mol⁻¹.l.cm⁻¹, and they generally occur in the visible or near infrared regions and are responsible for color of many inorganic complexes.

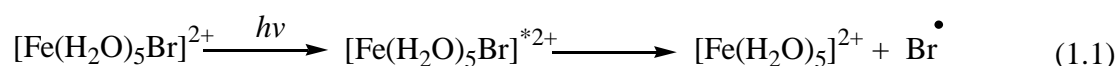
ii- Intraligand Transitions (IL):

These transitions arise from electronic transitions between molecular orbitals localized mainly on the ligand. These orbitals are not significantly perturbed by complex formation. IL transitions in the absorption spectra of the complexes are observed (e.g., $\pi \rightarrow \pi^*$, $n \rightarrow \pi^*$ and $\sigma \rightarrow \sigma^*$) which are equivalent to the transitions in the free ligand. In spite of the fact that many coordination compounds exhibit internal ligand bands, there are only a few cases where such bands have been recognized ⁽²⁵⁾. This is partly due to experimental difficulties, since the internal ligand bands lie in the uv spectral region and thus, they are often obscured by the very intense charge transfer bands. The few known examples of photoreactions caused by IL excitation are the trans-cis isomerization of trans-4-stilbene carboxylic acid⁽²⁶⁾. Coordination of either iridium (III) or ruthenium (III) ⁽²⁷⁾, and the isomerization that accomplished by IL excitation of tailbone ligand ⁽²⁵⁾. A furthermore illustration of IL photochemistry is the photochemical behavior of cis-dichloro-bis-(1-naphthylamine)-platinum(II) upon irradiation in the 250 nm region⁽²⁸⁾.

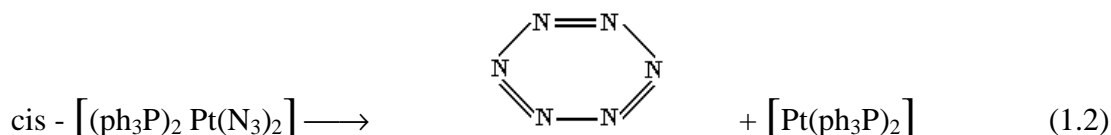
This photoreaction leads to the formation of the free 1-naphthylamine ligand with relatively high quantum yield. Irradiation of the naphthylamine ligand is known to produce an excited state with decreased base strength compared with the ground state, thus the reaction appears to be the result of an IL isomer.

iii- Charge Transfer Transitions (CT)

These transitions arise from electron transitions between a metal center orbital and ligand localized orbitals⁽²⁹⁾. Irradiation of a coordination compound with light of appropriate wavelength may induce transfer of an electron from ligand to metal (LMCT), as shown in the following photochemical reaction:



LMCT processes occur quite frequently because most strong complexing ligands are Lewis bases. Occasionally, metal to ligand electron-transfer (MLCT) absorption transition occur especially in metal carbonyls and nitrosyls compounds. Charge transfer absorption bands always occur at higher energies than d-d transitions, and are frequently found in the blue or ultraviolet regions⁽³⁰⁾. Generally, charge-transfer absorption followed by chemical steps results in oxidation of one or more ligand molecules with simultaneous reaction of the metal ion. Among the considerable number of surprising CT-generated photoredox reaction of coordination compound, and one of the most spectacular, is that described by Vogler and co-workers⁽³¹⁾, in which a two-electron reduction of cis-diazo-bis (triphenyl phosphine) platinum (II) leads to the formation of an intermediate tentatively assigned to hexazine as described in (equation 1.2).



The highly reactive LF, IL, CT-isomeric forms of appropriate ground state compounds can be achieved at very low temperature and can lead to the formation of formal oxidation numbers, even when these are not expected from classical thermal chemistry. Figure (1.1) illustrates the electronic state of coordination compounds in relation to their photochemical behavior⁽³²⁾.

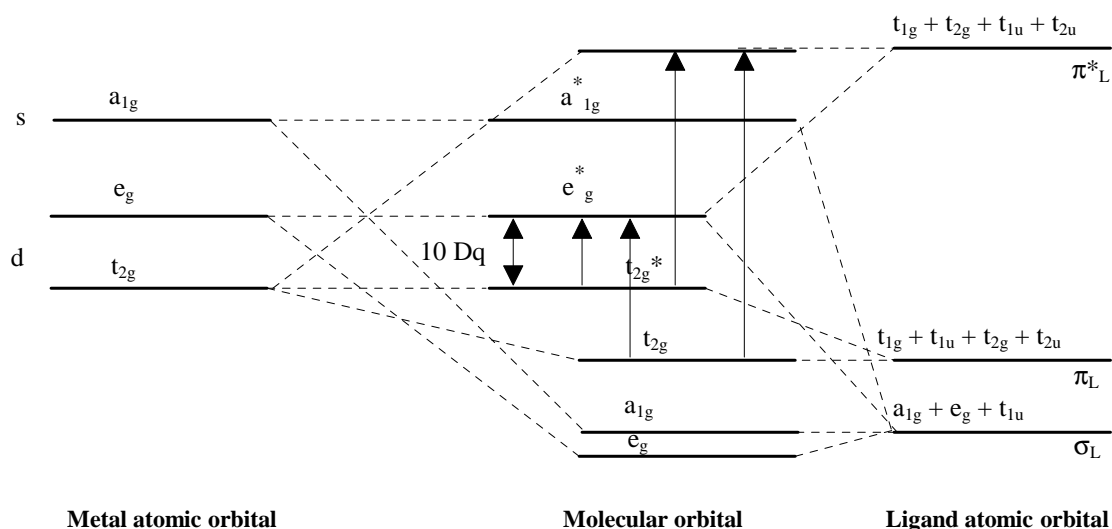


Figure (1.1): *Orbital energy diagram of electronic transition in octahedral complexes*⁽³²⁾.

1.6 Photophysical and Photochemical Processes

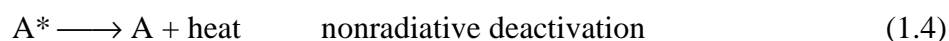
Absorption of a photon by a species, A, leads to the formation of a short - lived electronically excited molecule, A*.



The electronic energy can be dissipated physically or chemically⁽³²⁾.

1.6.1. Photophysical Processes:

These may be subdivided into radiative and non-radiative process:



(i) **Non-radiative processes:** Two main processes are involved, these are⁽³³⁾:

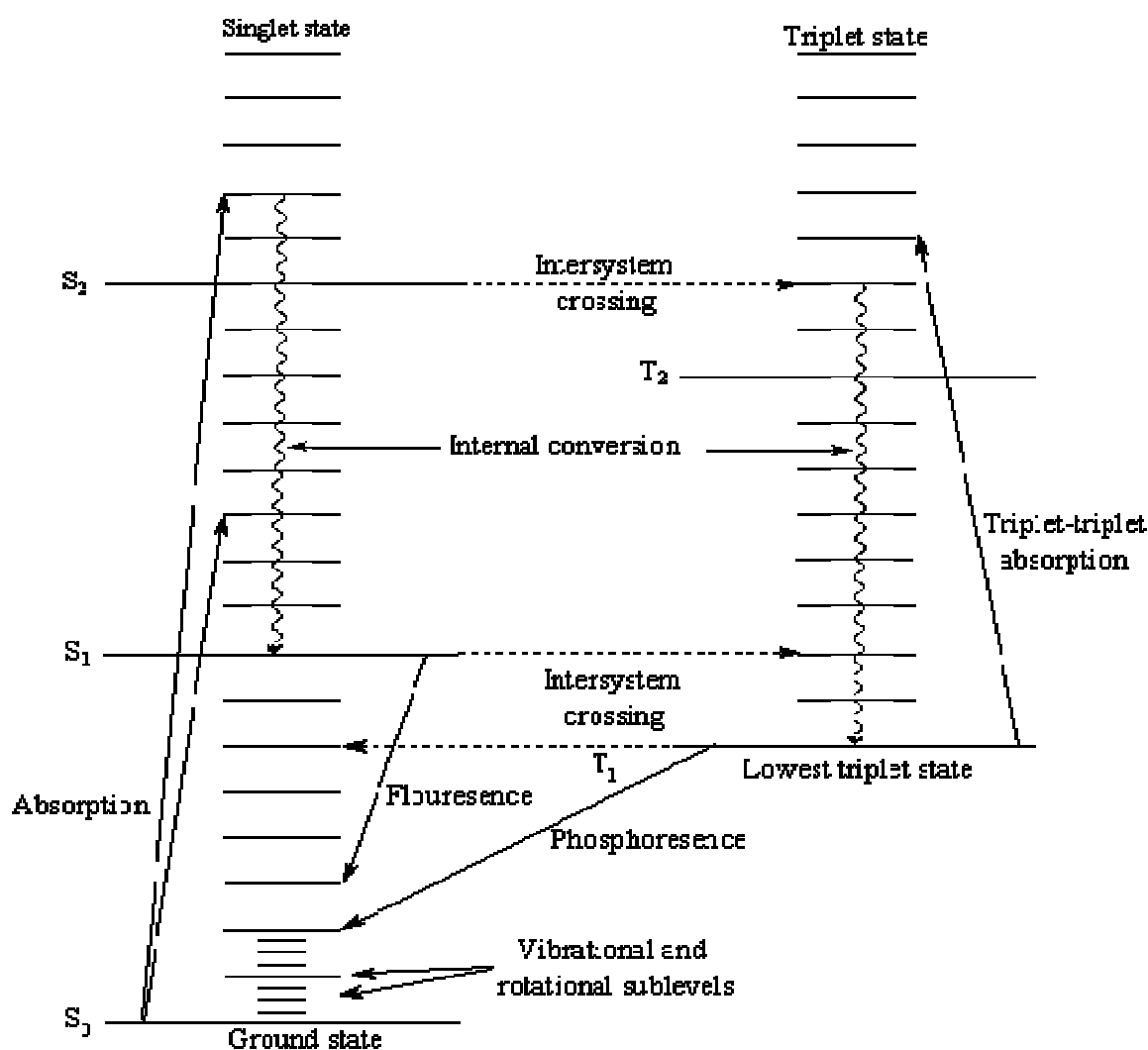
1- Internal Conversion (IC): An electronically excited complex may return directly to its ground state without emission of photon, converting the excitation energy into heat. Interconversion from the first excited to the ground state is believed to be significant process in coordination compounds⁽³⁴⁾ solutions (life time are ranged from 10^{-12} to 10^{-13} sec.).

2- Intersystem Crossing (ISC): Radiationless transition between electronic states of different multiplicity is forbidden, but it is a form of radiationless transitions which can lead to populate spin - forbidden states. This is a very important phenomenon in transition - metal complexes because it is well established that the rate constant for intersystem crossing is greatly enhanced in paramagnetic species⁽²⁹⁾. In many cases, their lifetime is sufficiently long to enable excited molecules to engage in chemical reaction⁽²⁸⁾.

(ii) **Radiative processes:** An electronically excited metal complex can return to the ground state by emission of a photon. If the multiplicities of ground and excited states are equal, the emission is called "fluorescence", if different it is called "phosphorescence". Fluorescence is relatively uncommon in transition metal complexes⁽³³⁾. If the ion is paramagnetic, intersystem crossing will lead to significant population of one or more

spin-forbidden excited states which can subsequently decay to the ground state via phosphorescence.

Figure (1.2) shows the most important processes which occur in the excited state of metal complexes⁽³⁵⁾.



Where: S_0 is singlet ground state
 S_1 and S_2 are the singlet first and second excited states
 T_1, T_2 are the first and second triplet state

Figure(1.2): Deactivation process for an excited molecule(Jablonski diagram)⁽³⁵⁾.

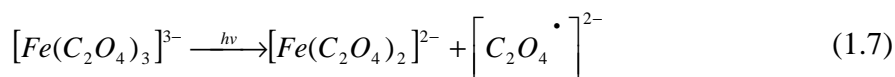
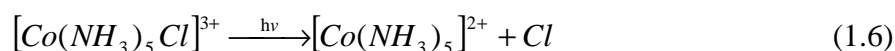
1.6.2. Photochemical Processes:

The photon excitation of coordination compounds may cause a number of different reactions whose nature depends on the type of the metal atom and the ligands involved, the wavelength of irradiation and other experimental conditions.

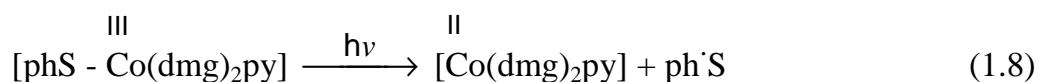
The photochemical reactions may be classified into four main types:

(i) Photochemical oxidation-reduction reaction:

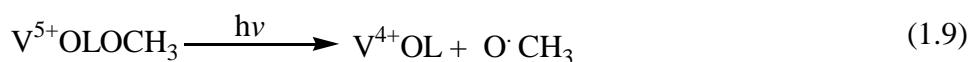
In a large number of photochemical processes, the overall results are the reduction of the metal and oxidation of one or more ligands. Examples are reactions in equations⁽³⁶⁾ (1.6) and (1.7)



In reactions shown in equations (1.6) and (1.7) the primary photochemical process is thought to be the scission of metal-chloride and metal oxalate bonds in (Co-Cl) and (Fe-C₂O₄) respectively. Benzene thiolatobis-(dimethylglyoximate) pyridine cobalt (III), [Co(dmg)₂Sph(py)], photochemically forms the appropriate cobalt (II) complex [Co(dmg)₂py] with concomitant formation of benzene thiolate radicals (ph·S) by homolytic scission of cobalt-sulfur bond⁽³⁷⁾ as shown in equation (1.8).



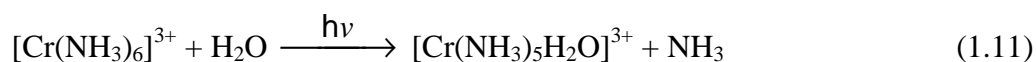
The generation of methoxy free radical (CH_3) from the photochemical decomposition in different solvents of vanadium (v) species has been studied⁽³⁸⁾. Irradiation of $[\text{VO}^{5+}\text{LOCH}_3]$ with $\lambda = 265\text{nm}$ has led to the redox reaction according to chemical reaction described in equation (1.9) below.



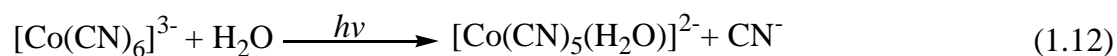
(Where L is a tetradentate Schiff base ligand).

(ii) Photosubstitution reaction:

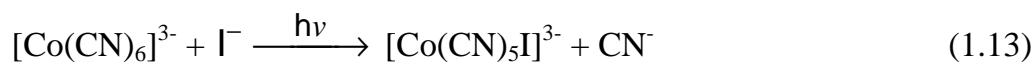
Excitation of coordination compounds may lead to ligand exchange reaction such as that shown in equations (1.10) and (1.11):



Photochemical ligand -exchange reaction are particularly common in metal carbonyls and their derivatives. Moggi and co-workers⁽³⁹⁾ have reported the photosolvation of cobalt (III) complex via irradiated with UV-light.



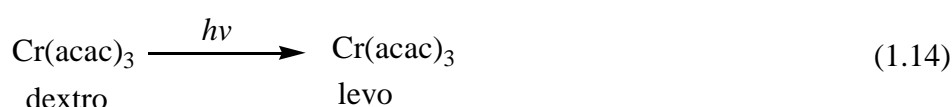
Some photosubstitution reactions could occur in aqueous solution involving anionic ligands, as shown in equation (1.13).



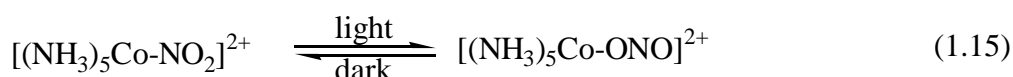
The reaction seems to involve primary photodissociation process, yielding $[\text{Co}(\text{CN})_5]^{2-}$ which is then scavenged by the coordinating iodide anion⁽³³⁾.

(iii) Photochemical isomerization and racemisation reactions:

A number of optically active coordination complexes exhibit a tendency to racemise photochemically. The chromium (III) acetylacetonate, $\text{Cr}(\text{acac})_3$, is one of this type of complexes. Irradiation of dextro $\text{Cr}(\text{acac})_3$ with visible light of $\lambda = 546 \text{ nm}$ has been reported the conversion (with high quantum efficiency) to the levo form⁽⁴⁰⁾ as shown in equation(1.14).



Balazani and co-workers⁽⁴¹⁾ have shown that linkage photoisomerization could occur in the $\text{Co}(\text{II})$ complexes containing the NO_2 group as shown in equation(1.15):



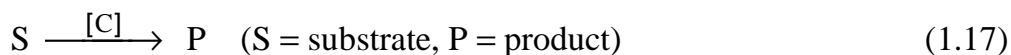
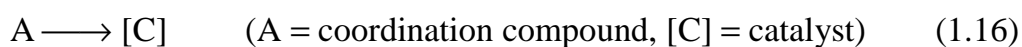
The reaction was found to be reversible; it goes back to the original compound in dark place. The photoisomerization has been also found to occur in octahedral $\text{Pt}(\text{IV})$ and square planar $\text{Pt}(\text{IV})$ complexes⁽⁴²⁾.

(iv) Photocatalytic reactions:

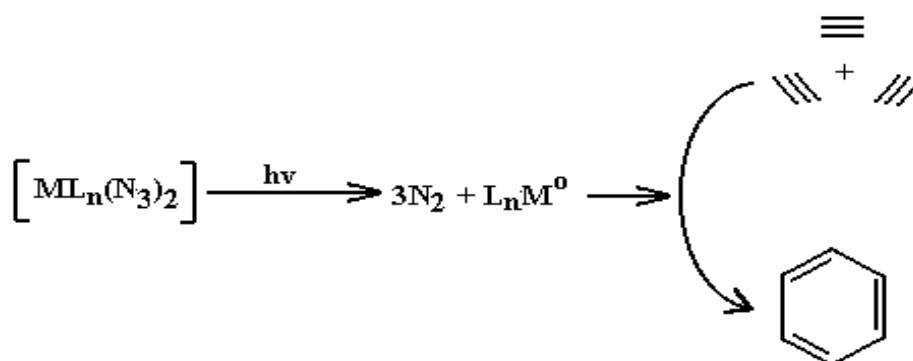
Photocatalysis reaction, and a number of reactions described in the literature as: photoinitiated, light initiated, light accelerated, photoenhanced, photosensitized ... etc, one often deal with the same aspects⁽⁴³⁾ considering the comments made by Mirbach⁽⁴⁴⁾ and Carassiti⁽⁴⁵⁾. It is suggested that the above terms have been used to distinguish between the different light-induced reactions which lead to the catalyzed conversion of diverse substrates.

1.7 The photoinduced catalytic reaction

The term implies the photochemical generation of a catalyst from a thermally stable and catalytically inactive compound. The catalyst can be a coordinative unsaturated complex species, a free ligand or a complex with a changed formal oxidation number. The reaction in equation (1.16) is a photochemical reaction and it is unlikely that reaction shown in equation (1.17) is an exclusively thermal process. The catalyst is not consumed in both reactions. ⁽⁴⁶⁾



Although light is required to generate the catalyst, other products are also formed after the light source is shut off ⁽⁴⁷⁾. The irradiation of mixed ligand azido complexes of nickel (II), palladium (II) and platinum (II) into the region of their charge transfer bands are examples of these kind of reactions ⁽⁴⁸⁾. This irradiation leads to the very efficient formation of coordinatively unsaturated electron-rich metallo-fragments ^(49, 50) which are catalytically active with respect to oligomerization or cyclization of acetylene and alkyne derivatives, as shown in scheme (1.1).



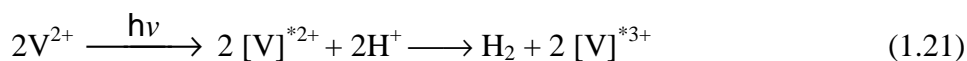
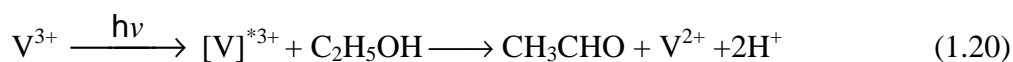
Scheme (1.1): Photoinduced Cyclotrimerization of acetylene in the presence of mixed ligand azido complexes (M: Ni, Pd, Pt; L; Mono- and diphosphane ligands) ⁽⁵⁰⁾.

The coordination compound is not consumed in this process. The catalyst can react with the substrate either by thermal or by further photochemical activation as shown in equations (1.18) and (1.19).

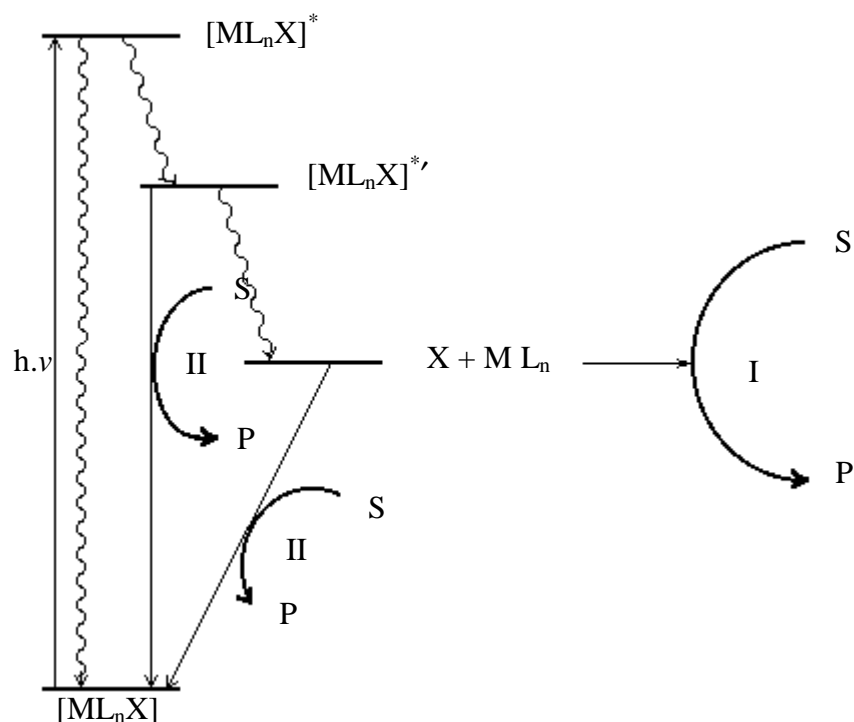


Unlike photoinduced catalyst reactions, photoassisted reactions do not proceed without continuous irradiation.

The oxidation of ethanol to acetyldehyde with simultaneous reduction of H^+ to hydrogen through photoassisted reaction by vanadium (III) complexes has been reported. The reactions are shown in equations (1.20) and (1.21)⁽⁵¹⁾ below.



Scheme (1.2) provides an illustration to differentiate photoinduced catalyst and photoassisted reactions⁽⁴⁷⁾.



where M is metal, L is Ligand, X is halogen

The wavy lines represent non-radiative relaxation

Solid lines represent radiative relaxation

Scheme (1.2): Schematic representation of photoinduced catalyst (I) and photoassisted reaction (II) ⁽⁴⁷⁾.

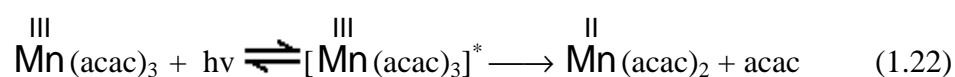
1.8 Photochemical application of transition metal chelate complexes

The photochemical activity of some chelate complex has found many interesting applications. These are:

(i) Photoinitiator of free radical polymerization and photocrosslinking agents:

A wide variety of coordination compounds has been investigated in terms of their photoinitiated polymerization reaction ⁽⁵²⁻⁵⁴⁾.

Photoinitiation by chelate complex probably constituted from the original work of Bamford and Ferrer⁽⁵⁵⁾. The authors have shown that $[\text{Mn}^{\text{III}}(\text{acac})_3]$ photosensitize by the free radical polymerization of methyl methacrylate (MMA) and styrene. It was found that $(\text{acac})\cdot$ radical derived from the ligand in chelate complex are responsible for the initiation process, according to the following equation (1.22):



Vanadium inelates, such as chloro-bis-(2,3-pentane-dionato) vanadium (V)⁽⁵⁶⁾ and alkoxo - oxobis (8-quinolinolato) vanadium (V)⁽⁵⁷⁾ can initiate a free radical polymerization in the presence of light. Vanadium chelate-containing polymers can also be used to polymerize grafts and used as a cross linking⁽⁵⁸⁾ compounds. A new type of polyolefin (V) chelate complexes, such as oxo-tris-(diakylthiocarbamate) vanadium (V), $\text{VOCS}_2\text{CN}(\text{CH}_3)_2)_3$ was reported⁽⁵⁹⁾ as photoinitiator for the polymerization of styrene (at $\lambda = 365 \text{ nm}$). Spectroscopic analysis has shown that initiation occurred predominately through the scission of the $(-\text{SC}(\text{S})\text{N}(\text{CH}_3)_2)$ ligand with reduction of vanadium (V), and $\text{VO}(\text{S}_2\text{CN}(\text{CH}_3)_2)$ was the final photolytic product. Recently, a chloro - oxobis - [(N, 4 - bromophenyl) salicydereiminato] vanadium (V), VOL_2Cl and its methoxy derivative VOL_2OCH_3 , were used as photo and thermal initiators. Vinyl polymerization, derived from Schiff base vanadium (V) chelate complexes which were capable of initiating free radical polymerization of styrene and methyl methacrylate monomers at 25°C and the incident light of wavelength 365 nm ⁽⁶⁰⁾.

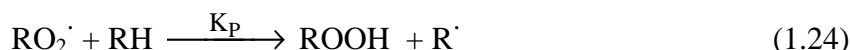
(ii) Photosensitizers:

Chemical conversion and storage of solar energy has drawn a lot of attention for converting solar energy to fuel⁽⁶¹⁾. Photochemical reduction of CO₂ and water cleavage to hydrogen and oxygen were the most promising approaches of photochemical conversion and storage of solar energy⁽⁶¹⁾. Because neither CO₂ nor H₂O molecules absorb light in the visible solar spectrum⁽⁶²⁾, photosensitizer was needed to approach these processes. Ruthenium tris (bipyridyl) chelate complex [Ru(bipy)₃]²⁺ has been extensively used as sensitizer for photochemical water cleavage to give H₂ and O₂ on exposure to visible light⁽⁶³⁾. Another study was made to photoreduce CO₂ in aqueous solution, to formic acid and formaldehyde, by hydroxo-oxobis(8-quinolyloxo) vanadium (V), (VOQ₂OH), as photosensitizer complex⁽⁶⁴⁾.

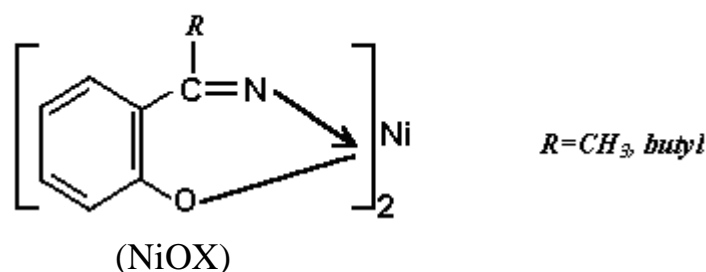
Metal chelates, such as V^{III} (acac)₃, Fe^{III} (acac)₃, and Co^{III} (acac)₃, were also used as sensitizer in a photogalvanic system to convert light energy to electrical energy⁽⁶⁵⁻⁶⁷⁾.

(iii) Photostabilizer for polyolefins:

The photo-oxidation of polyolefin generated hydroperoxide, alcohol and various types of carbonyl groups in the polymer, as they were exposed to sunlight. A carbon centered radical (R·) in the amorphous regions of the polyolefin rapidly combined with oxygen which permeated the amorphous regions to give a peroxy radical (RO₂·), this reacts quite slowly by hydrogen abstraction from C-H site on the backbone to generate a pendant hydroperoxide group (ROOH) and fresh carbon center which restarts the cycle as shown in reactions (1.23) and (1.24)⁽⁶⁸⁾.



The net effect of chain reaction was the consumption of O_2 and polymer and building up of hydroperoxide. Many Schiff bases oximes and Substituted salicylate chelates of transition metals have been studied as inhibitors of the photochemical oxidation process in polyolefins. Nickel (II) metal chelate complexes of the type:

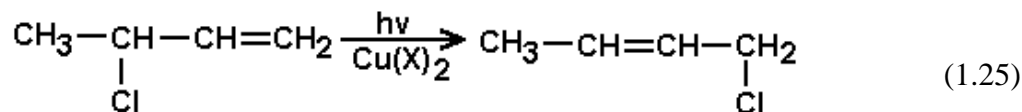


have proven to be effective quenchers of excited states and the hydrogen peroxide decomposers which were the main precursor of the photodegradation process. In photo-oxidation, chelates of the type (NiOX) have been shown to reduce the rate of radical initiation by absorbing UV light and functioning as an antioxidant⁽⁶⁹⁾. Co(II) salicylaldehyde oxime chelates were also considered as an effective singlet oxygen quenchers⁽⁷⁰⁾, and therefore they showed good stabilizing properties against photodegradation of polyolefin.

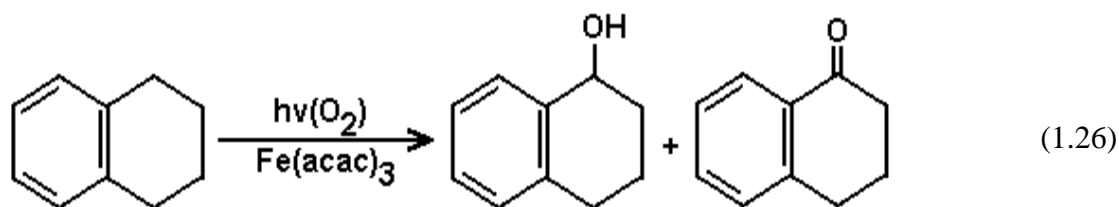
(iv) Photocatalysts for organic synthesis:

Photochemical reaction of organic compounds catalyst by transition metal complexes received a great deal of attention in the last 20 years,^(71,72). Metal chelates complexes have been shown to have some catalytic effects on photochemical isomerization rearrangement and hydrogenation of olefins and polyolefines⁽⁷³⁾. UV-irradiation of 3-chloro-1-butene, in presence of $Cu(OAc)_2$ or $Cu(acac)_2$, induced the

photoisomerization of the substrate to give 1-chloro-2-butene as shown in equation (1.25):



The photochemical oxidation of tetraline (1,2,3,4-tetrahydronaphthalene) was catalyzed by $\text{Fe}(\text{acac})_3^{(73)}$ as shown in equation(1.26):

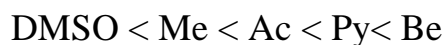


The results showed that the addition of $\text{Fe}(\text{acac})_3$ enhanced the rate of the photoinitiated reaction and this effect was more pronounced with increasing temperature. The effect of $\text{Co}(\text{III})$, $\text{Co}(\text{II})$, $\text{Fe}(\text{II})$ and $\text{Mn}(\text{II})$ chelate complexes on the photochemical oxidation of aromatic hydrocarbons has also been investigated⁽⁷⁴⁾.

The photochemistry of chelate complex tris(ethylxanthato) cobalt(III), $\text{Co}(\text{etx})_3$ and tris(diethyldithiocarbamate) Cobalt (III), $\text{Co}(\text{dtc})_3$ was studied in several organic solvents. Monochromatic light of wavelength 365nm was used for the irradiation process at 25⁰C. UV-visible spectral changes and other observations have indicated an intra oxidation – reduction reaction occur during the photolysis of $\text{Co}(\text{etx})_3$ and $\text{Co}(\text{dtc})_3$ complexes , with hemolytic scission of Co-S bond .

The quantum yields (Q_d), rate of photodecomposition and reactivity ratio (K_2/K_{-1}), were determined in each solvent. These values

were found always to increase as the polarity of the solvent increases and follow the order ⁽⁷⁵⁾:



1.9 Chromium complexes

The photochemistry of chromium coordination complexes in solution has been well investigated ⁽⁷⁶⁾.

The luminescence of Cr(III) complexes have been studied^(77,78) and a preliminary investigation of the partial photoresolution of some exalato-complexes of Cr(III) at room temperature has been published ⁽⁷⁹⁾. The first investigation of the photochemical behavior of chromium (VI) species was reported by Eder⁽⁸⁰⁾.

The effect of light on aqueous solution of Cr(II) was first reported by Dain and co-workers⁽⁸¹⁾. They found that the absorption of ultraviolet light (200-350nm) by aqueous solution of CrSO₄ caused the evolution of hydrogen gas and the formation of equivalent amount of chromic ion. In chromium carbonyls and complexes which contain π -bonding organic ligands, the chromium atoms are in low positive, zero, or low negative oxidation states, and the photochemistry (as well as the general chemistry) of these compounds were quite different from that of the "normal" Werner complexes.

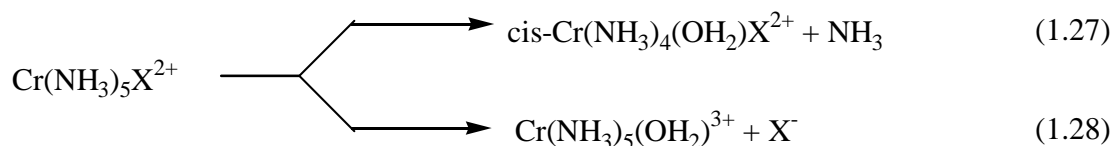
1.9.1 Photochemistry of Some chromium (III) Complexes

The classification of the excited states in organometallic compounds as ligand field, charge transfer, ligand-centered, and metal-metal was based on the assumption that molecular orbitals in these complexes have very large contribution from either metal or ligand orbitals ⁽⁸²⁾. Although such classification can be applied to Werner-type

complexes of the first and second row transition metals, organometallics were highly covalent compounds and the "metal-centered" d orbitals have considerable ligand character. The mixing ligand character in the d orbitals has an important effect on the transition probabilities: ligand field transitions have extinction coefficient in the range of thousands.

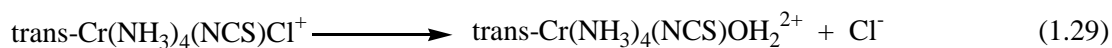
In other aspects, the pseudo ligand field states of organometallic compounds behave in manner that born strong resemblance to those of more simple coordination complexes⁽⁸³⁾.

In photoreactive transition- metal coordination complexes, the population of metal –centered excited states induced the reorganization of coordination sphere that were photosolvation, photoracemization, and photoanation reaction. The dark reaction of the d³ and d⁶ metal ions, such as Cr(III), Co(III), and Rh(III), were slower than the corresponding photochemical processes facilitating the photochemical studies and interesting experimental information has been obtained with their acido-ammine (or amine) complexes. The photochemical equation processes of Cr(III) were different from the thermal equation reaction with regard to the type of ligand labialized and the reaction stereochemistry . [Cr(NH₃)₅X]⁺² ions exhibited two photoprocesses : the photoequation of ammonia as in equation(1.27) and the photoequation of the acido ligand as in equation(1.28)

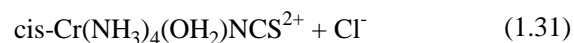
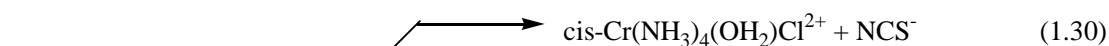


Although the equation of ammonia (equation 1.27) , has the largest yield of the two photoprocesses , equation(1.28) of X⁻ was the only thermal reaction observed with these compounds. The difference between

thermal and photochemical reaction can also be illustrated with acido-tetraammine complexes, such as $\text{trans-[Cr(NH}_3)_4(\text{NCS})\text{Cl}]^{(84)}$, the thermal equation(1.29) is for the hydrolysis of chloride with retention of the configuration:



The photoequation of Cl^- and SCN^- took place as shown in equations (1.30) and (1.31), however, with similar yields and configuration inversion⁽⁸⁰⁾



Photolabilization reactions of d^6 metal ion complexes, such as Co(III) , Ph(III) , Ir(III) and Ru(III) , have been studied to a large extent and as a result, there were more information available about these d^6 complexes than for any except for the d^3 transition metal complexes⁽⁸⁵⁾. A number of systematic features in the ligand field photochemistry of Cr(III) complexes led to the formulation of empirical rules known as Adamson's rules⁽⁸⁶⁾. The two rules are:

1) Consider the six ligands to lie in pairs at the ends of three mutually perpendicular axes. The axis with the weakest average ligand field will be the one labialized, and the total quantum yield will be about that for octahedral complexes of the same average field.

2) For a labialized axis with two different ligands, the ligand of greater field strength is preferentially equated.

The application of rule 1 to $[\text{Cr(NH}_3)_5\text{Cl}]^+$ (equation 1.27) shows that equation of ammonia from the $\text{H}_3\text{N-Cr-NCS}$ axis, that is, the axis with the weakest average field, must be the dominant photoprocess. Moreover, trans-diacidotetraammines and cis-diacidotetraammines, that

is, CrN_4XY^+ with $\text{N}_4=(\text{en})_2$ or $(\text{NH}_3)_4$ and $\text{X}, \text{Y}=\text{I}, \text{Br}^-, \text{Cl}^-, \text{NCS}^-, \text{N}_3^-$, undergo labialization along the X-Cr-Y axis according to rule 1. For $\text{trans-}[\text{Cr}(\text{NH}_3)_4(\text{NCS})\text{Cl}]^+$ the photoequation of NCS^- has a larger yield than the photoequation of Cl^- (equations 1.30 and 1.31) in good agreement with both rules. The rules have less than general validity within the family of Cr(III) compounds. This is illustrated by the photochemical behavior of $\text{trans-}[\text{Cr}(\text{en})_2\text{F}]^{2+}$, where the photoequation of ethylenediamine was the main photoprocess⁽⁸⁶⁾.

1.9.2 Photoreactive excited states of Cr(III) complexes

A typical absorption spectrum of a Cr(III) complex having practically octahedral microsymmetry is sketched in Figure (1.3). One could observe two or three weak bands (Q_1 , Q_2 and Q_3 in order of decreasing wavelength) with molar extinction coefficients of $\sim 10 \sim 100$ and half widths of ~ 1500 to $\sim 2000\text{cm}^{-1}$. In most cases, the band Q_3 was covered by the tail of very intense bands whose maximum was often inaccessible. In addition, in the range of $650 - 750 \text{ m}\mu$ (i.e. on the long-wavelength tail of band Q_1) there occurred a very sharp and weak band, D, with molar extinction coefficient ~ 1 and half-width of ~ 100 to $\sim 200 \text{ cm}^{-1}$. This band usually exhibited a vibrational structure⁽⁸⁷⁾.

The attribution of the bands D, Q_1 , Q_2 and Q_3 can be given using the ligand field theory. The system of energy levels for the d^3 configuration in octahedral symmetry is shown in Figure (1.4).

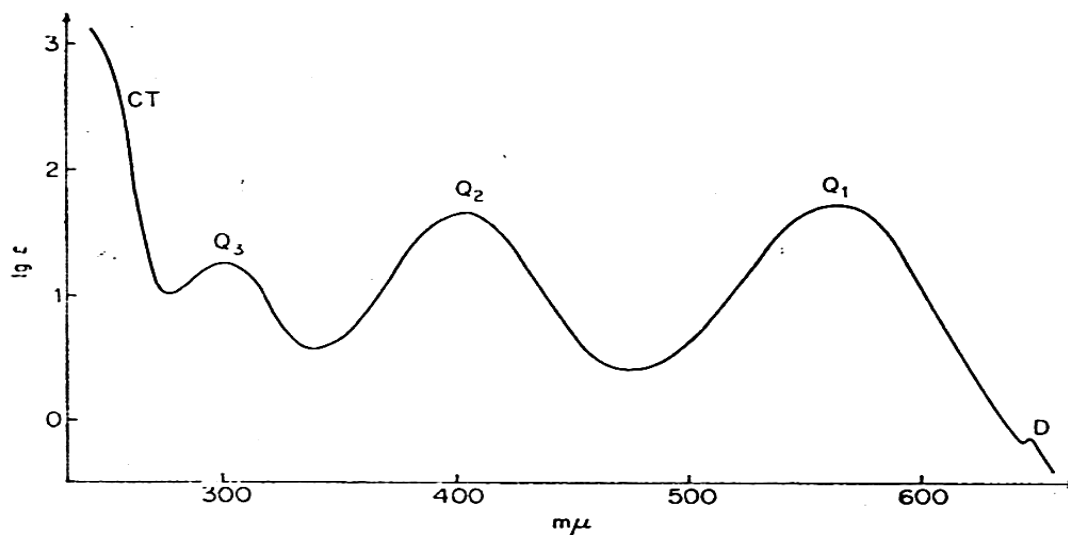


Figure (1.3): Absorption spectrum of a Cr (III) complex having practically octahedral microsymmetry⁽⁸⁷⁾.

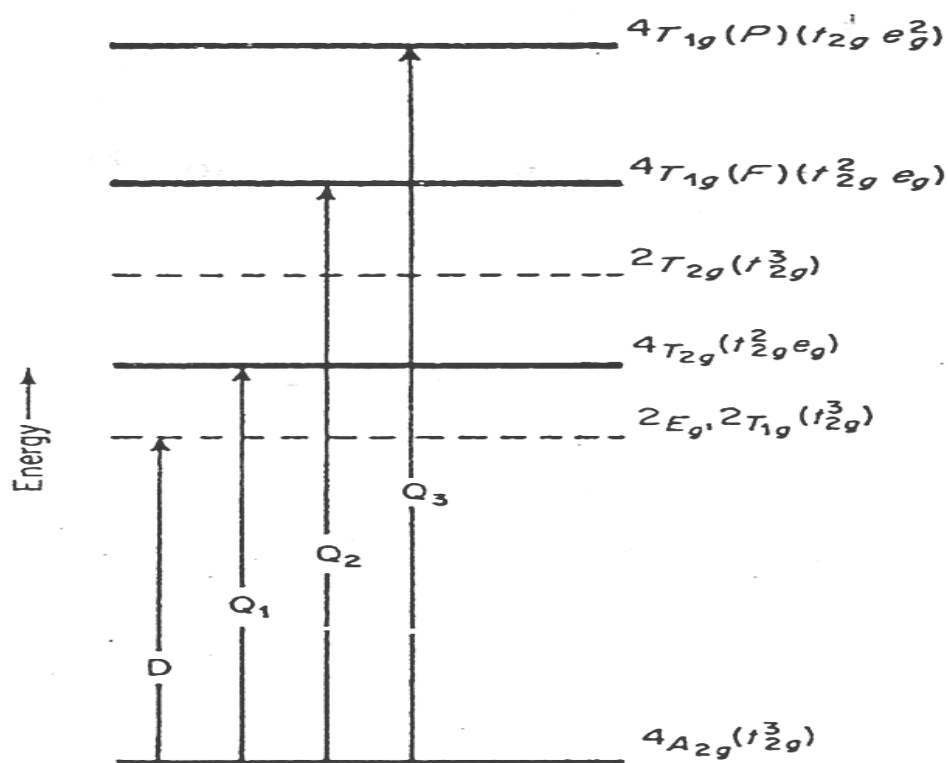


Figure (1.4): Energy levels for the d^3 configuration in octahedral symmetry⁽⁸⁷⁾.

The ground state was a quartet state (${}^4A_{2g}$) which corresponds, in the strong – field parentage, to the one electron configuration ${}^3t_{2g}$; the one-electron configurations of the lower excited states are shown on the right – hand side the figure.

Band D corresponds to the transition from the quartet ground state ${}^4A_{2g}$ to the lowest doublet states 2E_g and ${}^2T_{1g}$ which in a pure octahedral field and in the absence of spin-orbit interactions are degenerate⁽⁸⁷⁾. This transition was characterized by the following features: First, it was parity – as well as spin – forbidden, so that the corresponding band must be very weak; second, it consisted in a spin pairing within the non-bonding t_{2g} sub-shell: therefore, the 2E_g excited state must have almost the same metal-ligand bond distances as the ground state and thus, the absorption band was very sharp; third. The energy difference between the 2E_g and ${}^4A_{2g}$ levels is independent of the ligand field parameter Δ , and thus, the position of the band was relatively insensitive to the type of ligand.

The bands Q_1, Q_2 and Q_3 correspond to the parity-forbidden spin-allowed transitions from the ground state to the excited quartet states ${}^4T_{2g}$, ${}^4T_{1g}(F)$ and ${}^4T_{1g}(P)$, respectively (Figure 1.3). These transitions consisted in electron promotions from the non-bonding or slightly π antibonding t_{2g} orbitals to the σ -antibonding e_g orbitals; therefore, the equilibrium distances in the excited states were larger than those in the ground state and thus, the corresponding absorption bands were broad. The actual spectral positions of the quartet –quartet bands depend on the type of ligand since the energy differences between the quartet excited states and the ground state depended on the ligand field strength.

In the case of complexes of symmetry lower than O_h , the octahedral states split and the corresponding bands are expected to split. In many cases, however, the splitting cannot be actually observed. In the $Cr(NH_3)_5X^{2+}$ complexes ($X=Br, I$), the Q_1 band splits, while the Q_2 one

did not^(88,89). In the trans-[Cr(en)₂X]²⁺ complexes (X=OH, H₂O, F, Cl, Br, I), one band was clearly resolved, while only an ill-defined shoulder was generally observed in the other band^(89,90). In cis-[Cr(en)₂X₂]²⁺, no splitting could be observed⁽⁹⁰⁾. Predictions and explanations of the splittings have been given by various authors^(87,88-92), using ligand field or molecular orbital models, the state designations given above could not be applied to non-*O_h* complexes, although they were often used in general sense.

While the ligand field bands of Cr(III) complexes have been extensively investigated, scarce information existed concerning their charge transfer bands. Besides the more common (ligand → *e_g*(metal)) transitions, the occurrence of vacancies in the "metal" *t_{2g}* orbitals would make (ligand → *t_{2g}*(metal)) transitions possible. Except for a systematic shift to shorter wavelength, the charge transfer bands of the halophentannine chromium (III) complexes were not available. According to Orgel⁽⁹³⁾, which was suggested that in the chromic complexes the *t_{2g}* orbitals were not used in the lowest LMCT transitions, presumably because the energy required for spin pairing of the electrons in the *t_{2g}* orbitals more than balance the extra energy obtained by putting an electron in one of the stable orbitals. This was consistent with the fact that chromous complexes were usually spin-free. As an alternative explanation, the observed bands correspond to transitions to the *t_{2g}* orbitals, while the transitions to the high-energy *e_g* orbitals lie in the far ultraviolet.

The values of optical electronegativity given by Jorgensen⁽⁹⁴⁾ were 1.8 and 1.0-1.3 for the *t_{2g}* and *e_g* orbitals, respectively, compared with the value 1.6-1.9 given for the cobalt(III)*e_g* orbitals.

1.10 Aim of The Present Work

The photochemistry of metal chelate complexes have attracted considerable attention in the last three decades⁽⁵⁷⁾, because of their interesting applications in the photoinitiation of vinyl polymerization and photocross-linking⁽⁵⁸⁾, the photostabilization of polyofines and photoinduced degradation of polymers⁽⁶⁹⁾, the photochemical storage of solar energy as in water splitting process⁽⁶³⁾ and photofixation of carbon dioxide⁽⁶⁴⁾.

In the present work we prepared tris(alkylxanthato)chromium(III) and intended to study the photochemistry of these complexes in dimethyl sulfoxide.

These complexes might be useful in many applications. Moreover, metal chelate with metals at high oxidation state is active in the enhancement of photodegradation of plastic and therefore, might serve as photocatalyst to treat the plastic waste pollution problem⁽⁷⁵⁾.

The effect of number of methyl group in these complexes has been also studied.

This work also deals with the photochemical reaction and determination of quantum yields and reactivity ratios of the photodecomposition processes of the different complexes in DMSO.

Spectroscopic methods have been used for the elucidation of the photochemical reactions, and determination of the quantum yields of the photochemical decomposition processes.

Chapter Two

Experimental

2.1 Chemicals

The chemicals in this work were used, without any further purification. The chemicals are listed in Table (2.1) along with their suppliers and purities:

Table (2.1): Chemicals and their suppliers and purity

<i>Chemicals</i>	<i>Company</i>	<i>Purity</i>
Chromium chloride anhydride	BDH	A. R. Grade
Carbon disulfide	BDH	99.9%
Potassium hydroxide	BDH	98.9%
Methanol	BDH	99.9%
Ethanol	BDH	99.9%
Isopropanol	BDH	99.9%
Butanol	BDH	99.9%
Hexanol	BDH	97.9%
Dimethyl Sulphoxide	BDH	97.9%
Petroleum Ether	Fluka	99.9%
Hydrogen peroxide	BDH	97.9%
Sulfuric acid	BDH	96%
Ferrous Sulfate	BDH	A. R. Grade

<i>Chemicals</i>	<i>Company</i>	<i>Purity</i>
1,10-phenanthroline	BDH	A. R. Grade
Hydroxyl ammonium chloride	BDH	A. R. Grade
Sodium acetate	BDH	A. R. Grade

2.2 Instruments used

a) Fourier transforms Infrared spectroscopy (FTIR)

The FTIR spectra in the range (500-4000) or (250-4000) cm^{-1} cut were recorded as KBr and / or CsI discs on Shimadzu Spectrophotometer FTIR model 8300 (Japan).

b) Ultraviolet –Visible Spectroscopy (UV)

The UV-Visible spectra were measured using Shimadzu UV-VIS model 1650PC A-Ultraviolet Spectrophotometer in the range (200-900) nm (Japan).

c) Magnetic Susceptibility Measurements

The magnetic susceptibility values of the prepared complexes were obtained at room temperature using Magnetic Susceptibility Balance of Bruke Magnet B.M.6 (England).

d) Melting Points

Stuart Scientific melting point apparatus was used to measure the melting points of all the prepared compounds (U.K.).

e) The Photolysis Apparatus

The photolysis apparatus (Iwasaki Electric Co., Ltd.) was used for irradiation of all prepared complexes(Japan).

f) Atomic absorption measurements

Atomic absorption measurements of the prepared complexes were obtained at 25⁰C using Atomic absorption apparatus of Shimadzu 680cc-flame (Japan).

g) Conductivity measurements

The molar conductivity values of the prepared complexes were obtained by using conductivity apparatus

2.3 Preparations of materials

2.3.1 Preparation of potassium methyl xanthate (PMX)

PMX was prepared according to the method described by Malik and coworkers⁽⁹⁵⁾. A 0.25 mole of potassium hydroxide was added to 0.2 mole of absolute methanol. The mixture was stirred for three minutes.

The reaction mixture was led to settle. The unreacted potassium hydroxide was removed by decanting. A 0.2 mole of carbon disulfide was added gradually to the solution with cooling and stirring in an ice bath. The yellow pasty product was washed with petroleum ether, filtered and dried at room temperature for 24 hours to get yellowish crystals(yield 1.5021g). The melting point, FTIR spectrum, Magnetic Susceptibility and UV-Visible spectrum were measured .

The same procedure was used to prepare potassium ethyl xanthate (PEX) (yield 3.510g), potassium isopropyl xanthate (PPX) (yield 4.103g),

potassium butyl xanthate (PBX) (yield 1.0499g)and potassium hexyl xanthate(PHX) (yield 1.031g) using the appropriate alcohol.

2.3.2 Preparation of tris(methylxanthato) chromium (III) complex , $\text{Cr}(\text{mex})_3$

It was not possible to prepare the $\text{Cr}(\text{mex})_2$ complex to compare its spectrum to that of $\text{Cr}(\text{mex})_3$ after irradiation, because Cr (II) is readily oxidized to Cr (III) during complexation. Ligands containing the CS_2 moiety are known to form stable Cr (III) complexes and generally the Cr (II) complexes, if formed are difficult to isolate⁽⁹⁶⁾

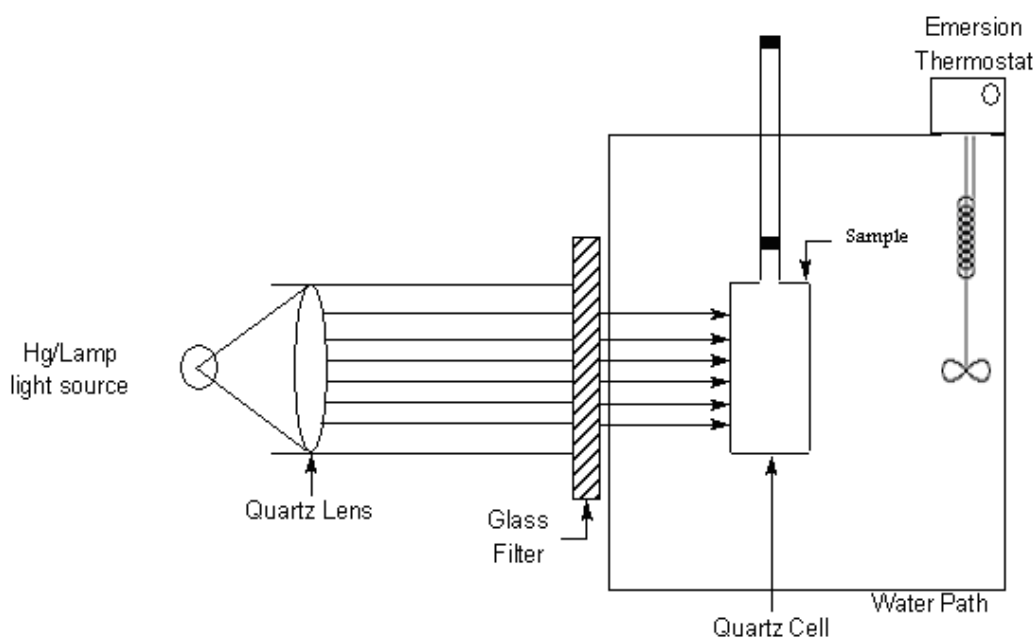
$\text{Cr}(\text{mex})_3 \cdot 3\text{H}_2\text{O}$ was prepared using method described by Al-Kassar⁽⁹⁷⁾ as follows . To 5 ml of a methanolic solution of 0.01 mole $\text{CrCl}_3 \cdot 6\text{H}_2\text{O}$, a 0.03 mole of potassium methyl xanthate (dissolved in small amount of methanol) was added. This mixture was stirred until a deep green as in crystalline solid was obtained. The product was crystallized from a mixture of petroleum ether. The recrystallized material dried at room temperature for 24 hours to yield deep green crystals of $\text{Cr}(\text{mex})_3$ (yield 0.7247g).

The above method was used to prepare the following complexes, however they gave different colored crystals.

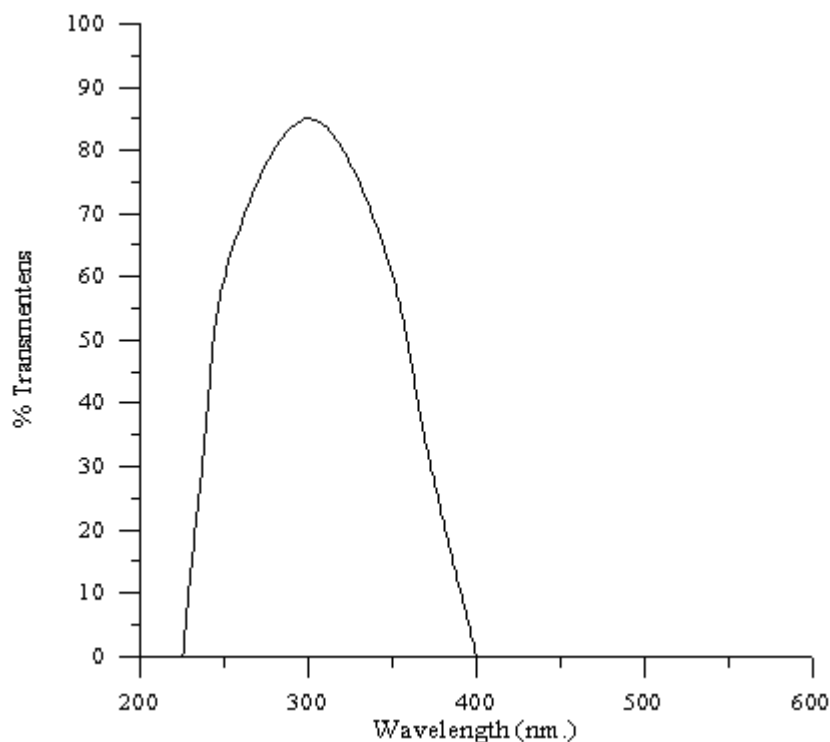
- Tris (ethylxanthato) chromium (III) complex $\text{Cr}(\text{etx})_3$ (yield 1.150g).
- Tris (isopropylxanthato) chromium (III) complex $\text{Cr}(\text{prx})_3$ (yield 0.354g).
- Tris (butylxanthato) chromium (III) complex $\text{Cr}(\text{bux})_3$ (yield 0.2670g).
- Tris (hexylxanthato) chromium (III) complex $\text{Cr}(\text{hex})_3$ (yield 0.189g).

2.4 The Photolysis Apparatus

The photolysis apparatus used in this work shown is Figure (2.1a). The apparatus is consisted of high pressure mercury lamp (1000 W. Iwasaki Electric Co., Ltd., Japan) and collecting quartz lens. The lamp was installed in a fixed vertical position, while the lens was adjusted to produce efficiently parallel beams of light. The light was passed through a glass filter. This filter had been calibrated with the aid of Perkin Elmer 1301 UV-visible double beam spectrophotometer. Calibration has shown that the transmitted light was predominately in wavelength range (230-400 nm). The transmitted spectrum of the filter is shown in Figure (2.1b). The distilled water bath was kept at room temperature.



(a) Photolysis apparatus



(b) % transmittens spectrum for filter used

Figure (2.1): (a) Photolysis apparatus set up and (b) Filter transmittance spectrum

2.5 Incident light intensity measurement

The intensity of the incident light (I_0), was measured by the use of potassium ferrioxalate actinometer method as described by Hatchard and Parker⁽⁹⁸⁾.

The actinometer solution (6×10^{-3} mol/l) was prepared by dissolving (3 gm.) of $K_3Fe(C_2O_4)_3 \cdot 3H_2O$ in 800 ml of distilled water. A 100 ml of 1 N of H_2SO_4 solution was added and the whole solution was diluted to one liter with distilled water. The actinometer solution absorbs 100% of the incident light at $\lambda = 311$ nm.

The light intensity measurement involves irradiation of the actinometer solution for a known period of time 3 minutes. Ferrous ion concentration was estimated spectrophotometrically using 1,10-phenanthroline (0.1 %) as complexing agent. According to Hatchard and Parker ferric ion is reduced to ferrous ion ($\text{Fe}^{3+} \longrightarrow \text{Fe}^{2+}$) using hydroxyl ammine solution reagent.

A phenanthroline complex is formed with Fe^{2+} which strongly absorbs at 510 nm. For Fe^{2+} formation, the quantum yield was known to be equal to 1.21⁽⁹⁸⁾.

The intensity of incident light (I_0) was calculated according to the following method⁽⁹⁹⁾. A 3 ml of actinometer solution was irradiated in the irradiation cell. A stream of nitrogen bubbles in the solution was used to remove the dissolved oxygen gas.

After illumination, a 1 ml of irradiation solution was transferred to 25 ml volumetric flask, 0.4ml of hydroxyl ammonium chloride solution, 2 ml of 1, 10-phenanthroline solution and 0.5 ml of buffer solution were added to the flask, and then diluted to 25 ml with distilled water. Blank solution was made by mixing 1 ml of unirradiated mixture solution with other components. The solution was left in dark for 30 mins. and then optical density (at $\lambda = 510\text{nm}$) was measured. The intensity of incident light was then calculated using the relationship⁽⁹⁹⁾ in equation (2.1) below:

$$I_0 = \frac{A \times V_2 \times N_A}{\phi_\lambda \times \epsilon \times V_1 \times t \times d} \text{ Einstein l}^{-1} \cdot \text{sec}^{-1}., \quad (2.1)$$

Where:

I_0 = Incident light (Einstein $\text{l}^{-1} \cdot \text{sec}^{-1}$)

A = Absorbance at ($\lambda = 510\text{nm}$)

V_2 = Final volume (25 ml)

ϕ_λ = Quantum yield = 1.21

ϵ = Molar extension coefficient (slope of the calibration curve),

V_1 = Volume taken from irradiated solution (1 ml)

t = Irradiation time in second

N_A = Avogadro's number

d = Thickness of the cuvette (1 cm)

The cell was irradiated in the same position used for irradiated samples. A calibration curve for Fe^{2+} was obtained using the following solutions:

- 1- 4×10^{-4} mol/L of FeSO_4 in 0.1 N H_2SO_4 .
- 2- 0.1 % w/v phenanthroline monohydrate in water.
- 3- Hydroxyl ammonium chloride solution was prepared by dissolving 10g of hydroxyl ammonium chloride in 100ml of water.
- 4- Buffer solution was prepared from mixing 600 ml of 1N sodium acetate with 360 ml. 1 N H_2SO_4 diluted to 1 liter.

Solutions of different concentrations of Fe^{2+} (ranged from 5.0×10^{-6} - 1×10^{-4} M) were prepared from solution (1) by taking different amounts in 25 ml volumetric flask, and each of the followings were added:

(a) a 0.4ml of hydroxyl ammonium chloride (b) a 2 ml Phenanthroline solution, (c) a 5 ml of buffer solution, (d) a 0.1 N H_2SO_4 to make the volume equal to 10 ml, diluting the whole solution with distilled water. The volumetric flask was covered with aluminum foil, and was kept in a dark for 30 minutes before the optical densities at $\lambda = 510$ nm were measured. A blank solution was used as a reference, which contained all ingredients except the ferrous ion solution.

The plot of optical density versus ferrous ion concentration was a straight line as shown in Figure (2.2) . The slope of the line represents the extinction coefficient of FeSO_4 solution which was equal to $(\epsilon=1.1027 \times 10^4 \text{ mol}^{-1} \cdot \text{L} \cdot \text{cm}^{-1})$. This value is in good agreement with that reported by Hatchard and Parker⁽⁹⁸⁾.

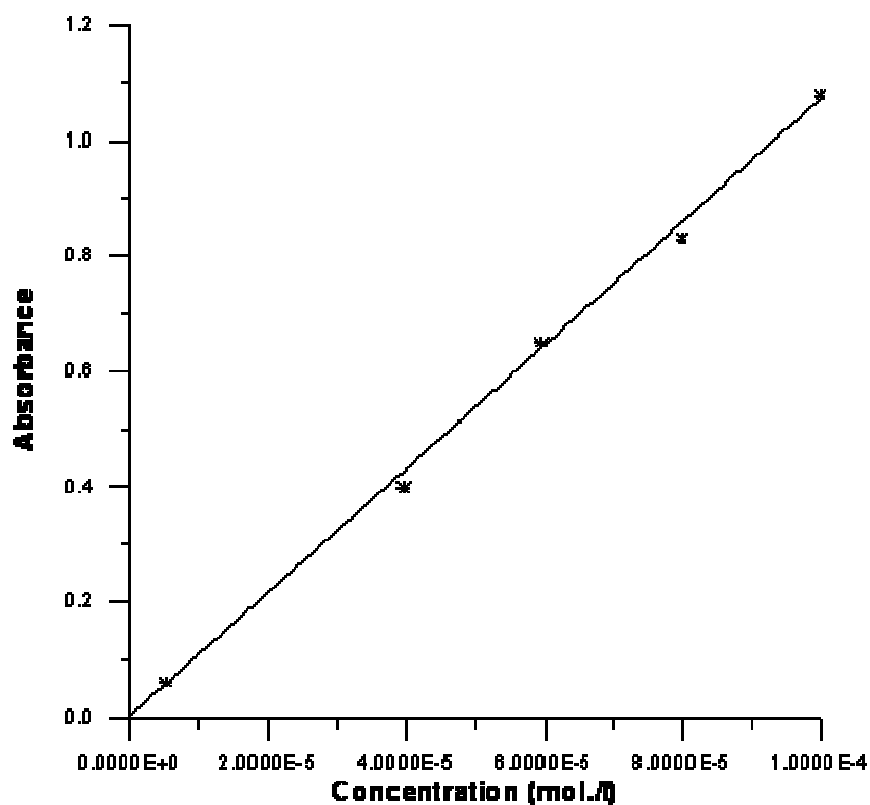


Figure (2.2): Calibration curve for Fe(II) complex at 510 nm.

2.6 The photodecomposition rate of complexes using Ultraviolet –Visible spectrophotometer

The absorption spectrum of each ligand and its complex was measured in the range of (200-600) nm. The λ_{max} of each complex was

recorded. The photodecomposition of the complexes at λ_{\max} at room temperature in the proper solvent was followed with time using a covered quartz uv-cell of 1cm bath length. A known concentration of complex solution in the proper solvent was introduced in the cell after degassing by nitrogen for 20 minutes. The cell was closed tightly and the absorbance was recorded. Pure DMSO solvent was used as a reference in order to study the kinetic of photodecay of the different complexes. The absorbance at infinite time (A_{∞}) was measured after the solution was irradiated for at least 10 half live of complex decomposition (more than 50 hours). The specific rate constant of the decomposition of the complex (K_d) was determined by the following first order equation ⁽⁷⁵⁾:

$$\ln(a - x) = \ln a - K_d t \quad (2.2)$$

Where:

a = Concentration of complex before irradiation.

x = Concentration of complex after t = time of irradiation.

t = Time of irradiation of complex solution.

A_0 = Absorbance of complex before irradiation.

A_t = Absorbance of complex after irradiation time

ϵ = Molar extension coefficient

$$a = (A_0 - A_{\infty}) / \epsilon, \quad x = (A_0 - A_t) / \epsilon, \quad a - x = (A_t - A_{\infty}) / \epsilon.$$

By substitution of a and $a - x$ in equation (2.2) and rearrangement

$$\ln (A_t - A_{\infty}) = \ln(A_0 - A_{\infty}) - K_d t \quad (2.3)$$

Thus a plot of $\ln |A_t - A_{\infty}|$ versus irradiation time (t) gives a line with a slope equal to K_d (S^{-1})

The rate of photodecomposition (R_d) was calculated for each complex using the following equation ⁽⁷⁵⁾ :

$$R_d = K_d \times [\text{concentration of complex}]$$

2.7 Decomposition Quantum yields (Q_d)

For determination of the quantum yield, reactions are carried out in closed quartz uv-cell of 1cm bath length so that the quantum input could be measured precisely; the absorbance measured by the technique as described below.

A knowledge of the incident light intensity (determined by actinometry using the method of Hatchard and Packer ⁽⁹⁸⁾ and the extinction coefficient of the compound enable the quantum input (I_{abs}) to be calculated .

The quantum yield of photodecomposition (Q_d) is defined by:

$$Q_d = \frac{\text{Rate of photodecomposition}}{\text{Quantum input}}$$

for each complexes using the following equation (2.4) ⁽²¹⁾:

$$Q_d = K_d \times [\text{conc.}] / I_{\text{abs}} \quad (2.4)$$

The quantum yield was plotted against the number of alkyl group of each complex.

The reactivity ratio (R_r) (K_2/K_1) was also calculated for each complex using the following equation ⁽²¹⁾:

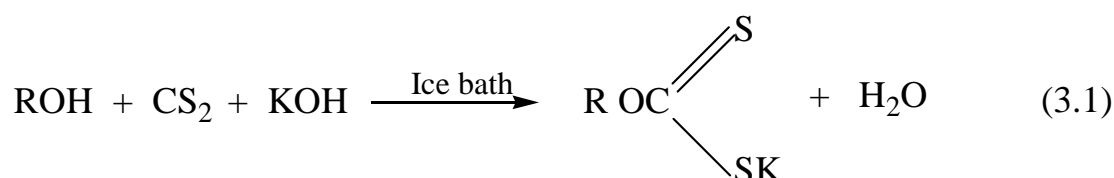
$$R_r = Q_d / 1 - Q_d$$

Chapter Three

Results & Discussion

3.1 Preparation of ligands

Potassium methyl xanthate, potassium ethyl xanthate, potassium isopropyl xanthate, potassium butyl xanthate, and potassium hexyl xanthate ligands were prepared according to the chemical reaction as shown in equation (3.1)

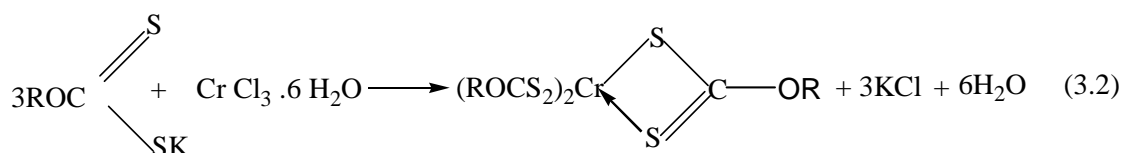


Where: R = CH₃-, C₂H₅-, C₃H₇-, C₄H₉-, or C₆H₁₃-

The reaction was one to one (1:1) stoichiometry. An excess of KOH solution was added to ensure complete reaction.

3.2 Preparation of complexes

Tris(methylxanthato)chromium(III), tris(ethylxanthato)chromium(III), tris(isopropylxanthato)chromium(III), tris(butylxanthato)chromium(III), and tris(hexylxanthato)chromium(III) complexes were prepared according to the chemical reaction as shown in equation (3.2)



The stoichiometry of the above reaction was 3: 1 with respect to ligand and metal salt, respectively

3.3 Physical properties of prepared ligands and complexes

Table (3.1) lists some of the physical properties of ligands and their complexes.

Table (3.1): Some physical properties of the prepared ligands and complexes

Compound	Color	Melting point ⁰C	M calc. %	M found %
PMX	Yellow	215-218	-	-
Cr(mex)₃	Deep green	>300*	2.53	3.84
PEX	Light brown	108-110	-	-
Cr(ety)₃	Greenish blue	>300	3.27	4.20
PPX	Yellowish white	208-210	-	-
Cr(prx)₃	Light blue	>300	6.51	7.32
PBX	Yellowish white	198-200	-	-
Cr(bux)₃	Light blue	>300	5.34	6.13
PHX	Yellowish white	210-212	-	-
Cr(hex)₃	Light grey	>300	4.88	5.10

* didn't melts below 300 ⁰C

The color of these ligands was all yellow but with different levels. The color of the prepared complexes has ranged from deep green to light grey. The melting points of the ligands were ranged from 108 to 218. However, the melting points of the complexes have be not recorded because they did not melt below 300 ⁰C. The data of metal were obtained

using flame atomic absorption technique. The calculation values were in a good agreement with the experimental values.

3.4 Magnetic susceptibility and molar conductivity measurements

The Experimental magnetic moment for each complex is listed in Table (3.2). Magnetic measurements are commonly used in studying transition metal complexes⁽¹⁰⁰⁾. The magnetic properties are due to the presence of unpaired electrons in the partially filled d-orbital in the outer shell of that element. These magnetic measurements give an idea about the electronic state of the metal ion in the complex.

The resultant magnetic moment of an ion is due to both orbital and spin motion⁽¹⁰¹⁾. The magnetic moment is given by the following equation⁽¹⁰²⁾:

$$\mu_{S+L} = \sqrt{4S(S+1) + L(L+1)} \text{ B.M}$$

μ = Magnetic moment

S = Spin quantum number

L = Orbital quantum number

B.M. = $9.27 \times 10^{-24} \text{ J. T}^{-1}$

Although detailed determination of the electronic structure requires consideration of the orbital moment. However, for most complexes of the first transition series the spin – only moment is sufficient, if the orbital contribution is small⁽¹⁰³⁾, therefore:

$$\mu_S = \sqrt{4S(S+1)} \text{ B.M.},$$

or

$$\mu_S = \sqrt{n(n+2)} \text{ B.M.}$$

$$S = n (1/2)$$

S = Spin multiplicity

n = Number of unpaired electrons.

The value of magnetic susceptibility of the prepared complexes at room temperatures was calculated using the following equation:

$$\mu_S = \sqrt{X_A \times T}$$

$$X_A = X_m + D$$

$$X_m = X_g \cdot \text{Mwt}$$

Where:

X_A = Atomic Susceptibility

X_m = Molar Susceptibility (corrected)

X_g = Mass Susceptibility

Mwt = Molecular weight of complex

D = Diamagnetic correction factor $\times 10^{-6}$

T = Temperature in Kelvin ($^{\circ}\text{C} + 273$)

B. M = Magnetic moment unit (Bohr magneton)

The observed magnetic moments for the prepared Cr(III) complexes is shown in Table (3.2). These values are typical of high spin octahedral complexes of Cr(III)⁽¹⁰⁴⁾. These values were in a good agreement with that given by Kazzer et al. for the Cr(etx)₃ which has been reported to be 4.18 B.M. However, the value for Cr(mex)₃ was reported to be 3.89 B.M.⁽¹⁰⁵⁾ compared to our value of 4.20. The values of the molar conductivity measurements in DMSO solvent at 25⁰C in Table (3.2)

showed, that tris(alkylxanthato)chromium (III) complexes were non-electrolyte

Table (3.2): Magnetic Moment and molar conductivity Measurements of complexes

<i>complex</i>	<i>Magnetic Moment (B.M)</i>	<i>Molar conductivity $\text{Ohm}^{-1}\text{cm}^2\text{mol}^{-1}$</i>	<i>Suggested Structure</i>
Cr(mex) ₃	4.20	18	octahedral
Cr(etx) ₃	4.18	17	octahedral
Cr(prx) ₃	4.15	10	octahedral
Cr(bux) ₃	4.12	16	octahedral
Cr(hex) ₃	4.16	13	octahedral

3.5 FTIR Spectra for ligands and their complexes

The FTIR spectra of the prepared potassium alkyl ligands and their chromium complexes are shown in Figures (3.1-3.10) for comparison. The FTIR spectra of the chromium complexes were run on both KBr and CsI discs. This is because the absorption bands below 500cm^{-1} were weak with CsI disc due to high absorption bands above 500cm^{-1} as shown in Figures 3.2, 3.4, 3.6, 3.8, and 3.10, (a) and (b) for KBr and CsI discs, respectively.

The main absorption bands for both ligands and their complexes are listed in Table (3.3).

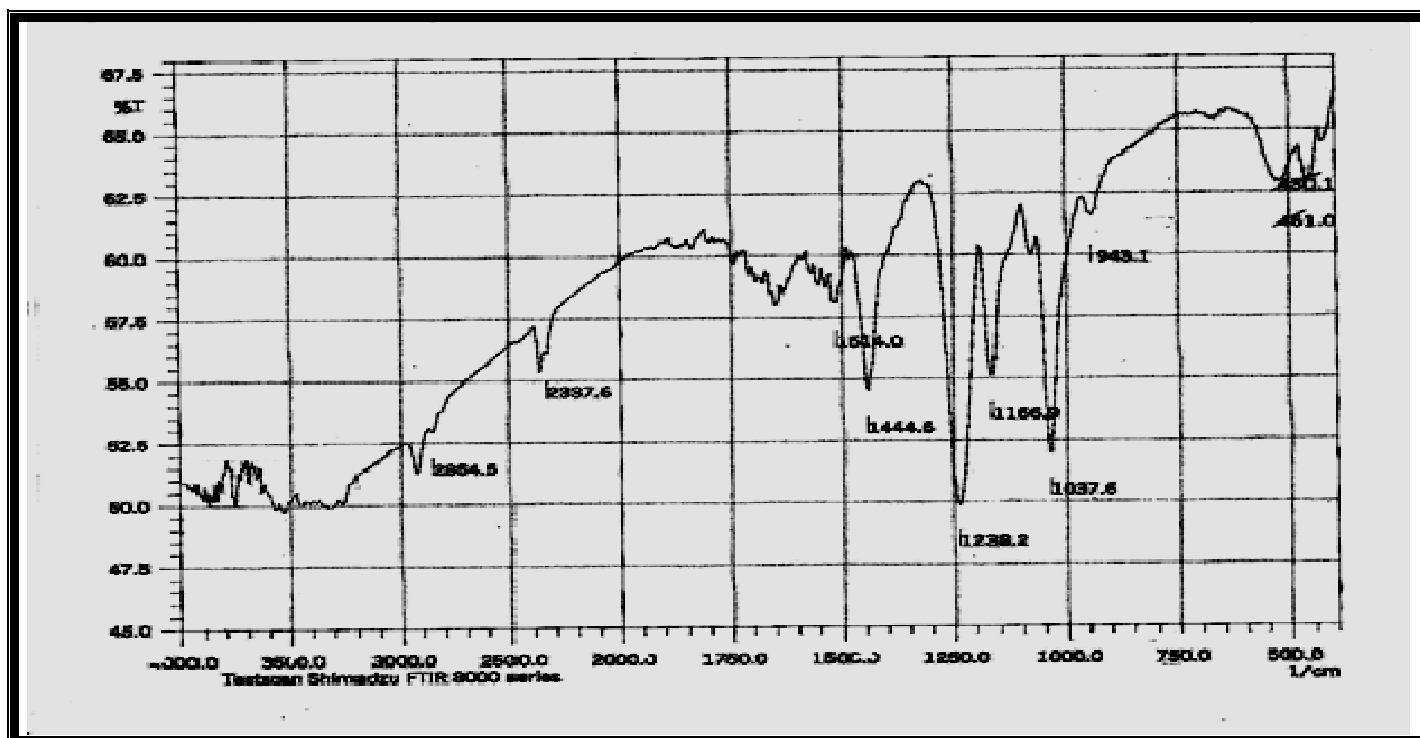
The absorption bands observed at ($1155\text{-}1188\text{ cm}^{-1}$) in the spectra of free xanthate ligands were may be assigned to $\nu(\text{O-C-O})$. This bands have shifted to higher values of ($1226\text{-}1250\text{ cm}^{-1}$) for chromium (III)

complexes which range from (44-81 cm⁻¹), indicating some involvement of oxygen of (C-O-C) in bonding with metals⁽¹⁰⁶⁾.

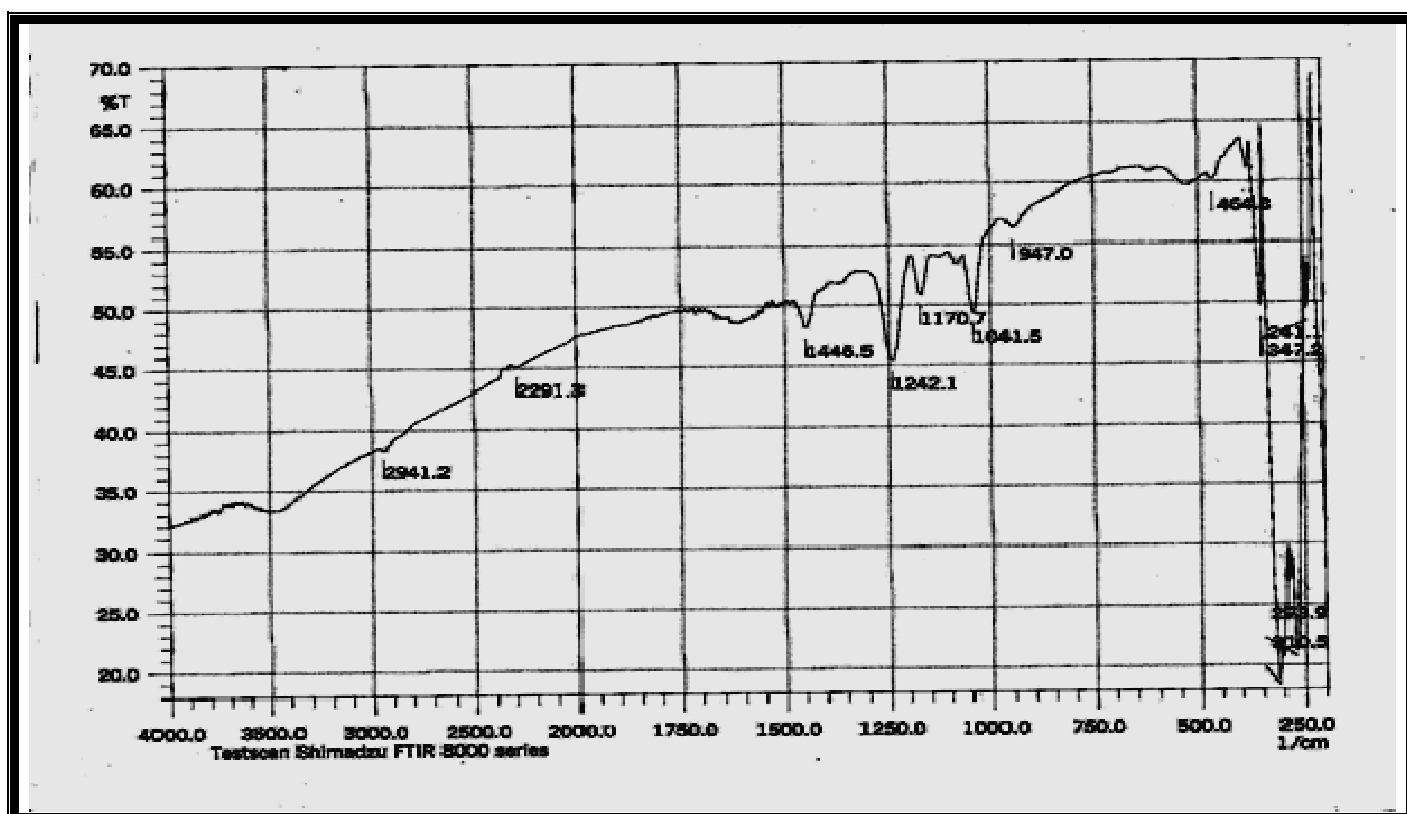
The bands at (1042-1065 cm⁻¹) in the spectra of xanthate ligands can be assigned to (C-S) stretching frequencies. In the spectra of all complexes, these bands shifted to lower frequencies ranged from (7-24 cm⁻¹) to give absorption bands for the complexes in the range (1032-1050 cm⁻¹) suggesting that sulphur is involved in bonding to the metal ion, this is in agreement with previous earlier assignment⁽¹⁰⁶⁾. Furthermore, the occurrence of this single band due to $\nu(\text{C-S})$ in all xanthate complexes showed the uninegative bidentate behavior of the xanthate ligands⁽¹⁰⁷⁾.

The bands at (1105-1145 cm⁻¹) in the spectra of xanthate ligands can be assigned to $\nu(\text{C=S})$. The absorption bands of the $\nu(\text{C=S})$ for the PMX was 1105 cm⁻¹ compared to 1145 cm⁻¹ for PHX which indicated a large shift from methyl to hexyl group in the ligands. This is in agreement with that reported previously⁽¹⁰⁸⁾. This has been attributed to the greater electron-releasing tendency of the hexyl compared to the methyl group⁽¹⁰⁸⁾. In the spectra of all complexes, these bands shifted to higher frequency of (1117-1190 cm⁻¹), which represented a shift to longer frequency of as much as 62 cm⁻¹.

The FTIR spectra of the complexes have shown new bands in the range of (347-352 cm⁻¹) for all complexes as listed in Table (3.3). These bands were assigned to (Cr-S) stretching vibration^(109,110).

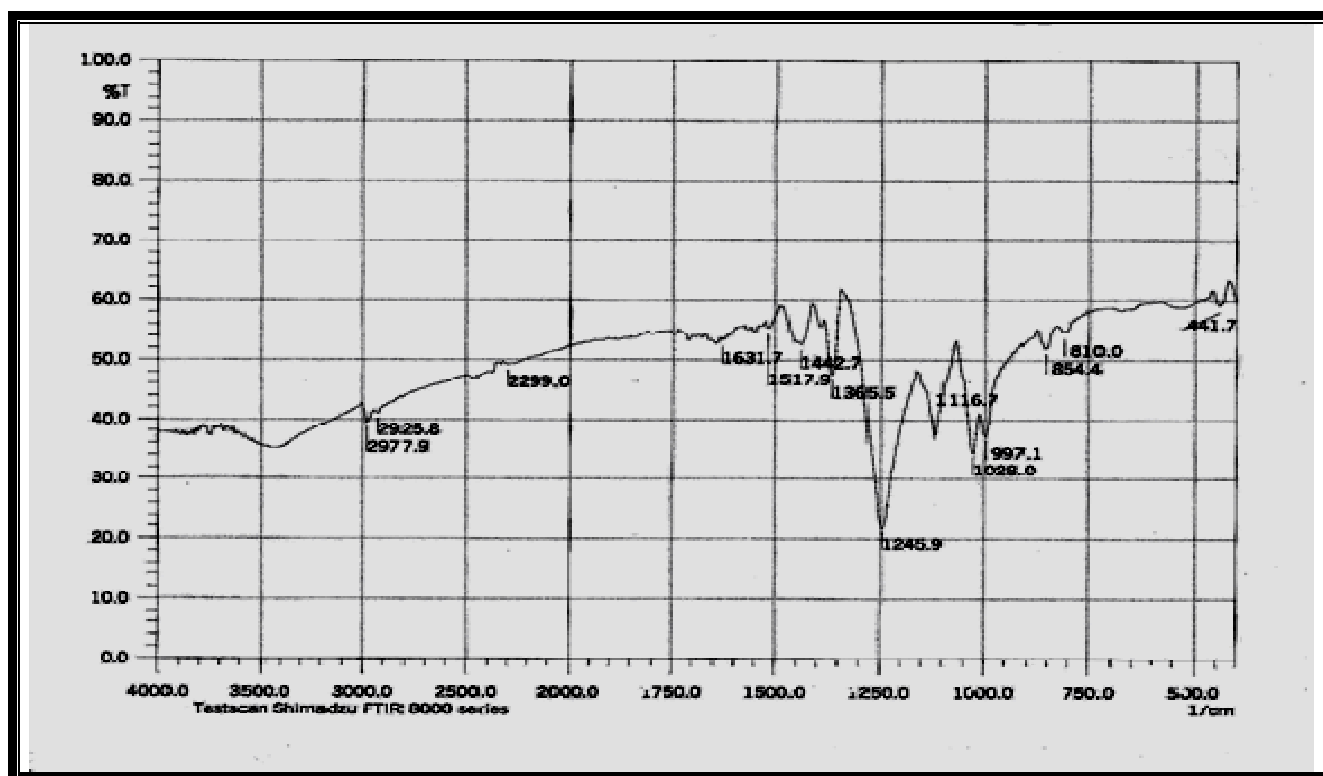


(a)

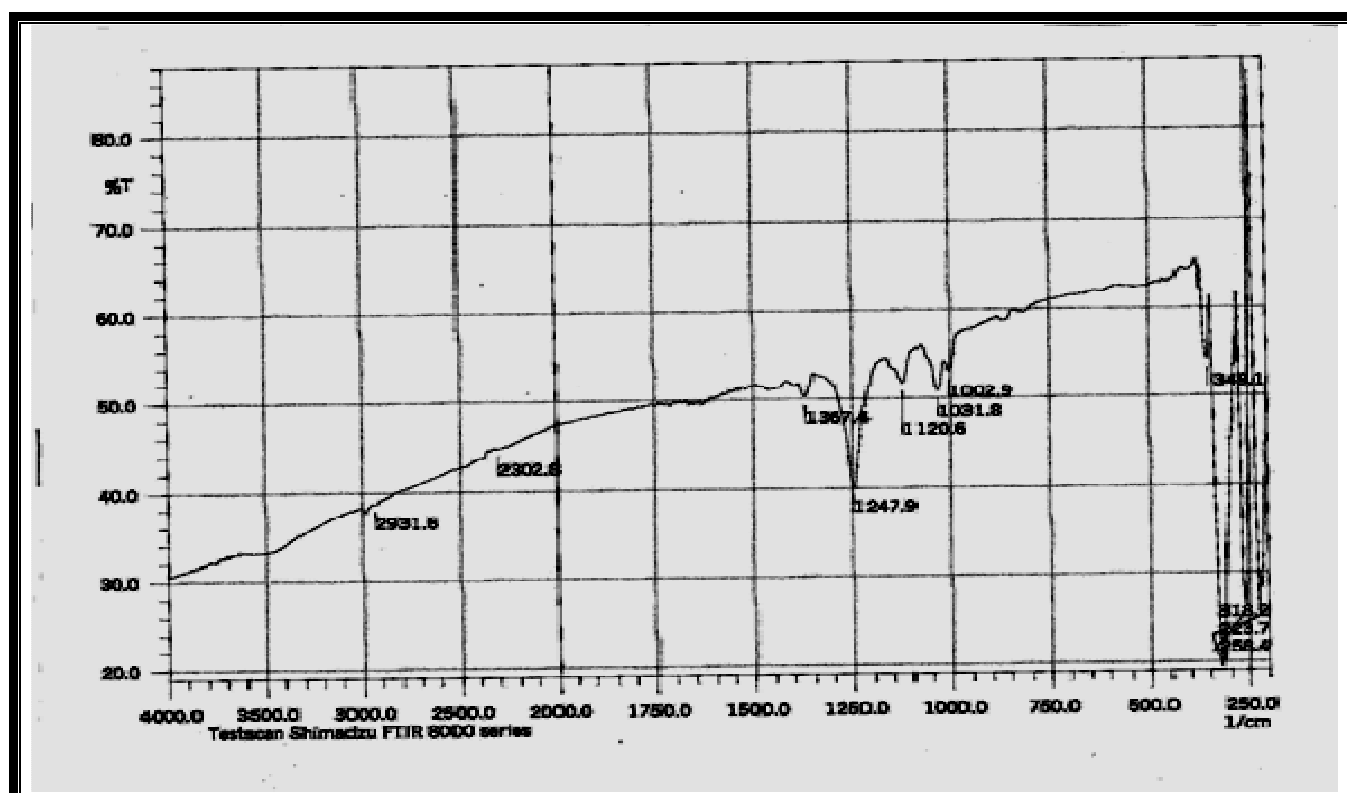


(b)

Figure (3.2): FTIR spectrum for tris (methylxanthato) chromium (III) complex using (a) KBr (b) CsI discs.

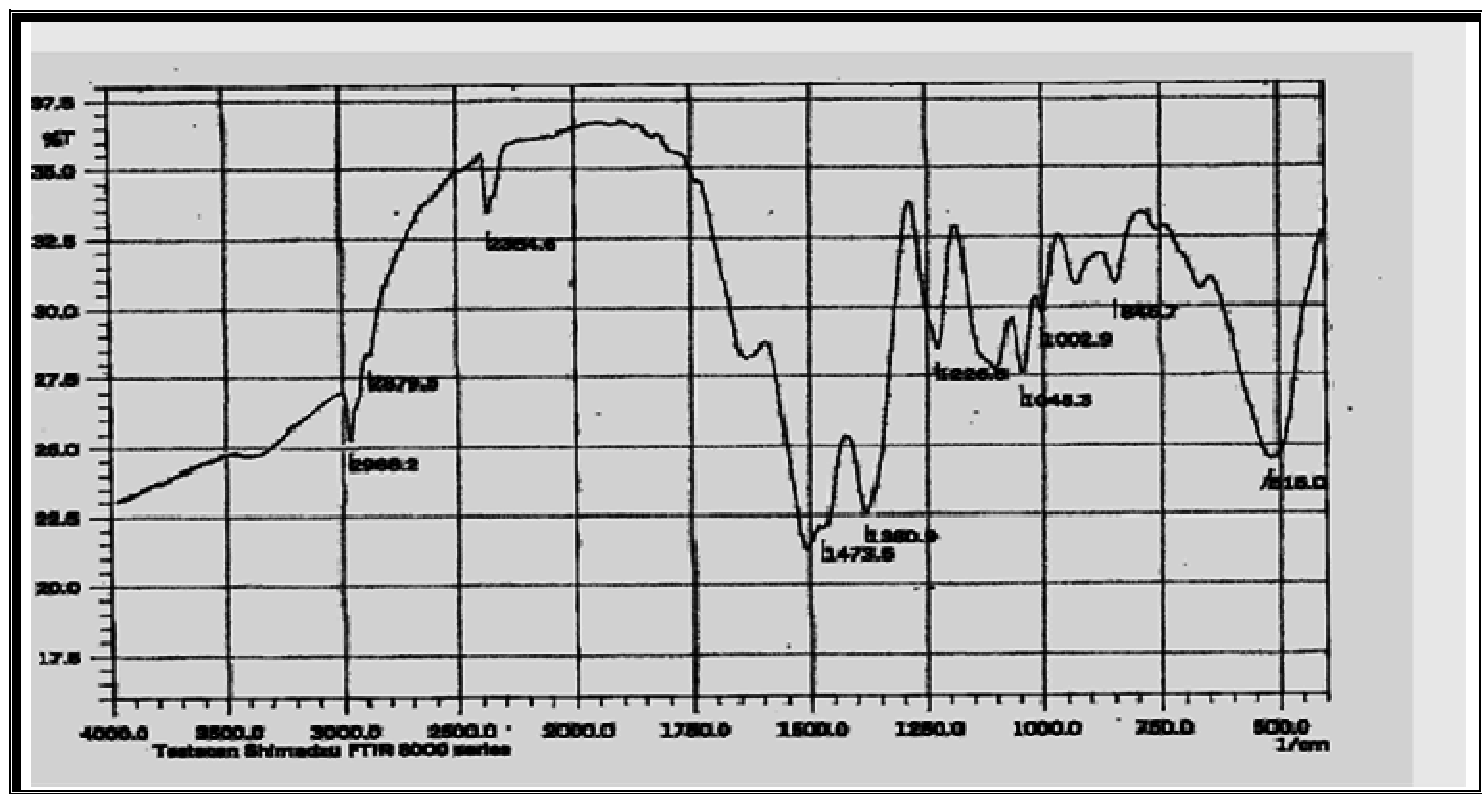


(a)

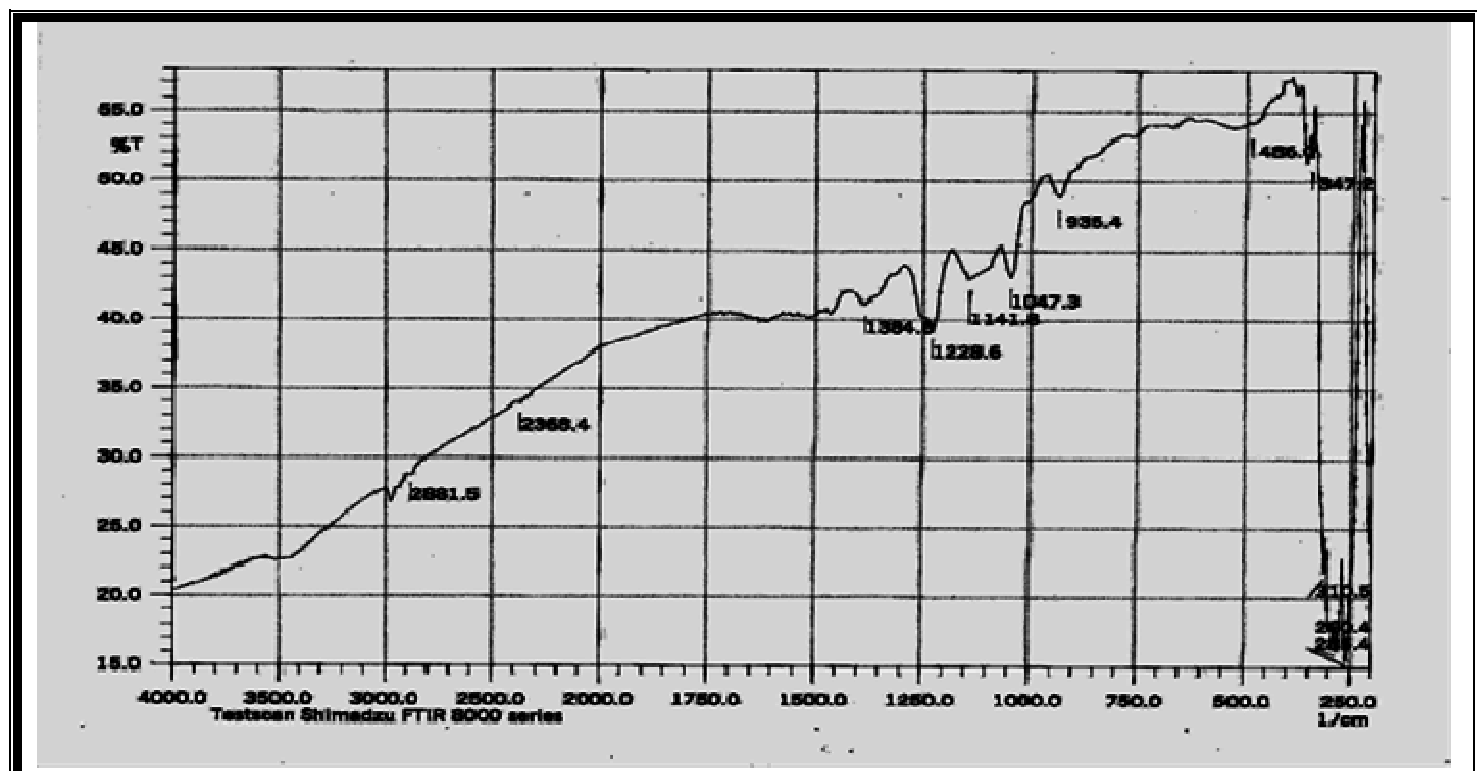


(b)

Figure (3.4): FTIR spectrum for tris(ethylxanthato)chromium(III) complex using (a) KBr (b) CsI discs.

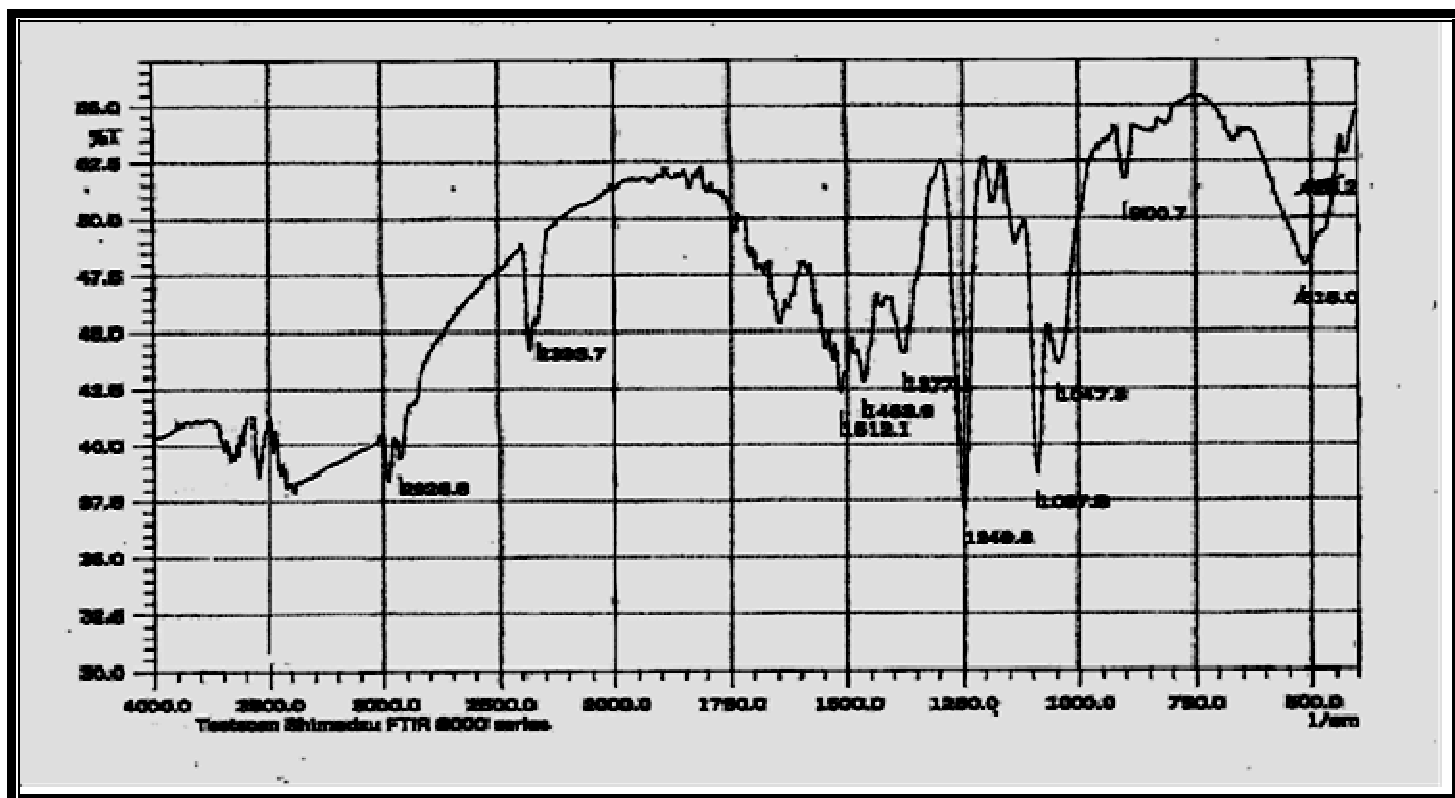


(a)

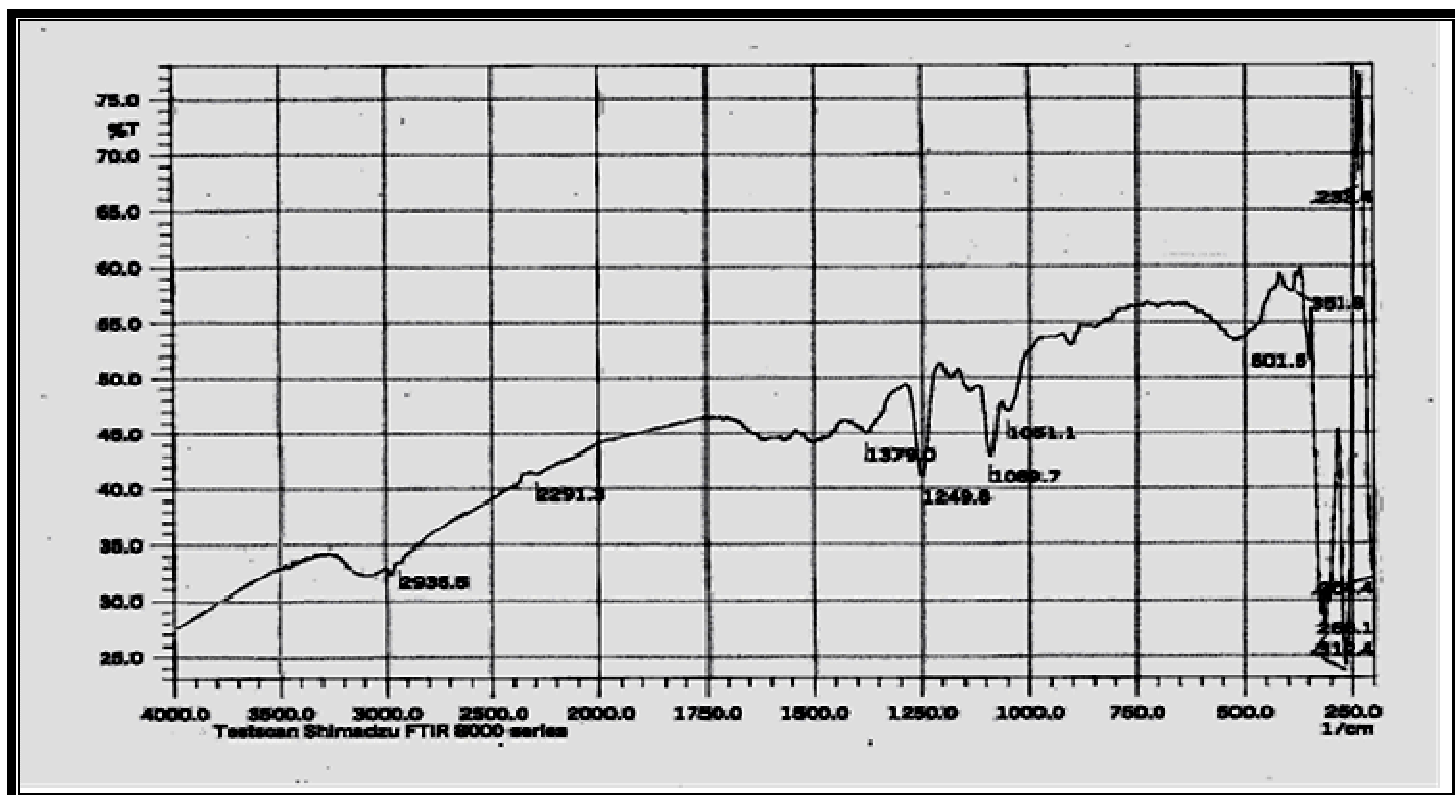


(b)

Figure (3.6): FTIR spectrum for tris(isopropylxanthato)chromium(III) complex using (a) KBr (b) CsI discs.

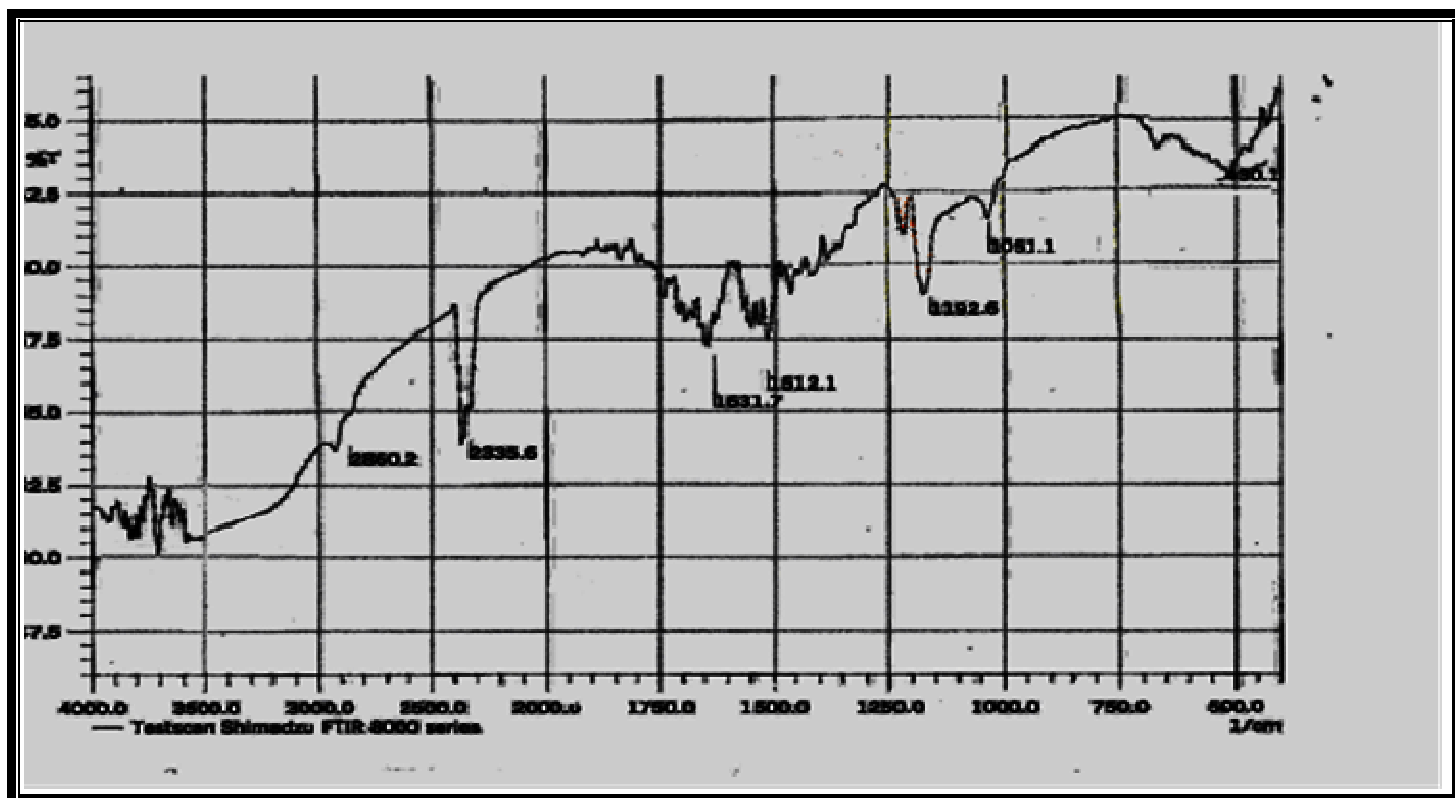


(a)

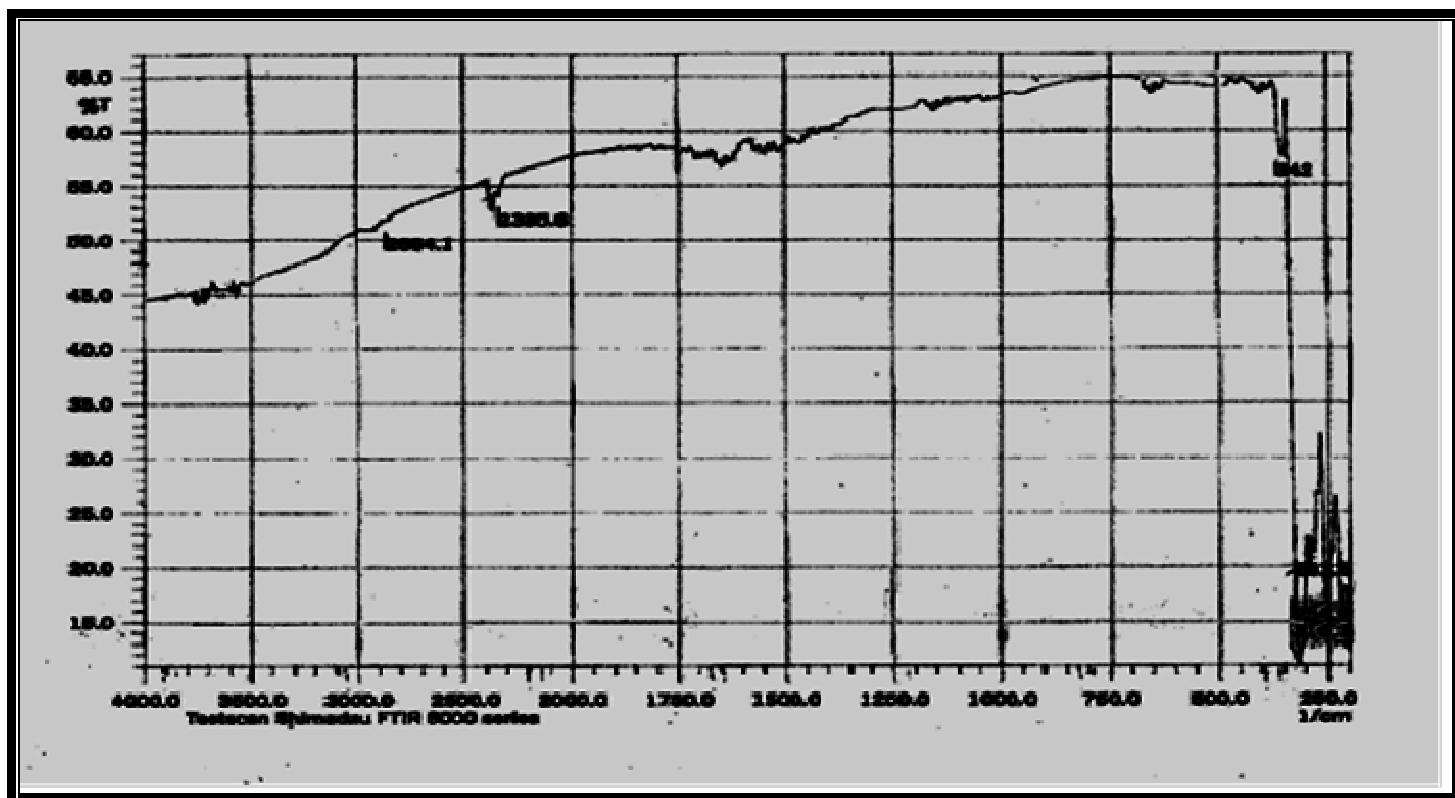


(b)

Figure (3.8): FTIR spectrum for tris(butylxanthato)chromium(III) complex using (a) KBr (b) CsI discs.



(a)



(b)

Figure (3.10): FTIR spectrum for tris(hexylxanthato)chromium(III) complex using (a) KBr (b) CsI discs.

Table (3.3): Infrared bands of xanthate ligands and their complexes

Compounds	$\nu(\text{C-O-C})\text{cm}^{-1}$	$\nu(\text{C-S})\text{cm}^{-1}$	$\nu(\text{C=S})\text{cm}^{-1}$	$\nu(\text{Cr-S})\text{cm}^{-1}$
<i>PMX</i>	1188	1045	1105	*
<i>Cr(mex)₃</i>	1238	1038	1167	347
<i>PEX</i>	1165	1042	1113	*
<i>Cr(etc)₃</i>	1246	1032	1117	349
<i>PPX</i>	1155	1065	1123	*
<i>Cr(prx)₃</i>	1227	1041	1141	347
<i>PBX</i>	1184	1055	1136	*
<i>Cr(bux)₃</i>	1250	1047	1180	352
<i>PHX</i>	1182	1062	1145	*
<i>Cr(hex)₃</i>	1226	1050	1190	347

* Not found

3.6 Ultraviolet – Visible Spectroscopy

The ultraviolet-visible absorption spectra of potassium alkyl xanthate (PAX) ligands in DMSO were recorded and shown in Figures (3.11a-3.16a). A maximum absorption wavelengths were observed at (450-486nm) of moderate absorbance and off-scale high absorbance reading below 400nm. These transitions may be attributed to $n \rightarrow \pi^*$, and $\pi \rightarrow \pi^*$ electronic transition respectively. The absorbencies of these transitions were employed to follow the decomposition of the complex. Although, the $\pi \rightarrow \pi^*$ transition which occur at shorter wavelength, below 400nm, with very high absorbance reading, for this reason it was

difficult to follow any decrease in the absorbance. Therefore, the decomposition reaction was followed using $n \rightarrow \pi^*$ electronic transitions.

The absorption spectra of tris(alkylxanthato) chromium (III) complexes have shown different absorption wavelength from that of the free ligand as shown in Figures (3.1b-3.16b). These complexes absorbance wavelengths were shifted to different wavelengths than the corresponding bonds in their ligands, which appears in the wavelength range between 310 to 620nm. These values are listed in Table (3.4).

These blue shift may be attributed to the formation of chromium(III) complex which was in agreement with the color of the resultant prepared complexes as shown in Table (3.3) and their FTIR spectra.

The ligand field electronic transitions between the metal d orbitals appear in Cr(III) bands located in the visible region for tris(alkylxanthato)chromium(III) complexes at (576-620nm) assigned to the transition ${}^4A_{2g}(F) \rightarrow {}^4T_{1g}(F)$ and (442-460 nm) assigned to the transition ${}^4A_{2g}(F) \rightarrow {}^4T_{1g}(F)$ and (310-312nm) ${}^4A_{2g}(F) \rightarrow {}^4T_{2g}(P)$. These transitions are showed in Table (3.4).

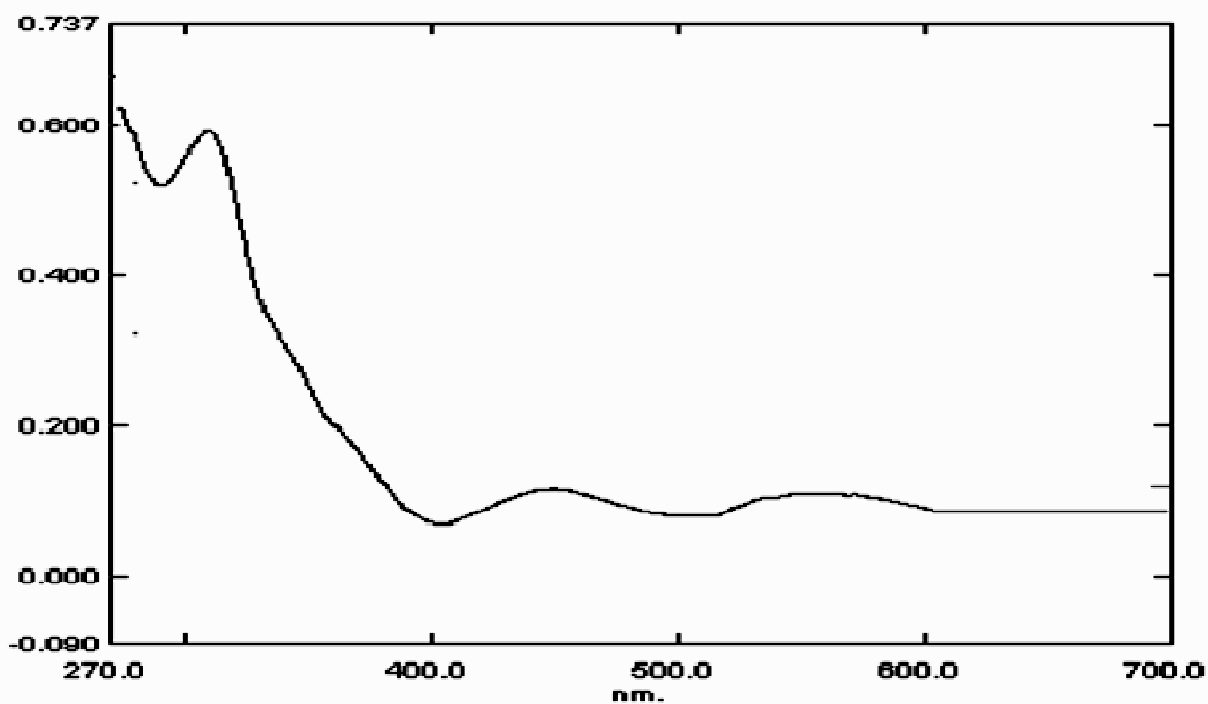
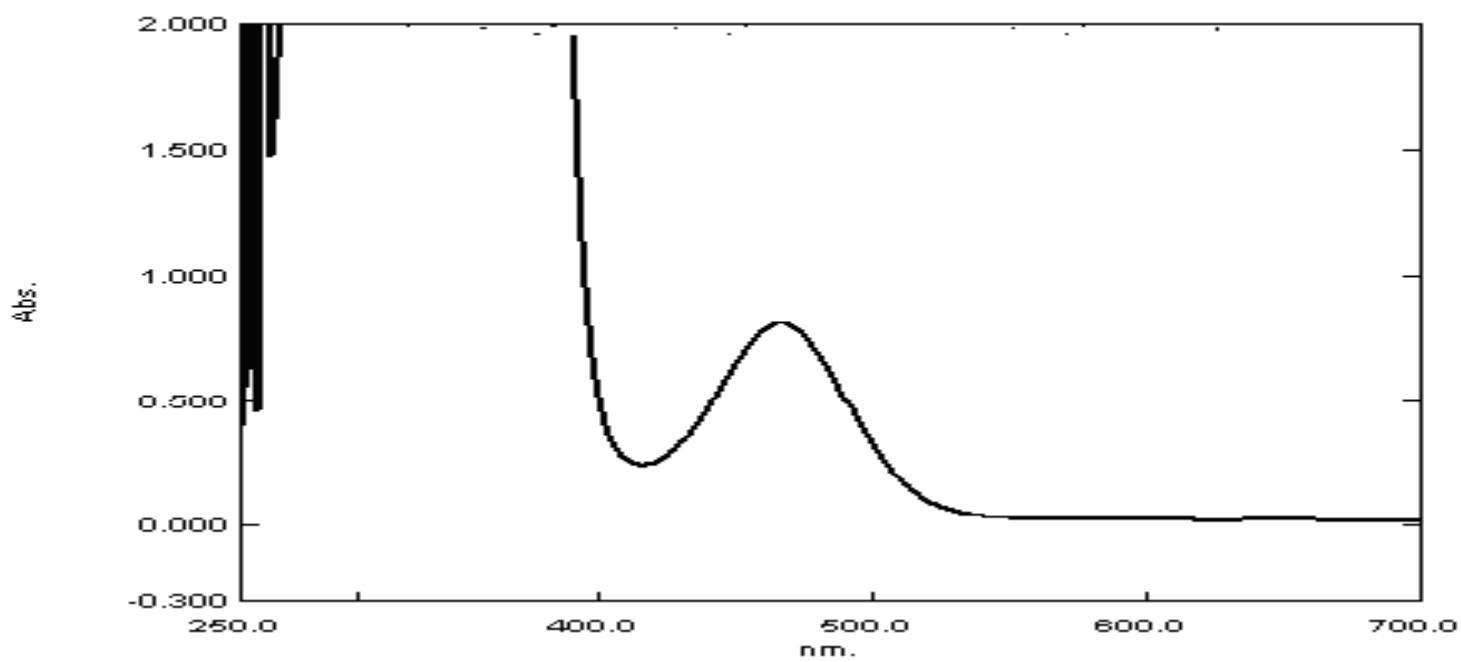


Figure (3. 11): The ultraviolet visible spectrum for a) potassium methyl xanthate and b) tris(methylxanthato)Chromium (III) complex.

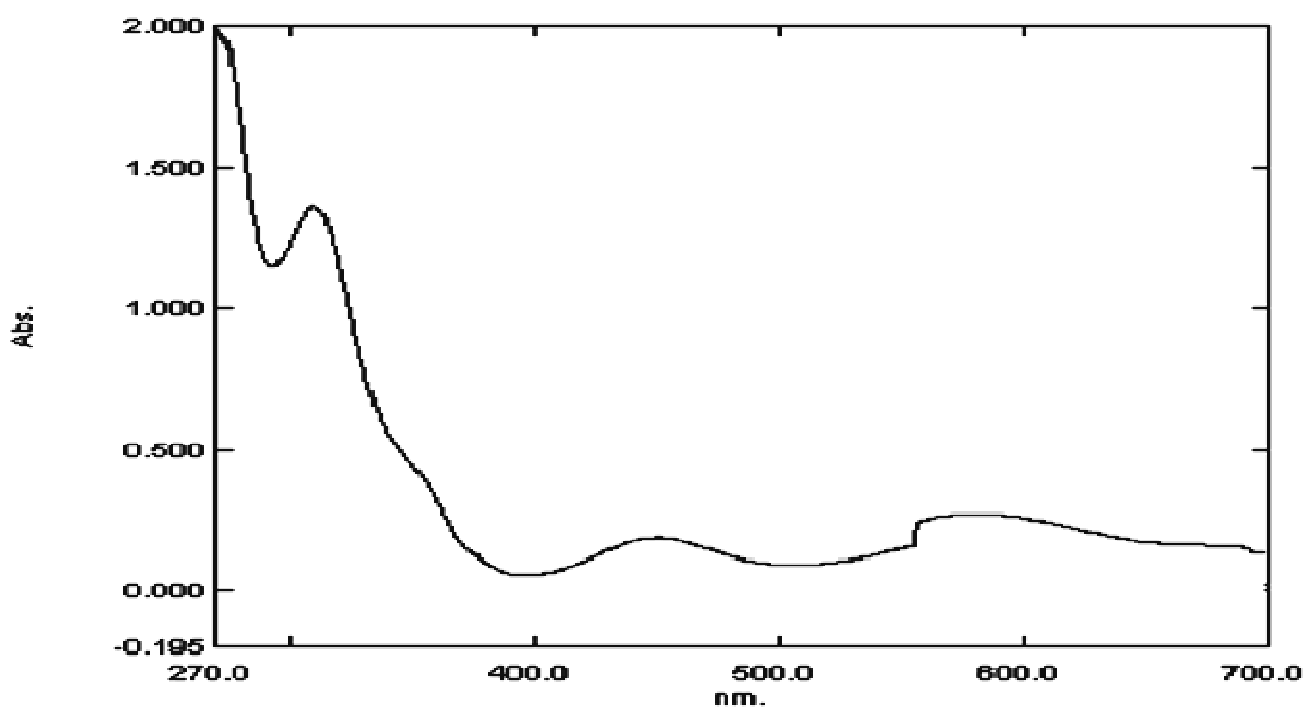
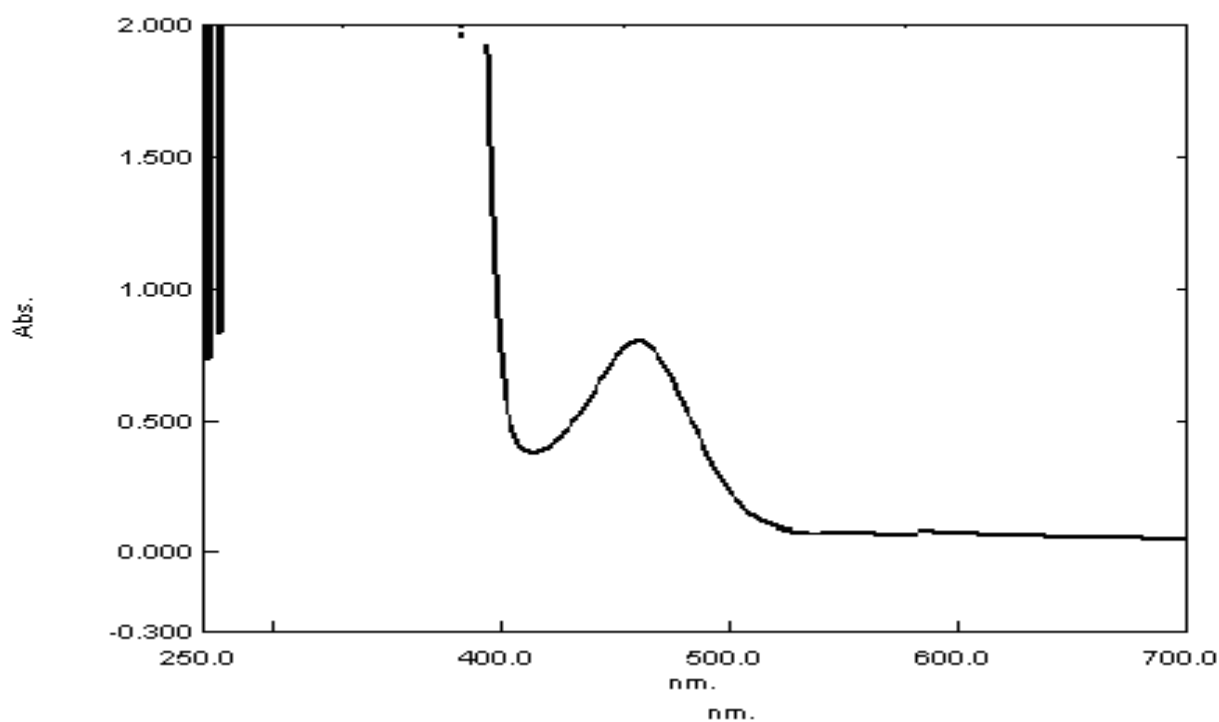


Figure (3. 12): The ultraviolet visible spectrum for a) potassium ethyl xanthate and b) tris(ethylxanthato)Chromium (III) complex.

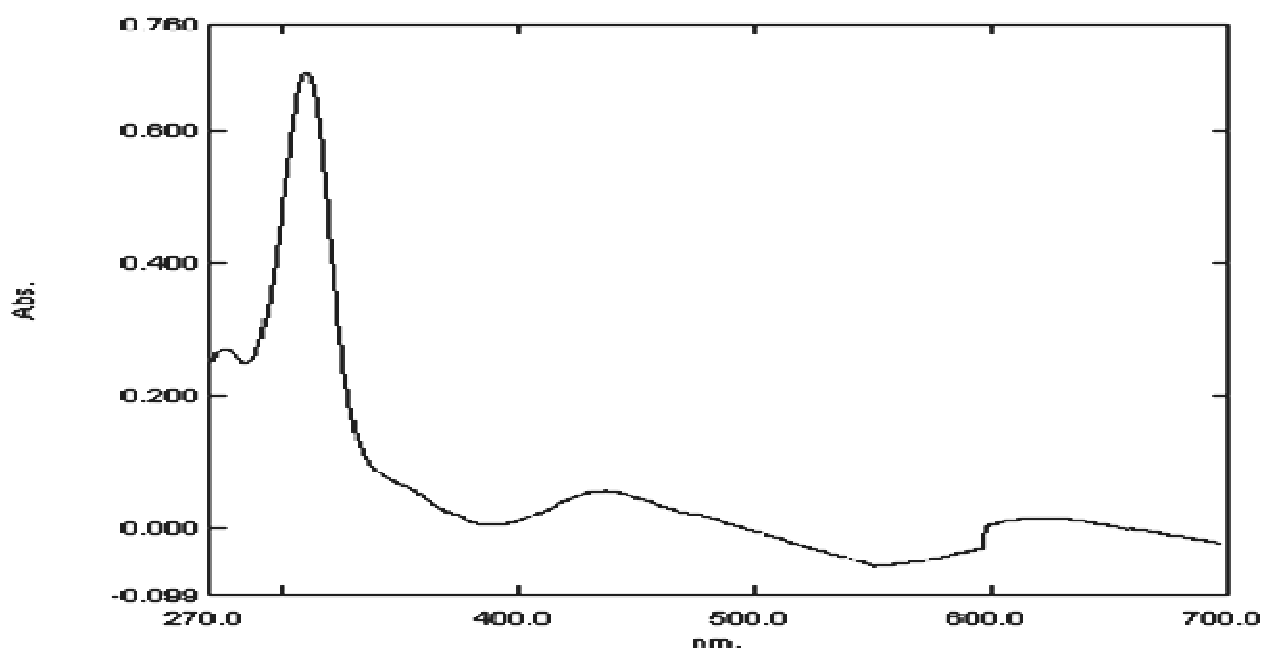
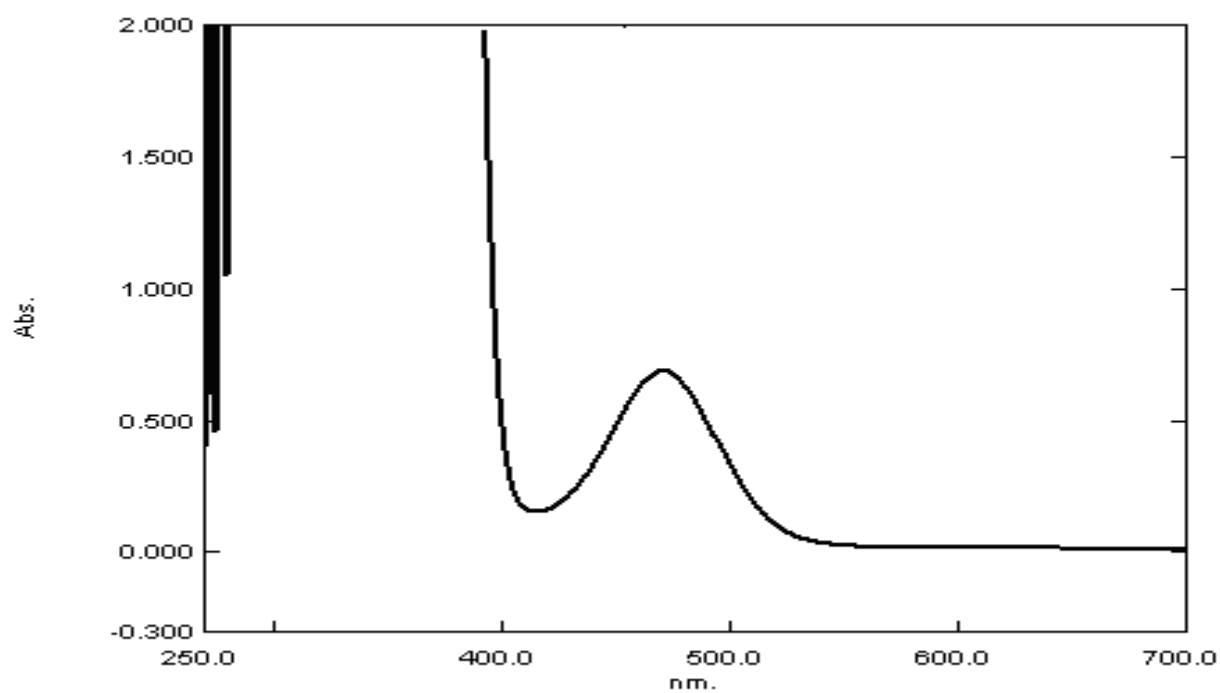
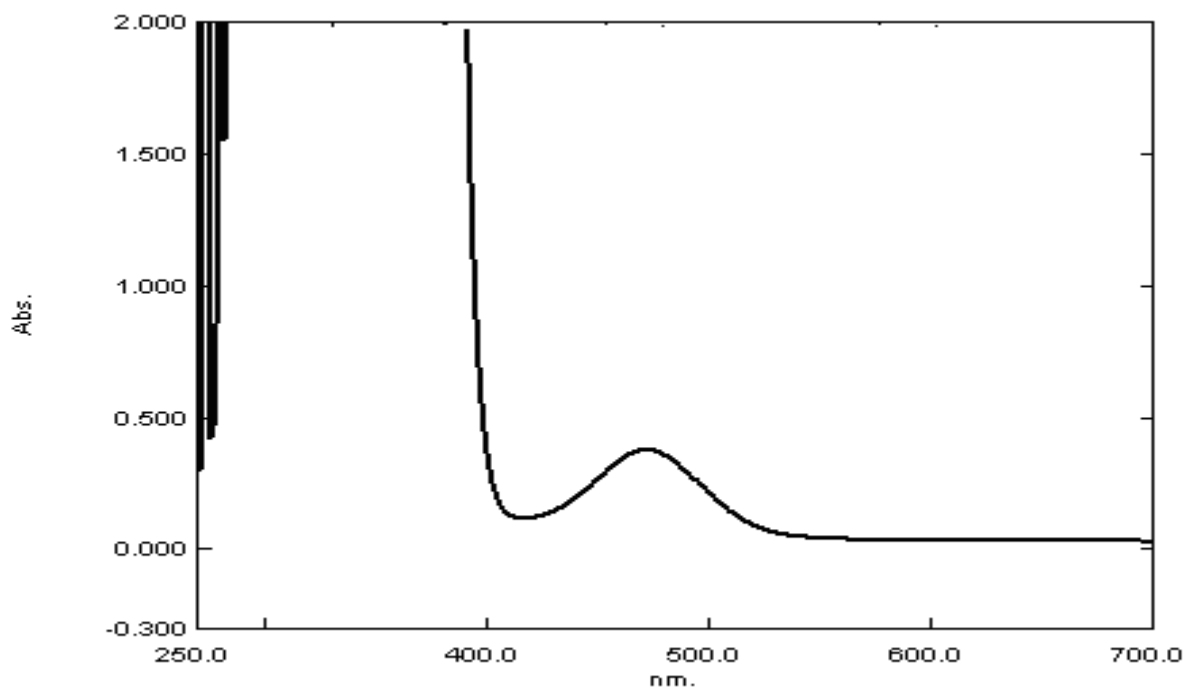
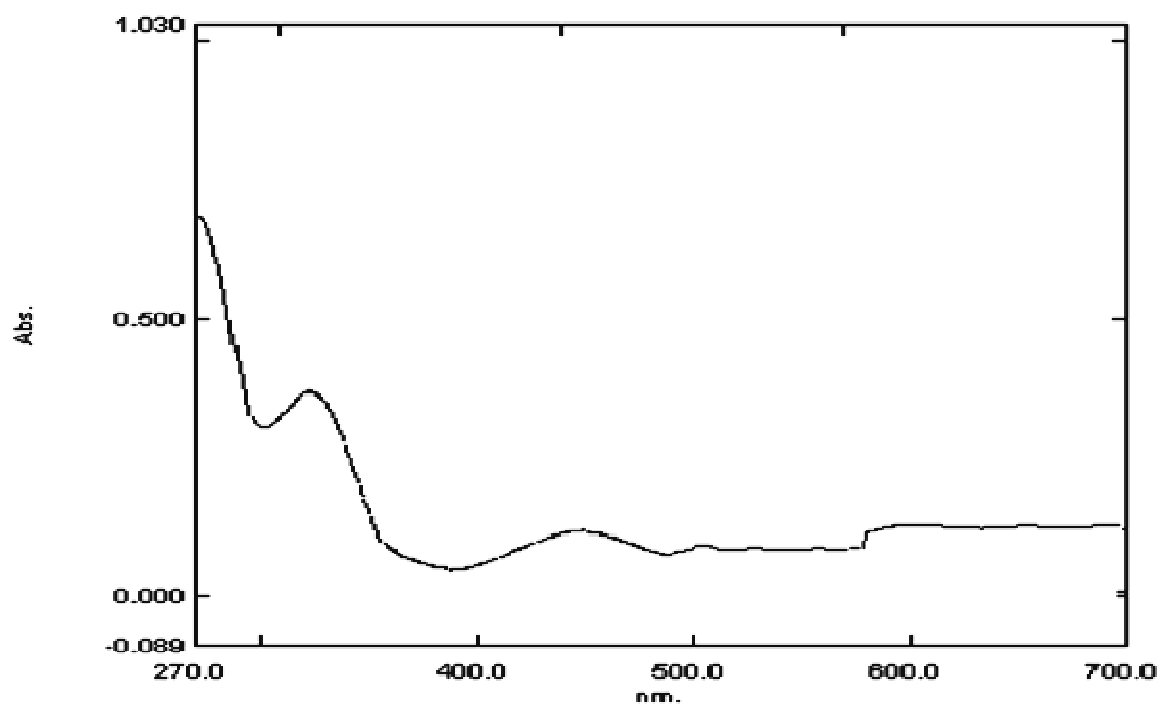


Figure (3. 13): The ultraviolet visible spectrum for a) potassium propyl xanthate and b) tris(isopropylxanthato)Chromium (III) complex.



(a)



(b)

Figure (3. 14): The ultraviolet visible spectrum for a) potassium butyl xanthate and b) tris(butylxanthato)Chromium (III) complex.

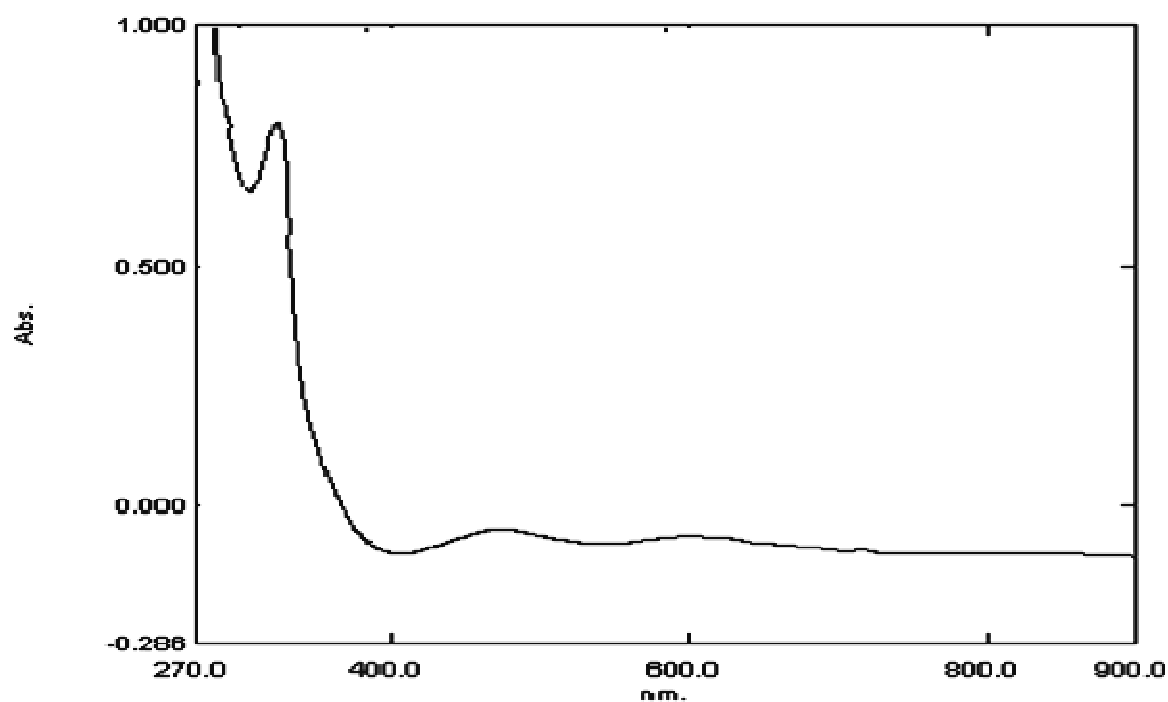
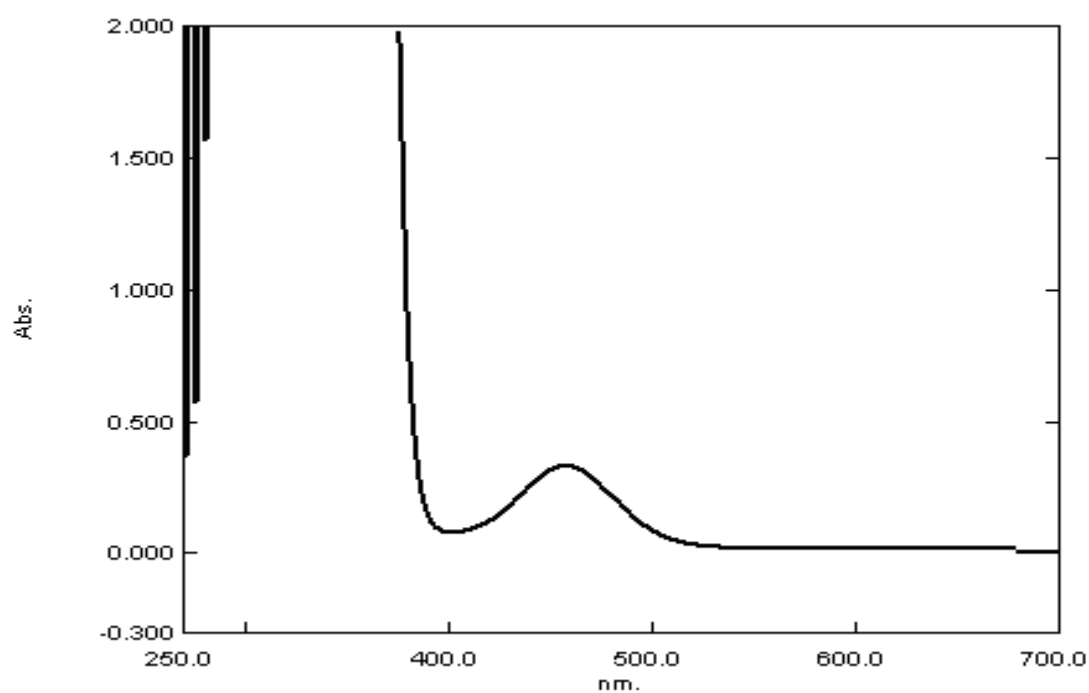


Figure (3. 15): The ultraviolet visible spectrum for a) potassium hexyl xanthate and b) tris(hexylxanthato)Chromium (III) complex.

Table (3.4): Absorption wavelengths of the prepared ligands and their complexes

Ligand complex	wavelength nm(cm^{-1})	Assigned transition
PMX	472(21186)	$n \rightarrow \pi^*$
Cr(mex)₃	590(16949)	${}^4A_{2g}(F) \rightarrow {}^4T_{1g}(F)$
	455(21978)	${}^4A_{2g}(F) \rightarrow {}^4T_{1g}(F)$
	311(32154)	${}^4A_{2g}(F) \rightarrow {}^4T_{2g}(P)$
PEX	478(20921)	$n \rightarrow \pi^*$
Cr(etx)₃	576(17361)	${}^4A_{2g}(F) \rightarrow {}^4T_{1g}(F)$
	450(22222)	${}^4A_{2g}(F) \rightarrow {}^4T_{1g}(F)$
	312(32051)	${}^4A_{2g}(F) \rightarrow {}^4T_{2g}(P)$
PPX	486(20576)	$n \rightarrow \pi^*$
Cr(prx)₃	615(16260)	${}^4A_{2g}(F) \rightarrow {}^4T_{1g}(F)$
	445(22472)	${}^4A_{2g}(F) \rightarrow {}^4T_{1g}(F)$
	310(32258)	${}^4A_{2g}(F) \rightarrow {}^4T_{2g}(P)$
PBX	481(20790)	$n \rightarrow \pi^*$
Cr(bux)₃	603(16584)	${}^4A_{2g}(F) \rightarrow {}^4T_{1g}(F)$
	460(21739)	${}^4A_{2g}(F) \rightarrow {}^4T_{1g}(F)$
	312(32051)	${}^4A_{2g}(F) \rightarrow {}^4T_{2g}(P)$
PHX	465(21505)	$n \rightarrow \pi^*$
Cr(hex)₃	620(16129)	${}^4A_{2g}(F) \rightarrow {}^4T_{1g}(F)$
	442(22624)	${}^4A_{2g}(F) \rightarrow {}^4T_{1g}(F)$
	310(32258)	${}^4A_{2g}(F) \rightarrow {}^4T_{2g}(P)$

3.7 Photodecomposition of tris(alkylxanthato)chromium

(III) complexes

The primary concern was to follow the spectral changes which occurred on irradiation of $\text{Cr}(\text{Ax})_3$ chelate complex in DMSO. UV-visible spectral techniques and FTIR identification methods were used to follow the photodecomposition reaction. The uv-visible spectral technique was also used to determine the rate of photodecomposition of the chelate complexes.

3.8 Spectrophotometric measurements

On irradiation of 5×10^{-5} mol/l $\text{Cr}(\text{Ax})_3$ in DMSO at room temperature, the complex absorption spectrum changes with the irradiation time. A decrease in the absorbance intensity was observed at wavelength of its maximum absorbencies as shown in Figures (3.16-3.20) for ($n \rightarrow \pi^*$) transitions in all prepared complexes. Table (3.5) lists the changes in absorbance (A_t) values with the irradiation time. From these changes in absorbance values during irradiation, one could say that the intra oxidation-reduction reaction occurs with homolytic scission of Cr-S bond and $\overset{\text{II}}{\text{Cr}}(\text{Ax})_2$ was formed.

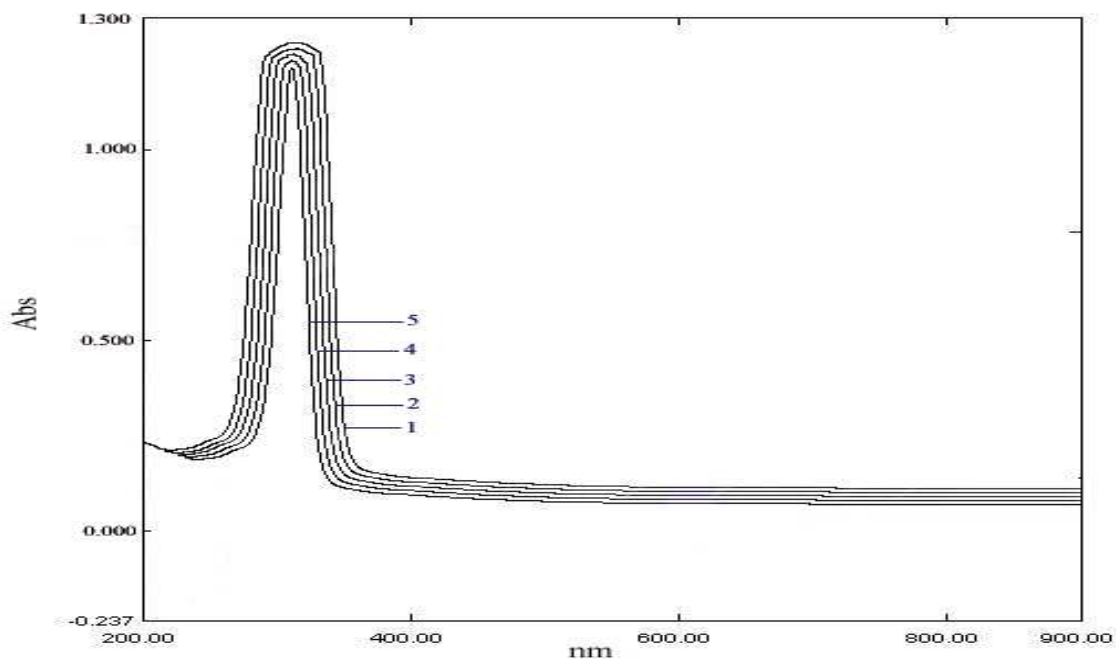
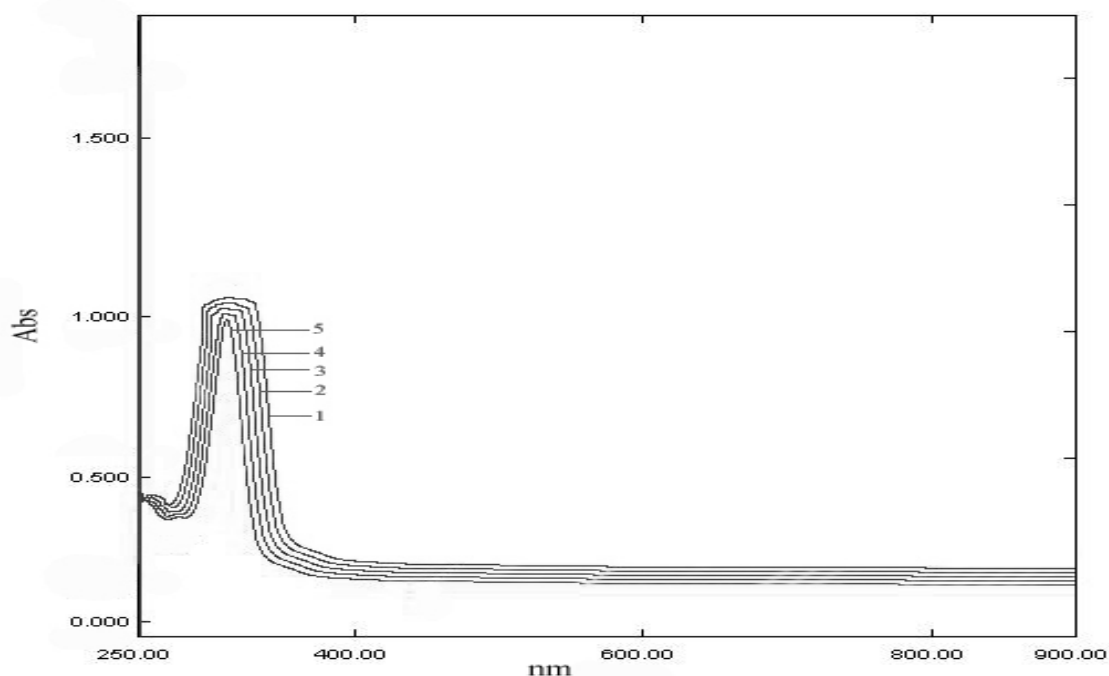


Figure (3.16): Uv-visible spectral changes in the absorbance of Cr(mex)₃ during irradiation; (1) Before irradiation (zero time) (2) After 15 min. (3) After 30 min. (4) After 45 min. (5) After 60 min. irradiation measured at $\lambda_{irr.} = 311\text{nm}$. at room temperature.



Figure(3.17): Uv-visible spectral changes in the absorbance of Cr(etx)₃ during irradiation; (1) Before irradiation (zero time) (2) After 15 min. (3) After 30 min. (4) After 45 min. (5) After 60 min. irradiation measured at $\lambda_{irr.} = 311\text{nm}$. at room temperature.

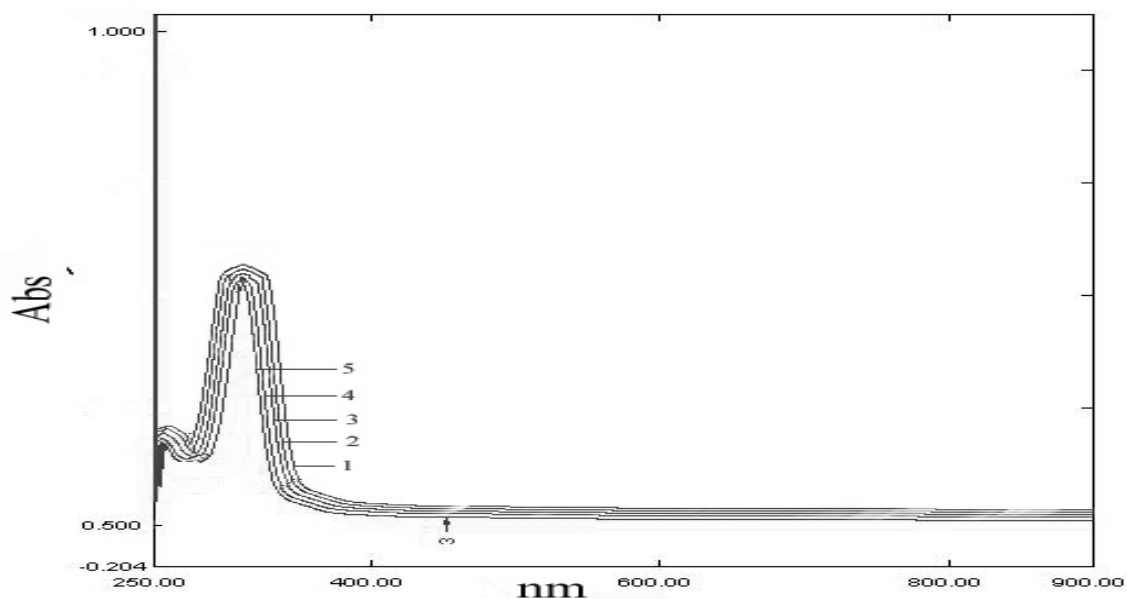


Fig.(3.18): *Uv-visible spectral changes in the absorbance of Cr(prx)₃ during irradiation; (1) Before irradiation (zero time) (2) After 15 min. (3) After 30 min. (4) After 45 min. (5) After 60 min. irradiation measured at $\lambda_{irr.} = 311\text{nm}$. at room temperature.*

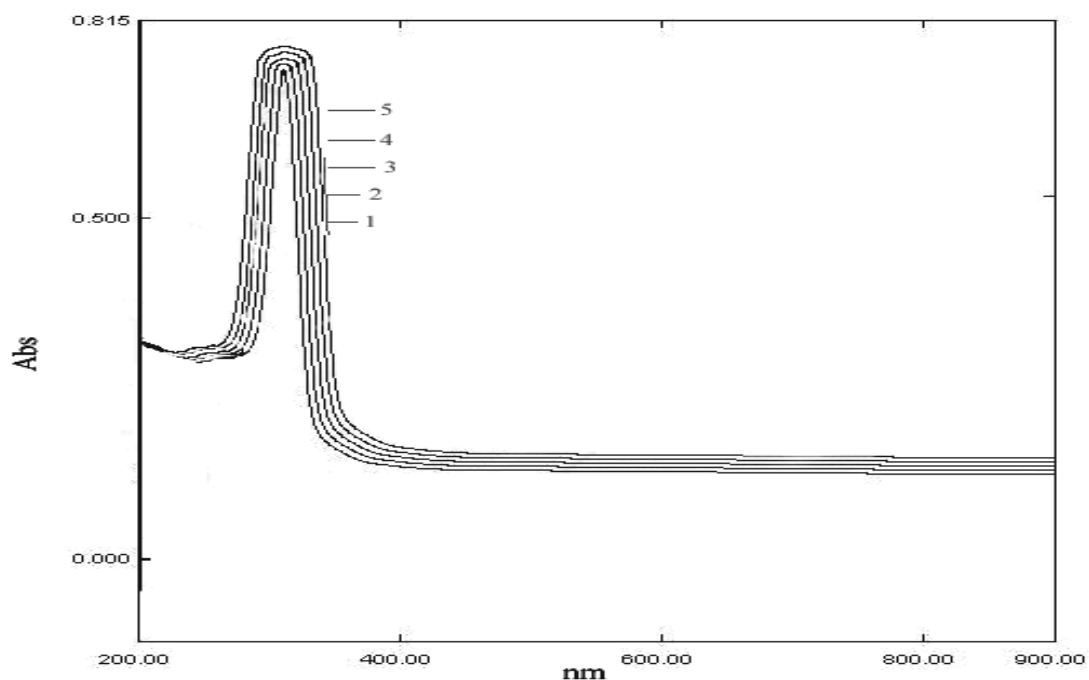


Figure (3.19): *Uv-visible spectral changes in the absorbance of Cr(bux)₃ during irradiation; (1) Before irradiation (zero time) (2) After 15 min. (3) After 30 min. (4) After 45 min. (5) After 60 min. irradiation measured at $\lambda_{irr.} = 311\text{nm}$. at room temperature.*

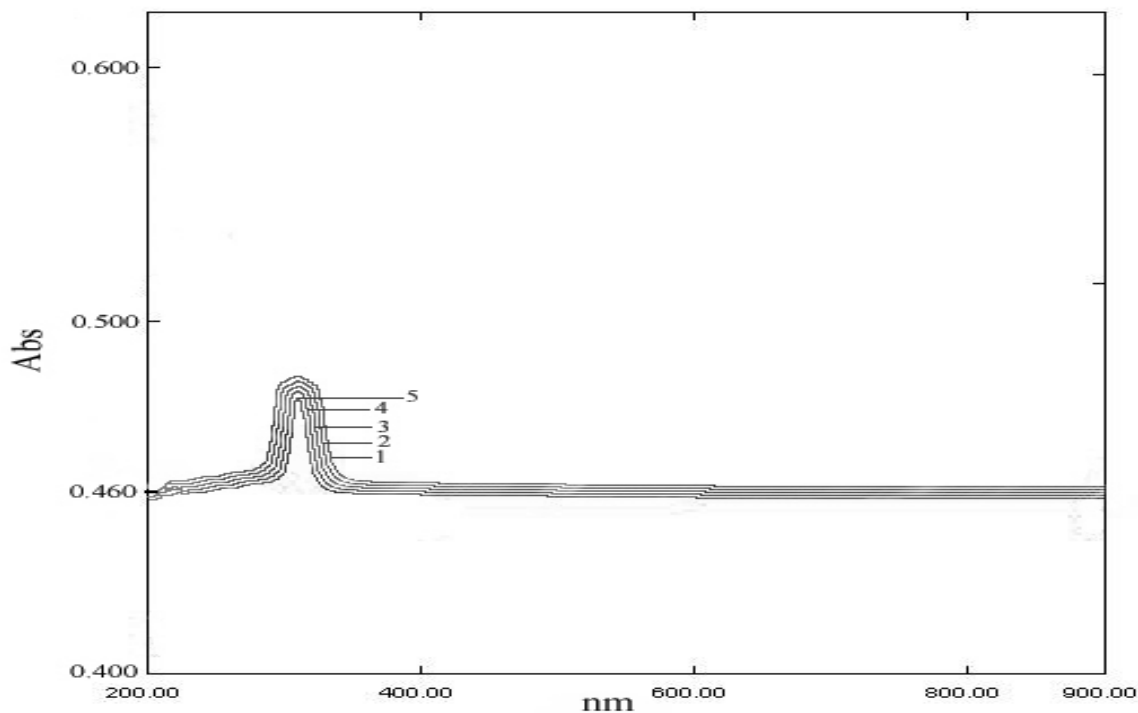


Figure (3.20): Uv-visible spectral changes in the absorbance of $\text{Cr}(\text{hex})_3$ during irradiation; (1) Before irradiation (zero time) (2) After 15 min. (3) After 30 min. (4) After 45 min. (5) After 60 min. irradiation, measured at $\lambda_{\text{irr.}} = 311\text{nm}$, at room temperature.

Table (3.5): Variation of absorbance with irradiation time of the complexes

Irradiation time (sec.)	Absorbance at $\lambda_{\text{irr.}} = 311 \pm 1\text{nm}$ for				
	$\text{Cr}(\text{mex})_3$	$\text{Cr}(\text{etx})_3$	$\text{Cr}(\text{prx})_3$	$\text{Cr}(\text{bux})_3$	$\text{Cr}(\text{hex})_3$
0	1.205	1.037	0.814	0.632	0.459
900	1.134	0.978	0.786	0.616	0.449
1800	1.060	0.930	0.741	0.601	0.441
2700	1.011	0.897	0.717	0.589	0.433
3600	0.959	0.854	0.687	0.580	0.425
4500	0.913	0.818	0.657	0.569	0.418
5400	0.868	0.783	0.630	0.558	0.412

The absorbencies at infinite irradiation (A_∞) of each compound were measured after a period of more than 50 hours. Each absorbance was subtracted from (A_∞) as listed in Tables (3.6 - 3.10). The natural logarithm of each value was taken. To convert the negative values of the resulting logarithm, one was added to each value.

Table (3.6): Natural logarithm of absorbance with irradiation time of $Cr(mex)_3$

Irradiation time(sec.)	A_t	$(A_t - A_\infty)$	$\ln(A_t - A_\infty)$	$1 + \ln(A_t - A_\infty)$
0	1.205	0.897	-0.109	0.891
900	1.134	0.828	-0.191	0.809
1800	1.060	0.752	-0.285	0.715
2700	1.011	0.703	-0.352	0.648
3600	0.959	0.651	-0.429	0.570
4500	0.913	0.605	-0.503	0.497
5400	0.868	0.560	-0.579	0.420
$A_\infty = \text{Absorbance at infinite time} = 0.308$				

Table (3.7): Natural logarithm of absorbance with irradiation time of $Cr(etx)_3$

Irradiation time(sec.)	A_t	$(A_t - A_\infty)$	$\ln(A_t - A_\infty)$	$1 + \ln(A_t - A_\infty)$
0	1.037	0.771	-0.260	0.740
900	0.978	0.712	-0.339	0.660
1800	0.930	0.664	-0.409	0.590
2700	0.897	0.631	-0.460	0.540
3600	0.854	0.588	-0.531	0.469
4500	0.818	0.552	-0.594	0.406
5400	0.783	0.517	-0.659	0.340
$A_\infty = \text{Absorbance at infinite time} = 0.266$				

Table (3.8): Natural logarithm of absorbance with irradiation time of $Cr(prx)_3$

<i>Irradiation time(sec.)</i>	A_t	$(A_t - A_\infty)$	$\ln(A_t - A_\infty)$	$1 + \ln(A_t - A_\infty)$
0	0.814	0.604	-0.540	0.496
900	0.786	0.576	-0.551	0.448
1800	0.741	0.531	-0.633	0.367
2700	0.717	0.507	-0.679	0.320
3600	0.687	0.477	-0.740	0.260
4500	0.657	0.447	-0.805	0.195
5400	0.630	0.460	-0.867	0.133
$A_\infty = \text{Absorbance at infinite time} = 0.210$				

Table (3.9): Natural logarithm of absorbance with irradiation time of $Cr(bux)_3$

<i>Irradiation time(sec.)</i>	A_t	$(A_t - A_\infty)$	$\ln(A_t - A_\infty)$	$1 + \ln(A_t - A_\infty)$
0	0.632	0.480	-0.734	0.266
900	0.616	0.464	-0.768	0.233
1800	0.601	0.449	-0.800	0.200
2700	0.589	0.437	-0.828	0.172
3600	0.580	0.426	-0.849	0.151
4500	0.569	0.417	-0.875	0.125
5400	0.558	0.406	-0.901	0.098
$A_\infty = \text{Absorbance at infinite time} = 0.152$				

Table (3.10): Natural logarithm of absorbance with irradiation time of $\text{Cr}(\text{hex})_3$

<i>Irradiation time(sec.)</i>	A_t	$(A_t - A_\infty)$	$\ln(A_t - A_\infty)$	$1 + \ln(A_t - A_\infty)$
0	0.459	0.425	-0.855	0.144
900	0.449	0.415	-0.879	0.120
1800	0.441	0.407	-0.898	0.101
2700	0.433	0.399	-0.919	0.081
3600	0.425	0.391	-0.939	0.061
4500	0.418	0.384	-0.957	0.043
5400	0.412	0.376	-0.973	0.027

$A_\infty = \text{Absorbance at infinite time} = 0.034$

These values were then plotted against irradiation time, as shown in Figures (3.21-3.25). The slopes of these plots represent the inverse photodecomposition rate constant (K_d) of each complex.

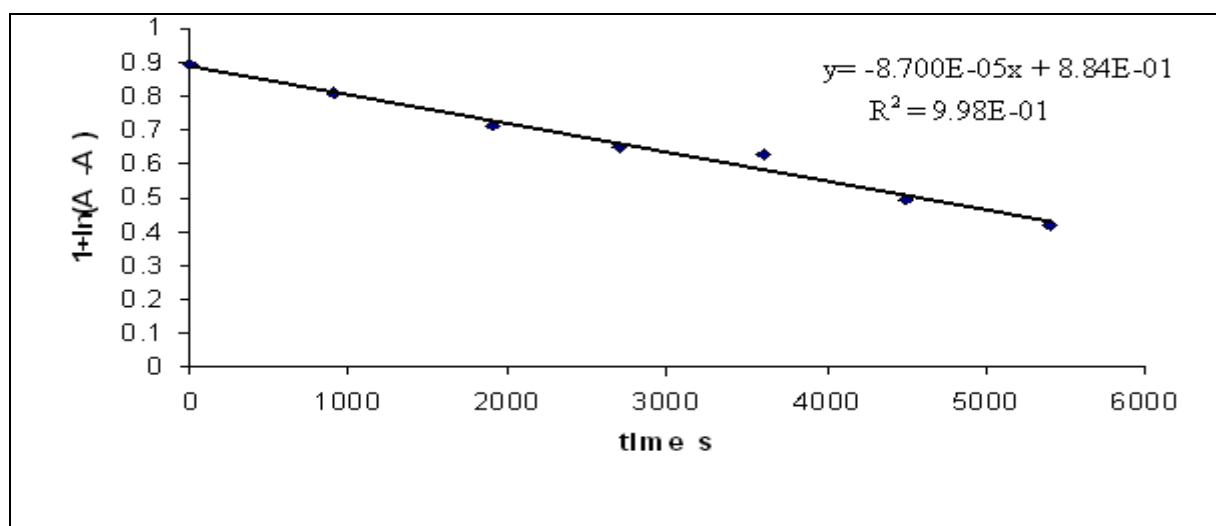


Figure (3.21): Plot of natural logarithm of absorbance against irradiation time for $\text{Cr}(\text{mex})_3$

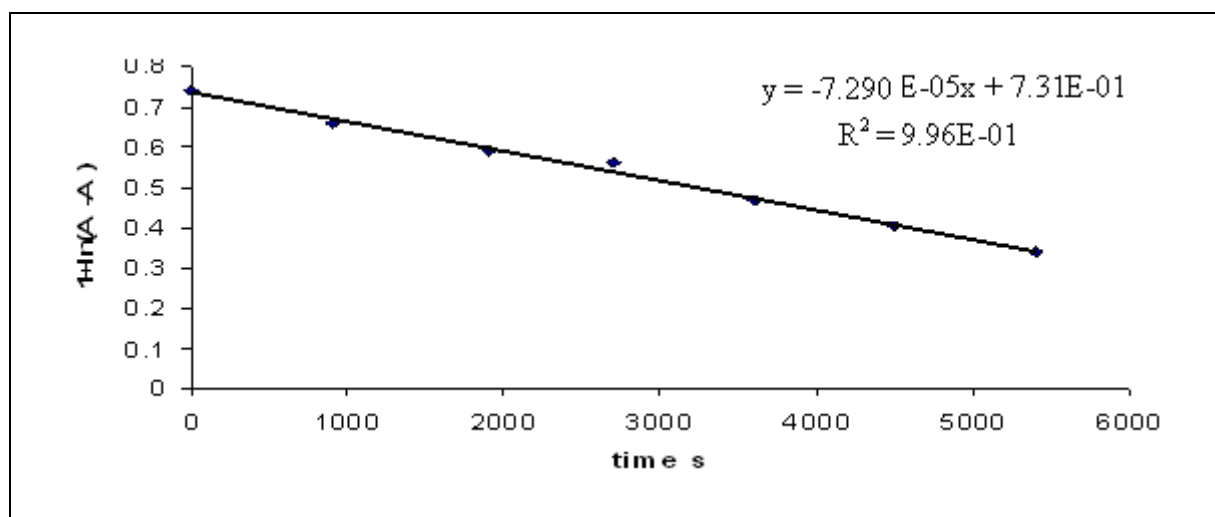


Figure (3.22:) Plot of natural logarithm of absorbance against irradiation time for Cr(etx)_3 .

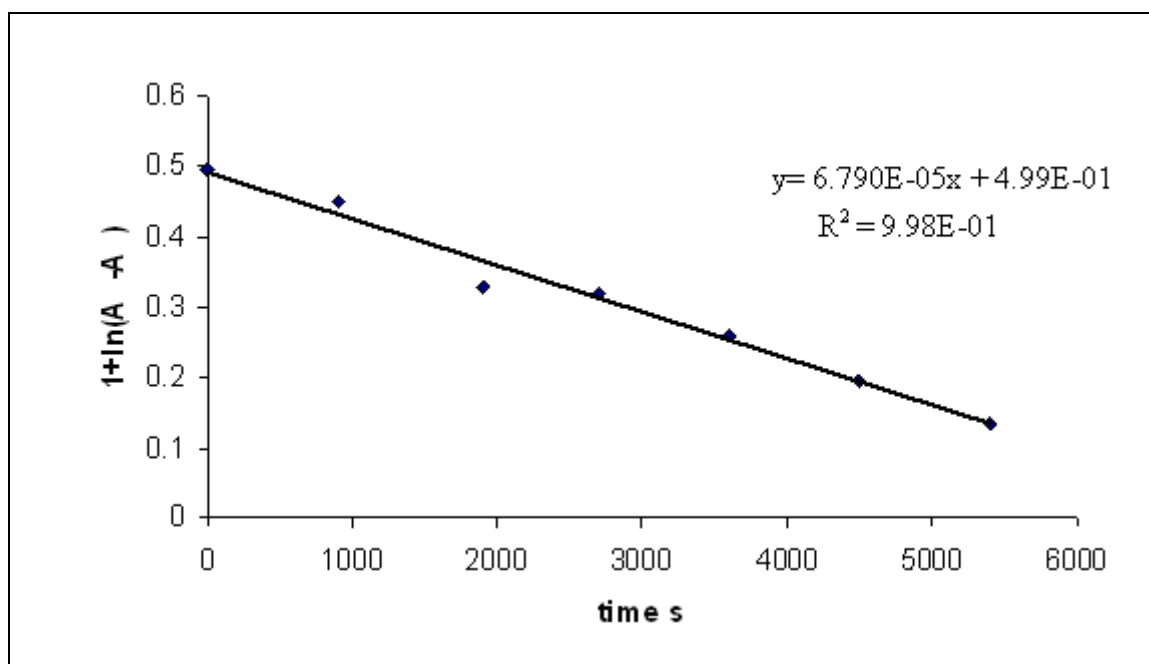


Figure (3.23): Plot of natural logarithm of absorbance against irradiation time for Cr(prx)_3 .

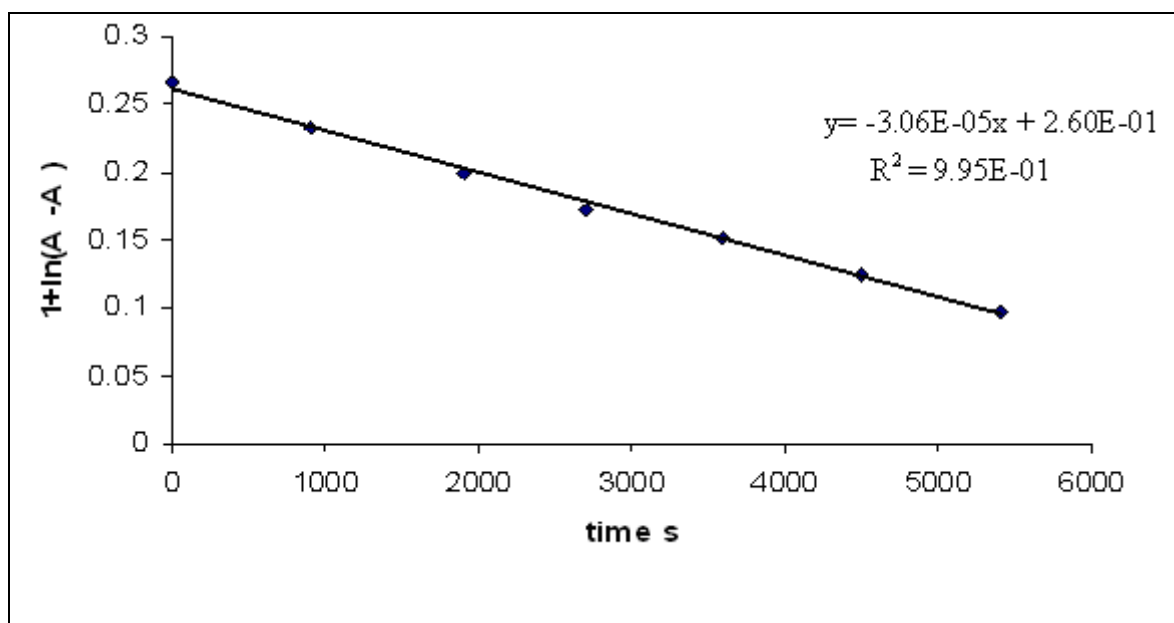


Figure (3.24:) Plot of natural logarithm of absorbance against irradiation time for $Cr(bux)_3$.

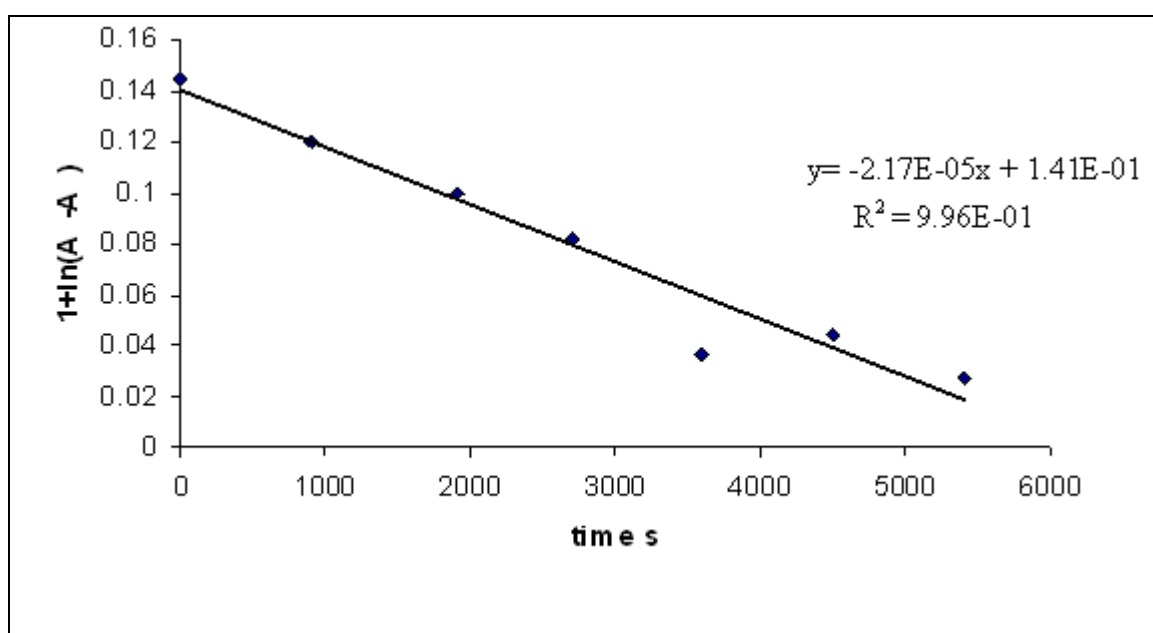


Figure (3.25): Plot of natural logarithm of absorbance against irradiation time for $Cr(hex)_3$.

3.9 Kinetic of the photodecomposition reactions using uv-visible spectrophotometric measurements

The change in the uv-visible absorptions spectra during irradiation were monitored through the photolysis experiments. The decay of tris(alkylxanthato)chromium(III) complexes during the irradiation at 311 ± 1 nm, was followed by the change in the chelate concentration spectrophotometrically. In order to determine the rate of photodecomposition of $\text{Cr}(\text{Ax})_3$ complexes. From this change, it was found that the value of $(A_t - A_\infty)$ decreased exponentially with irradiation time corresponding to the first order chelate decomposition and was consistent with first order reaction.

At wavelength 311 ± 1 nm, the value of $|A_t - A_\infty|$ decreased exponentially with irradiation time as summarized in Figure(3.26) for the variation of $1 + \ln(A_t - A_\infty)$ with irradiation time (t) of $\text{Cr}(\text{Ax})_3$ complexes. The straight lines are consistent with the first order chelate decomposition processes. Therefore, from the slopes of these straight lines, the values of specific rate constants (K_d) were evaluated. Using the value of (K_d), the rate of photodecomposition were calculated ($\text{Rate} = K_d [\text{Concentration of } \text{Cr}(\text{Ax})_3]$) and the quantum yield of this process is deduced.

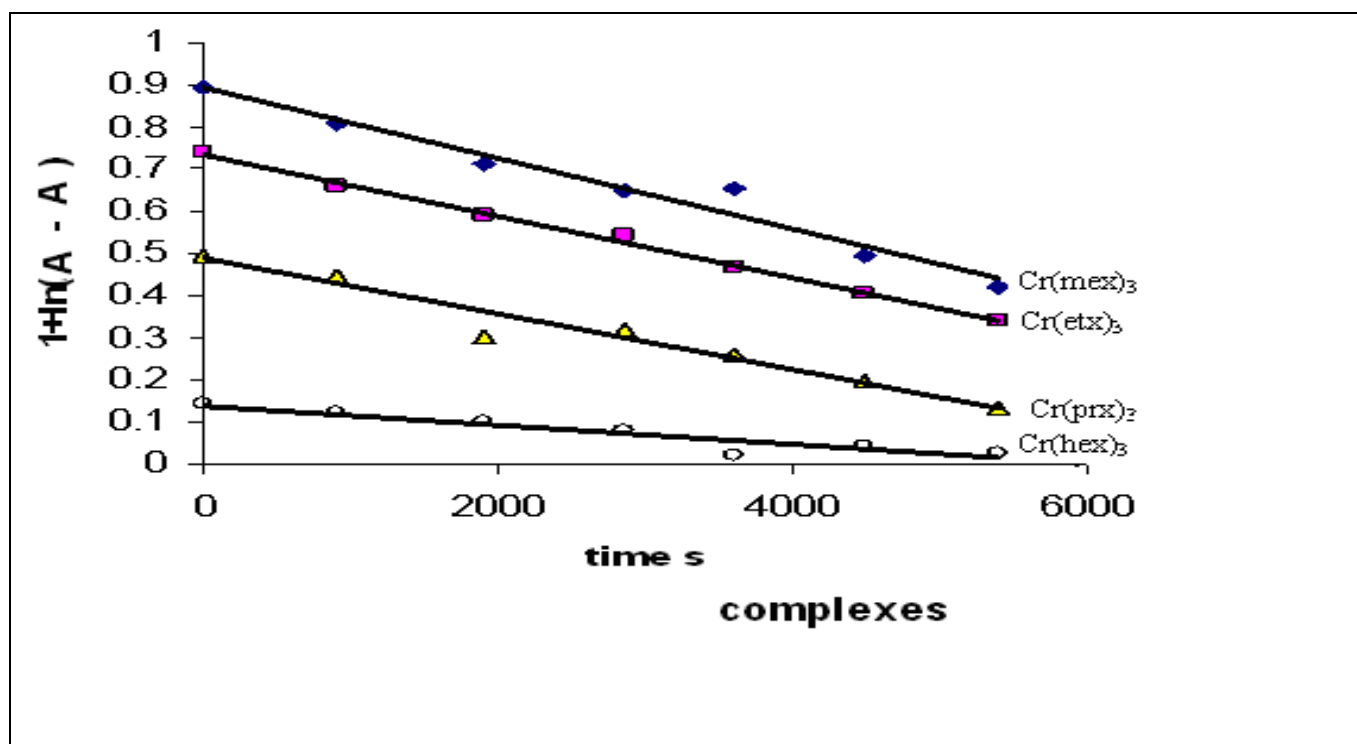


Figure (3.26): Variation of natural plot logarithm of absorbance with irradiation time of the $Cr(Ax)_3$ complexes in DMSO ($\lambda_{irr} = 311 \pm 1$ nm. at room temperature).

The following kinetic equilibria⁽⁷⁵⁾ might be followed for the reactions in equation (3.1) of scheme (3.1) :

$$-\frac{d[Cr(Rx)_3]^*}{dt} = I_{abs} - K_{-1} [Cr(Rx)_3]^* \quad (3.3)$$

Where I_{abs} is absorbed intensity radiation. I_0 and I_{abs} of DMSO were calculated using equation (2.1) and found to be equal to 1.3891×10^{-5} Ein.l⁻¹.S⁻¹ and 5.114×10^{-7} Ein.l⁻¹.S⁻¹, respectively. These values were used in the calculation of the quantum yield according to equation (3.4):

$$Q_d = \text{rate of photodecomposition} / I_{abs} \quad (3.4)$$

Since the rate of excited state decomposition can be expressed as in equation (3.5) is:

$$-\frac{d[\text{Cr}(\text{Rx})_3]^*}{dt} = I_{\text{abs}} - K_2 [\text{Cr}(\text{Rx})_3]^* - K_{-1} [\text{Cr}(\text{Rx})_3]^* \quad (3.5)$$

Assuming that the $[\text{Cr}(\text{Rx})_3]^*$ excited state concentration is fixed, then:

$$[\text{Cr}(\text{Rx})_3]^* = \frac{I_{\text{abs}}}{K_{-1} + K_2} \quad (3.6)$$

The value of excited state concentration, $[\text{Cr}(\text{Rx})_3]^*$, in equation (3.6) is substituted in equation (3.3), one can get:

$$\begin{aligned} -\frac{d[\text{Cr}(\text{Rx})_3]}{dt} &= I_{\text{abs}} - \frac{I_{\text{abs}} K_{-1}}{K_{-1} + K_2} \\ &= I_{\text{abs}} \left(1 - \frac{K_{-1}}{K_{-1} + K_2} \right) \end{aligned} \quad (3.7)$$

Then equation (3.4) can take the form:

$$Q_d = \frac{\text{Rate of photodecomposition}}{I_{\text{abs}}} = -\frac{d[\text{Cr}(\text{Rx})_3]}{dt} / I_{\text{abs}} \quad (3.8)$$

The value of quantum yield of photodecomposition (Q_d) can then be given by equation (3.9):

$$Q_d = 1 - \frac{K_{-1}}{K_{-1} + K_2} \quad (3.9)$$

or

$$Q_d = \frac{K_2}{K_{-1} + K_2} \quad (3.10)$$

By rearranging equation (3.9) and equation (3.10), we can obtain equation (3.11) for the value of reactivity ratio (K_2 / K_{-1}).

$$\frac{K_2}{K_{-1}} = \frac{Q_d}{1 - Q_d} \quad (3.11)$$

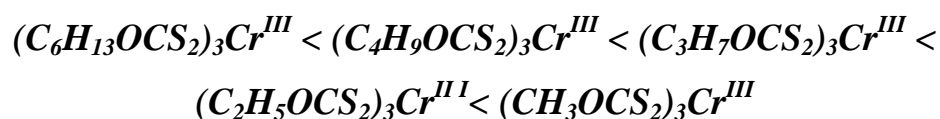
Equation (3.11) was used to calculate the reactivity ratio of the photodecomposition of $\text{Cr}(\text{Ax})_3$ in DMSO. These values are listed in Table (3.11). The results of Table (3.11) for the reactivity ratio indicated that these values decreased as the number of CH_3 -group in complexes increased and that should be expected since the value of Q_d decreased in the same manner. This also may be explained as the number of methyl group in complexes decreased, the excitation of the complex become much easier, i.e., the probability of excitation (ϵ) became larger compared to longer saturated alkyl chain⁽¹¹¹⁾. However, the small difference in the above values between the ethyl and the isopropyl group ligands may be due to the similarity in the spacial configuration of the two-alkyl group. Therefore, the concentration of the populated excited state will be larger for the small alkyl containing complexes (equation 3.1 in mechanism Scheme (3.1)). Consequently, the photodecomposition step (K_2) which dependent on the concentration of excited state will be larger for the less number alkyl group containing complexes.

Table (3.11): Specific rate constant (K_d), photodecomposition constant (R_d), the quantum yield (Q_d) and the reactivity ratio (K_r) for different complexes in DMSO (Irradiation wavelength 311 ± 1).

Complexes	Concentration $10^{-5}M$	K_d $10^{-5} s^{-1}$	R_d $10^{-9} s^{-1}M$	Q_d 10^{-3}	K_r 10^{-3}
$Cr(mex)_3$	5.000	8.700	4.350	7.702	7.762
$Cr(etx)_3$	5.000	7.290	3.645	6.454	6.496
$Cr(prx)_3$	5.000	6.790	3.395	6.011	6.047
$Cr(bux)_3$	5.000	3.060	1.530	2.709	2.716
$Cr(hex)_3$	5.000	2.170	1.080	1.921	1.925

From the results shown in Table (3.11), one could notice that K_d and Q_d values were dependent on the number of CH_3 - group in the complexes.

The photodecomposition increased as the number of CH_3 - group in the complexes decrease. Also the rate constant and quantum yield decrease from the higher number of CH_3 - group as in hexane complex (1.925×10^{-3}) compared to the lower number of CH_3 - as in methyl complex (7.762×10^{-3}) following the order:



The effect of the number of CH_3 - group in the complexes on the rate of photodecomposition process is, therefore, correlated with the value of quantum yield. The relationship of the Q_d values for the complexes in DMSO were plotted against the type of complex. The results shown

schematically in Figure(3.27), which indicated that Q_d increases as the number of CH_3 - group in complex decrease.

This shape of Figure (3.27) could be explained by considering that -OR group is electron-withdrawing group that would cause less electron density on the metal ion. The presence of the highly positive center, Cr(III), made the dissociation of this weak adduct that produce a higher quantum yield. This may be explain the observation of higher Q_d of $\text{Cr}(\text{Ax})_3$ complexes in DMSO.

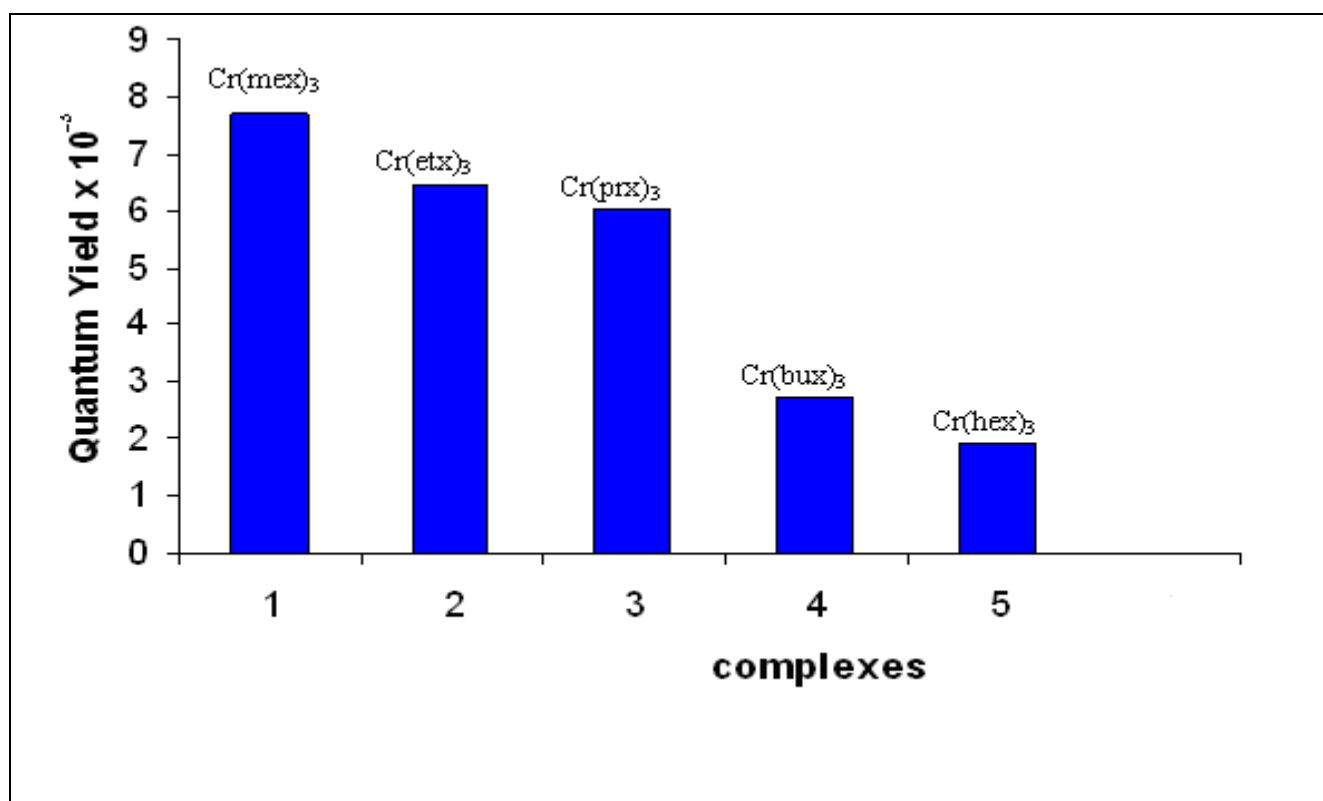
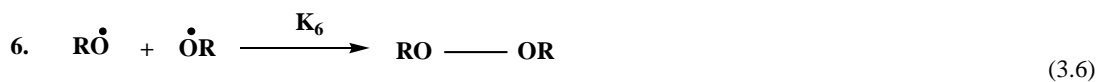
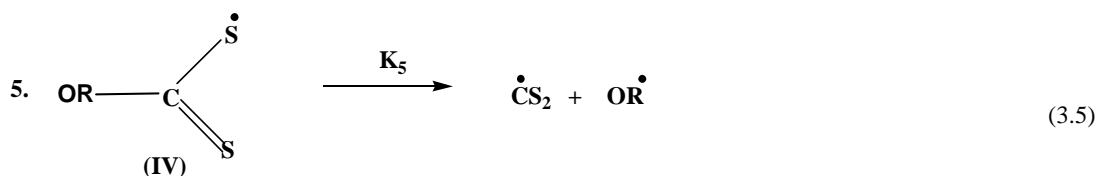
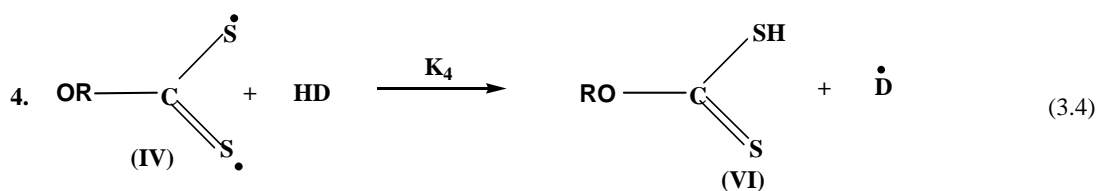
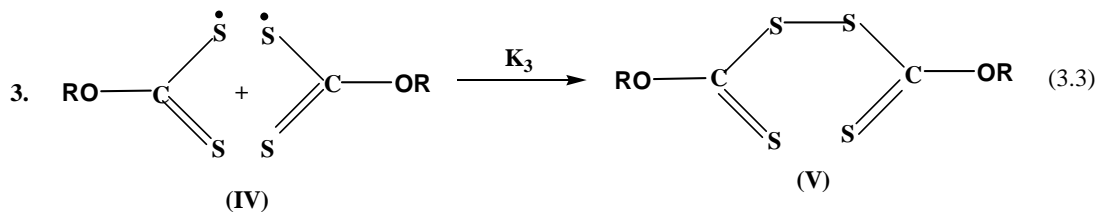
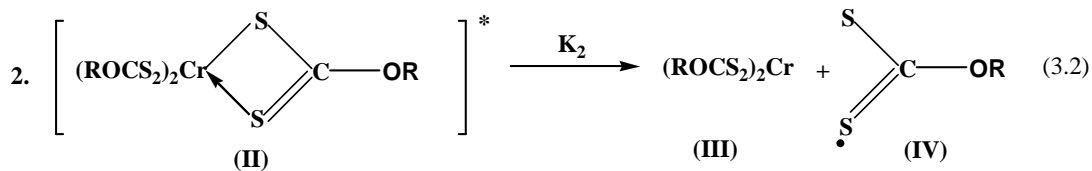
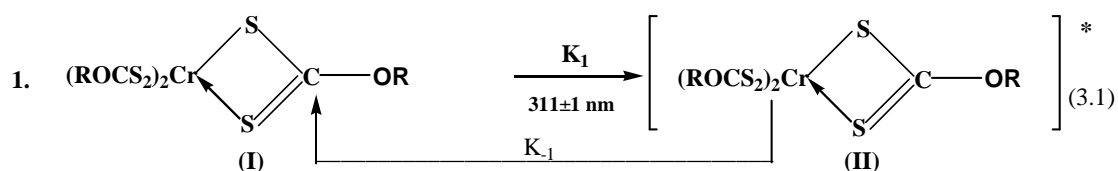


Figure (3.27): Variation in quantum yields (Q_d) with the number of methyl group in complexes for the photodecomposition of $\text{Cr}(\text{Ax})_3$ complex DMSO

3.10 Photolytic Reaction mechanism for the prepared tris(alkylxanthato) chromium (III) Complexes

The mechanism that may be suggested for the photodecomposition processes is shown in Scheme (3.1). The uv-visible spectra of the photolytic products indicated that the primary photolysis step might be the hemolytic scission of a Cr-S bond as shown in equation (3.2). After that, the obtained xanthate radical was rapidly decomposed to CS₂ and R[•] radicals, which were then expected to abstract hydrogen from the solvent (HD) forming alcohol.



Where: $K_{-1}, K_1, K_2, K_3, K_4, \dots$, etc. are the rate constants for the above reactions.

Scheme (3.1): The suggested reaction mechanism for the prepared complexes⁽⁷⁵⁾

The compound (I) has been excited to compound (II) by uv-radiation at $311 \pm 1 \text{ nm}$. The bonds between the chromium atom and the two sulphur atoms in the excited state of this compound break to yield compounds (III) and radical (IV) as shown in equation (3.2). The radical compound (IV) may undergo different radical reactions. It may either recombine to yield the dimer (V), or abstract hydrogen from the solvent (HD) as in equations (3.3) and (3.4), respectively. The bond between the oxygen and carbon may break to yield carbon disulphide and alkoxy radical (equation 3.5). The alkoxy radicals may be combined to yield peroxy as in equation (3.6) or abstract hydrogen from the solvent to yield alcohol (equation 3.7). The solvent radicals produce from equations (3.4) and (3.7) may finally recombine as in equation (3.8). However, these suggestions need further investigation using modern instrumentation such as ESR, mass spectrometry and other spectroscopic and separation techniques to validate the above reactions scheme. The reaction rate constant K_3 , K_4 , K_5 , K_6 , K_7 , and K_8 in equations (3.3-3.8) were very large, since, they involved very reactive radical reactions. However, excitation irradiation reaction in equation (3.1) was assumed to be the slowest step followed by the decomposition reaction in equation (3.2). Consequently, this reaction was considered as the rate-determining step.

Therefore, the dissociation reaction was followed by uv-visible spectrophotometry by measuring the decrease in the absorbance of the prepared tris(alkylxanthato)chromium(III) complexes as will be described thereafter.

3.11 Conclusion Remarks

In the work described in this thesis, the photochemistry of tris(alkylxanthato) chromium (III) complexes in DMSO was studied. The results have suggested that these complexes were photosensitive when irradiated with uv radiation of wavelength 311 ± 1 nm. and decomposed through the scission of the Cr-S bond. The $\text{Cr}(\text{Ax})_3$ complexes after irradiation produced $\text{Cr}^{\text{II}}(\text{Ax})_2$ and $[(\text{CS}_2)\text{OR}]^\cdot$ radical which ultimately decomposed to CS_2 and R^\cdot radical. The latter abstracted hydrogen from solvent molecular to produce alcohol as suggested by the propose mechanism. It was also found that the photochemical reaction is first order accordingly. The specific rate constants (K_d) at room temperature, were evaluated by monitoring the spectral changes during irradiation process.

The quantum yield of photodecomposition process is generally low and is greatly affected by the type of ligands in Cr(III) chelate complexes and the number of CH_3 - group. The value of quantum yield of photodecomposition in these complexes increases as the number of CH_3 -group decreased in the order, from $(\text{C}_6\text{H}_{13}\text{OCS}_2)_3\text{Cr}^{\text{III}}$, $(\text{C}_4\text{H}_9\text{OCS}_2)_3\text{Cr}^{\text{III}}$, $(\text{C}_3\text{H}_7\text{OCS}_2)_3\text{Cr}^{\text{III}}$, $(\text{C}_2\text{H}_5\text{OCS}_2)_3\text{Cr}^{\text{III}}$, to $(\text{CH}_3\text{OCS}_2)_3\text{Cr}^{\text{III}}$

It is well established that transition metal chelate are photochemically active in polymer photochemistry. These complexes might be useful in many applications. Moreover, as mentioned earlier, metal chelate with metals at high oxidation state is active in the enhancement of photodegradation of plastic and therefore, might serve as photocatalyst to treat the plastic waste pollution problem.

3.12 Suggestion for future work

- 1- It is recommended to study the photodecomposition reactions of these and other complexes using modern instrumentation as mentioned above.
- 2- The use of different metal complexes to compare the photodecomposition of these metals.
- 3- The use of unsaturated, phenyl and other aromatic compounds instead of alkyl group to compare their photodecomposition constants and other values.
- 4- Study the effect of polar and nonpolar solvent on the photodecomposition reactions.
- 5- Using these complexes as photoinitiator for polymerization process might be good extension of the present work.

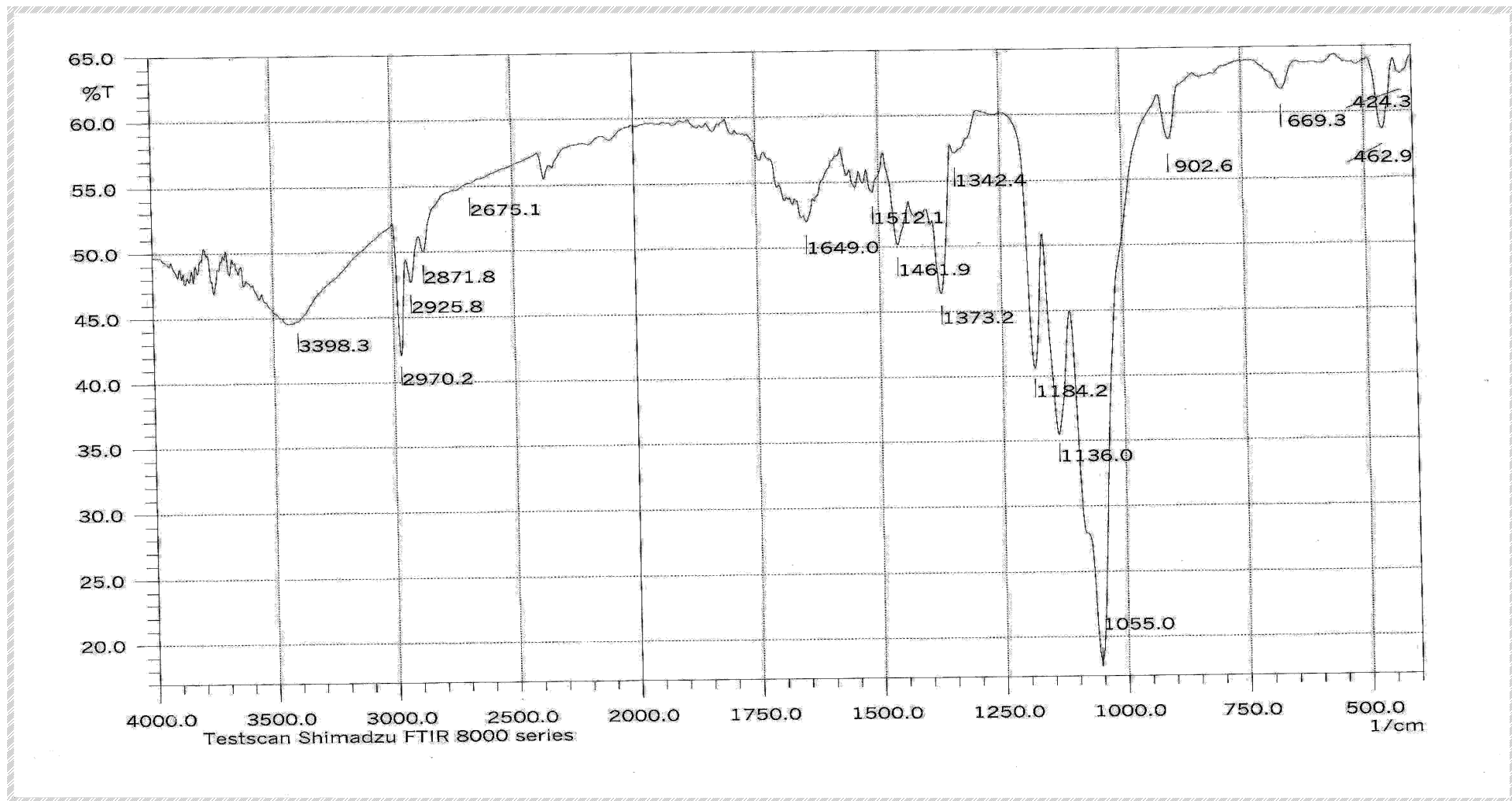


Figure (3.7): FTIR spectrum for potassium butyl xanthate ligand (PBX)

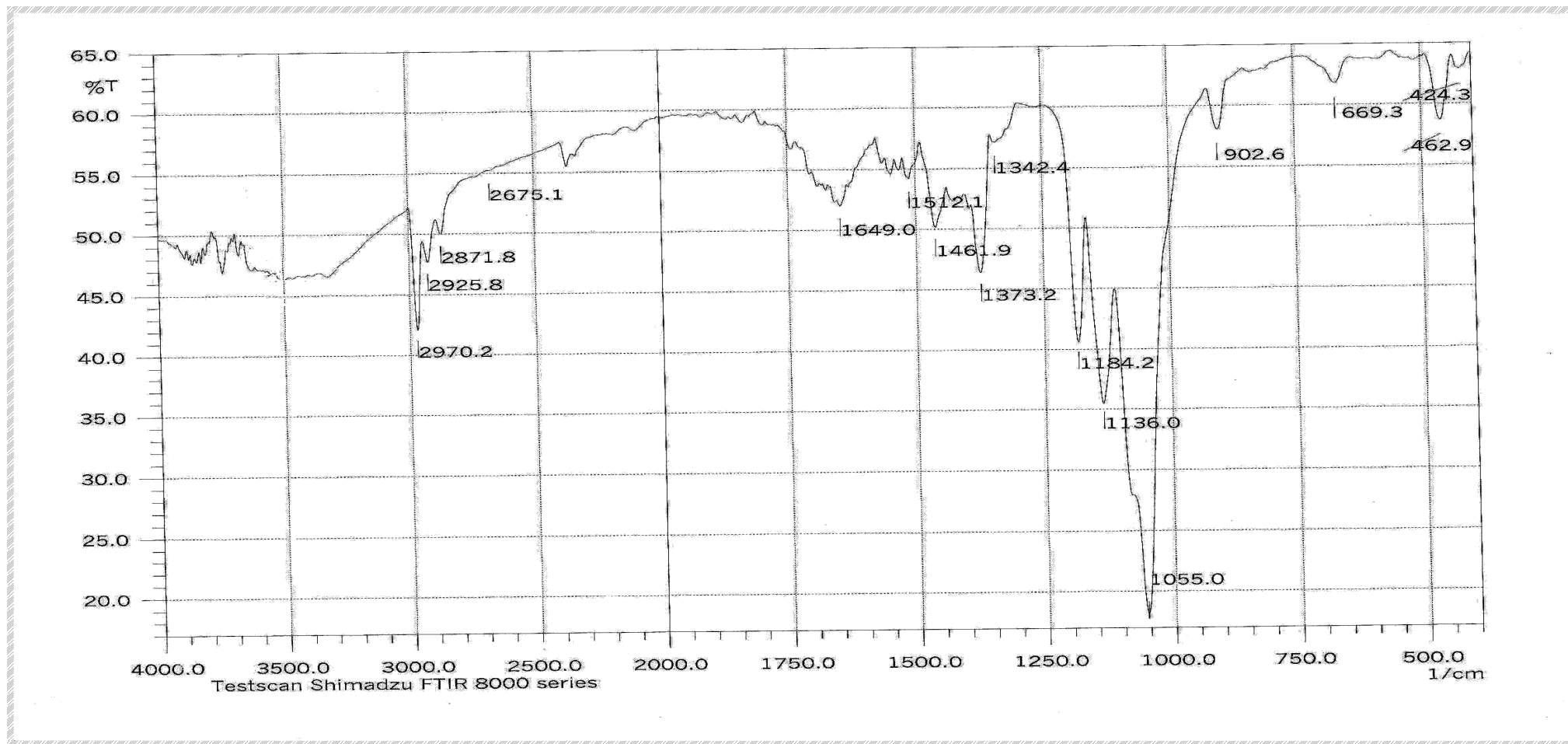


Figure (3.7): FTIR spectrum for potassium butyl xanthate ligand (PBX)

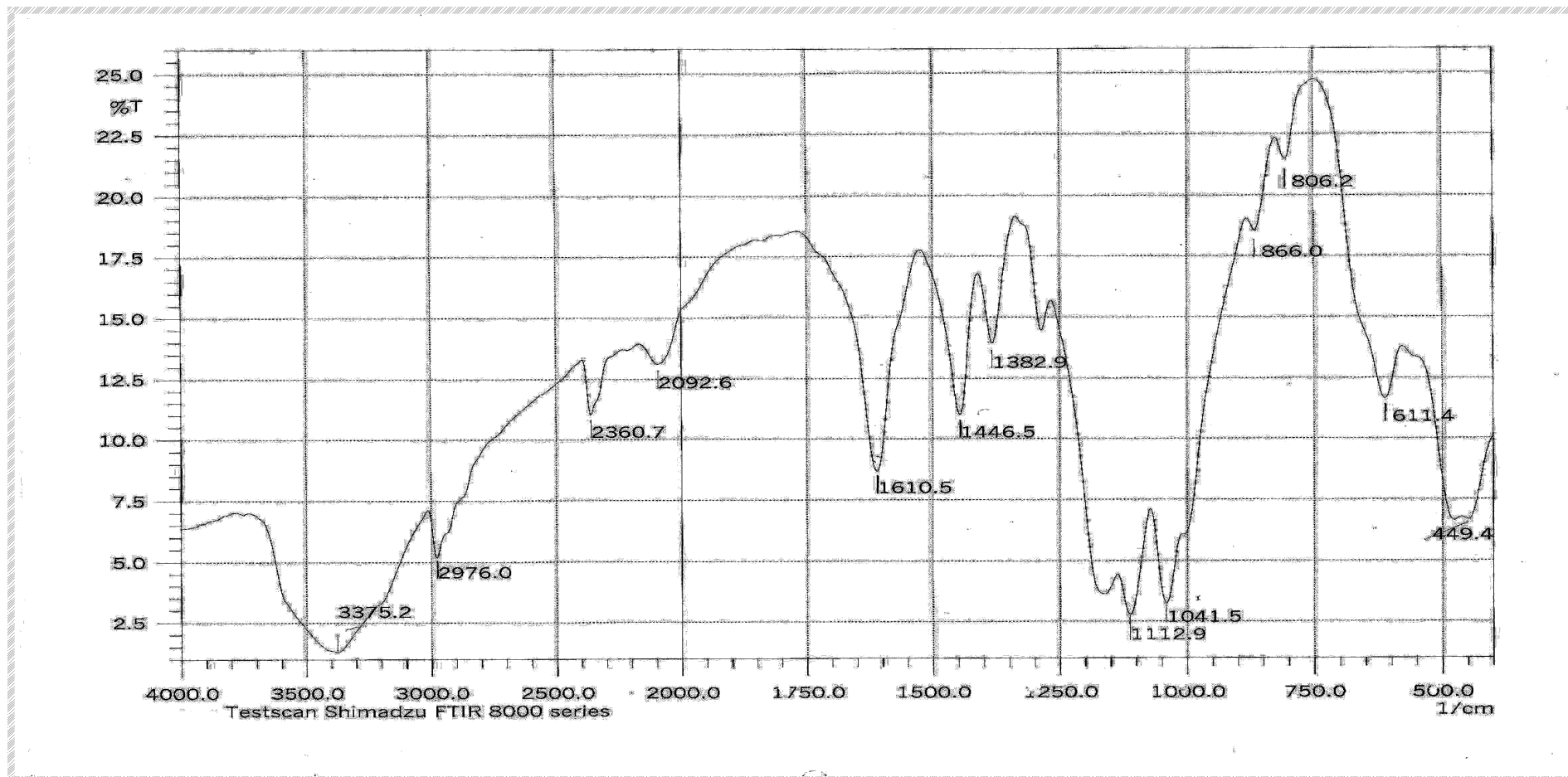


Figure (3.3): FTIR spectrum for potassium ethyl xanthate ligand (PEX)

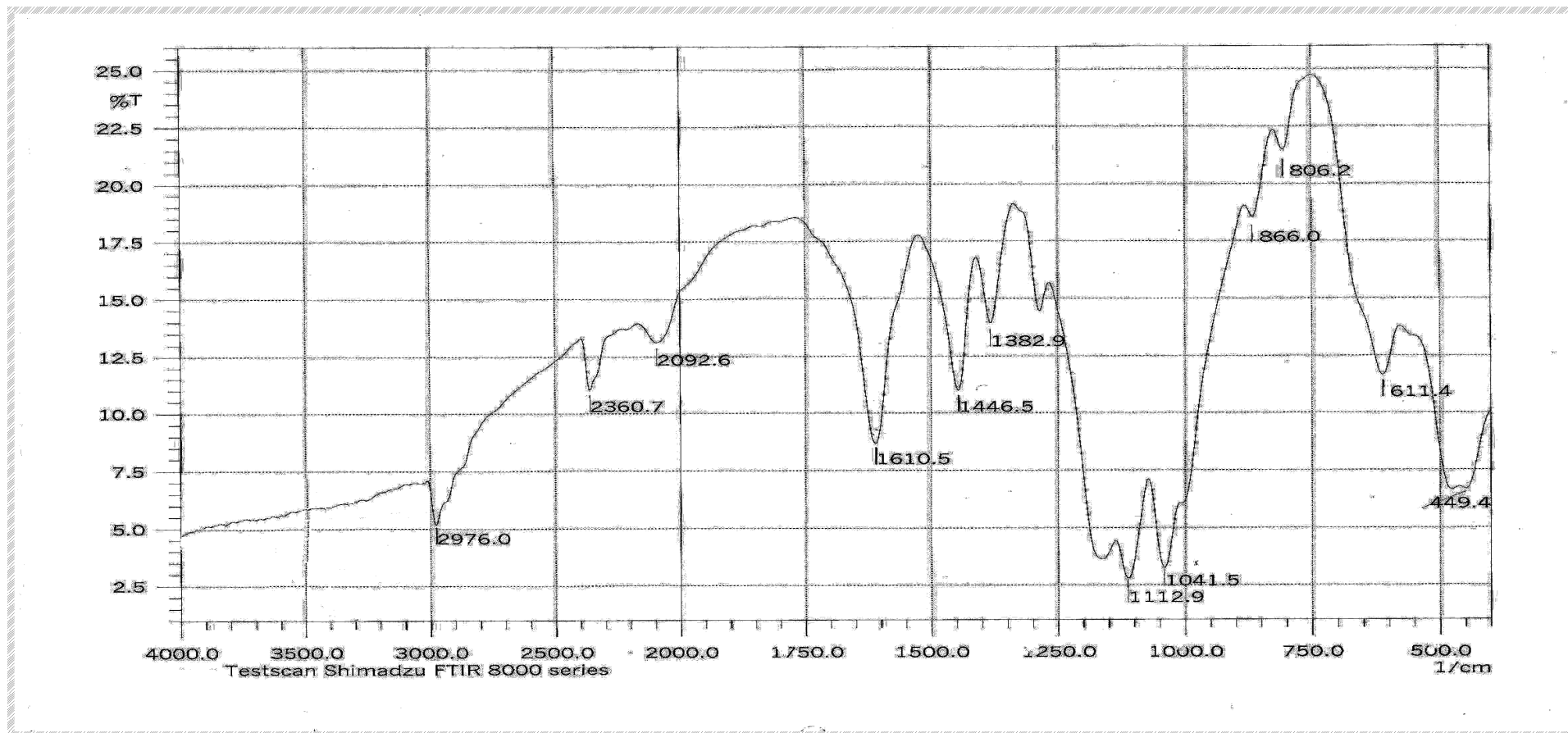


Figure (3.3): FTIR spectrum for potassium ethyl xanthate ligand (PEX)

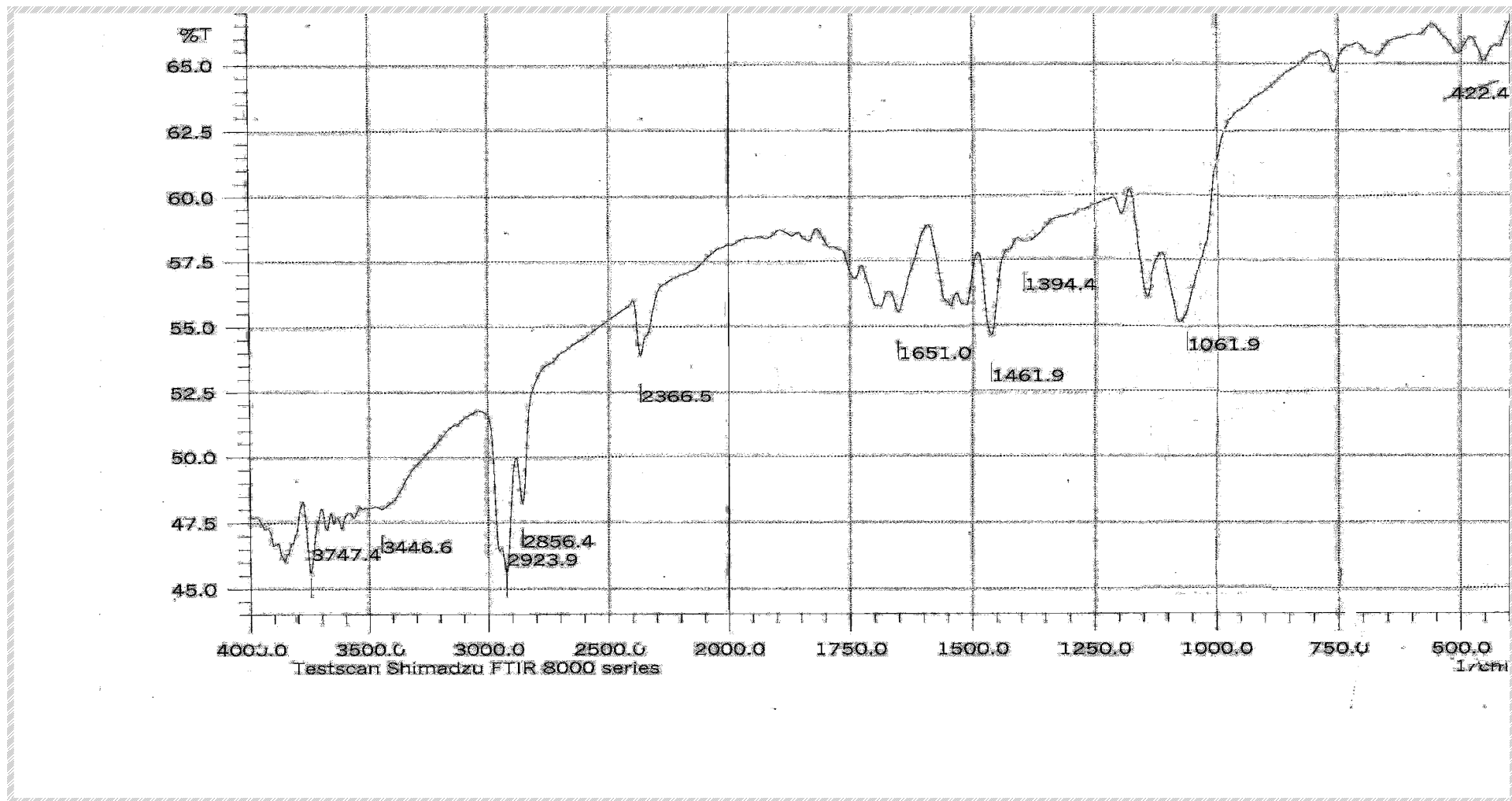


Figure (3.9): FTIR spectrum for potassium hexyl xanthate ligand (PHX)

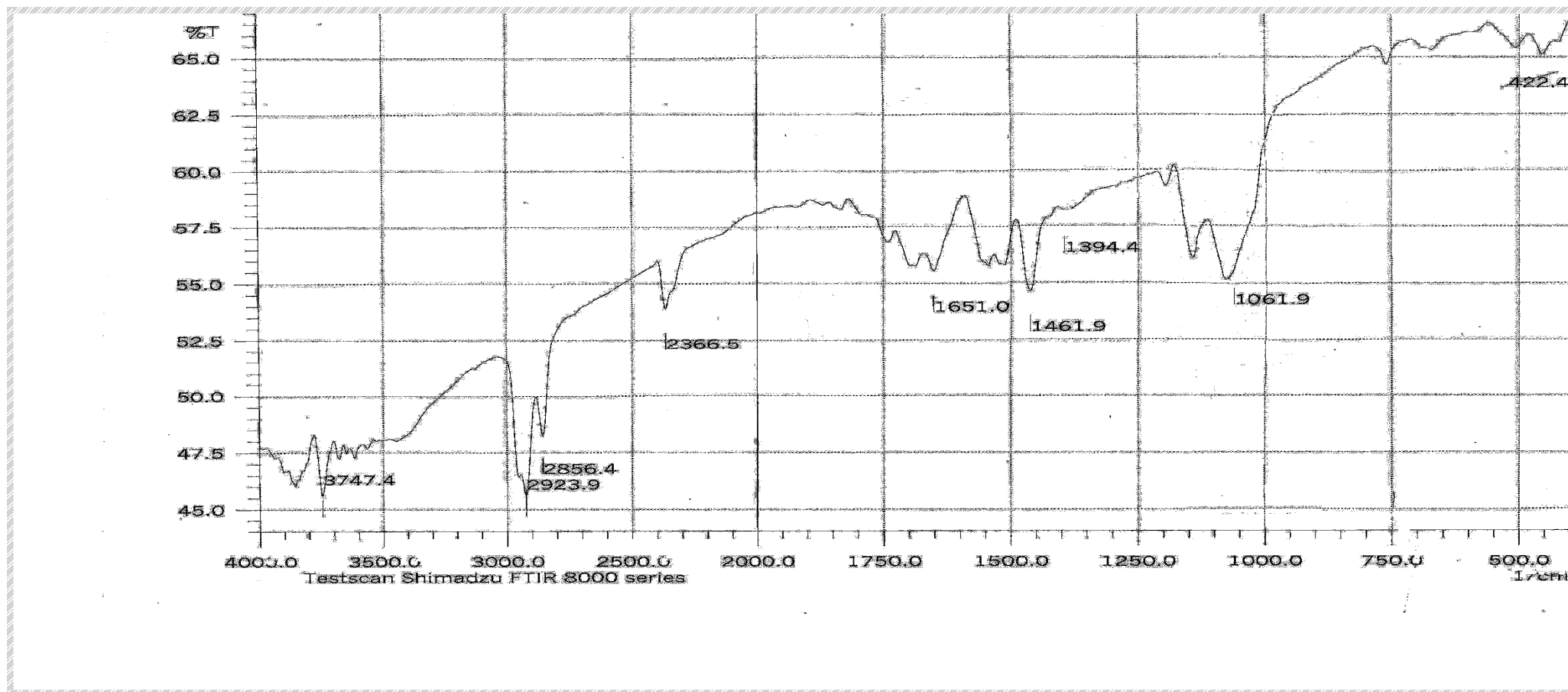


Figure (3.9): FTIR spectrum for potassium hexyl xanthate ligand (PHX)

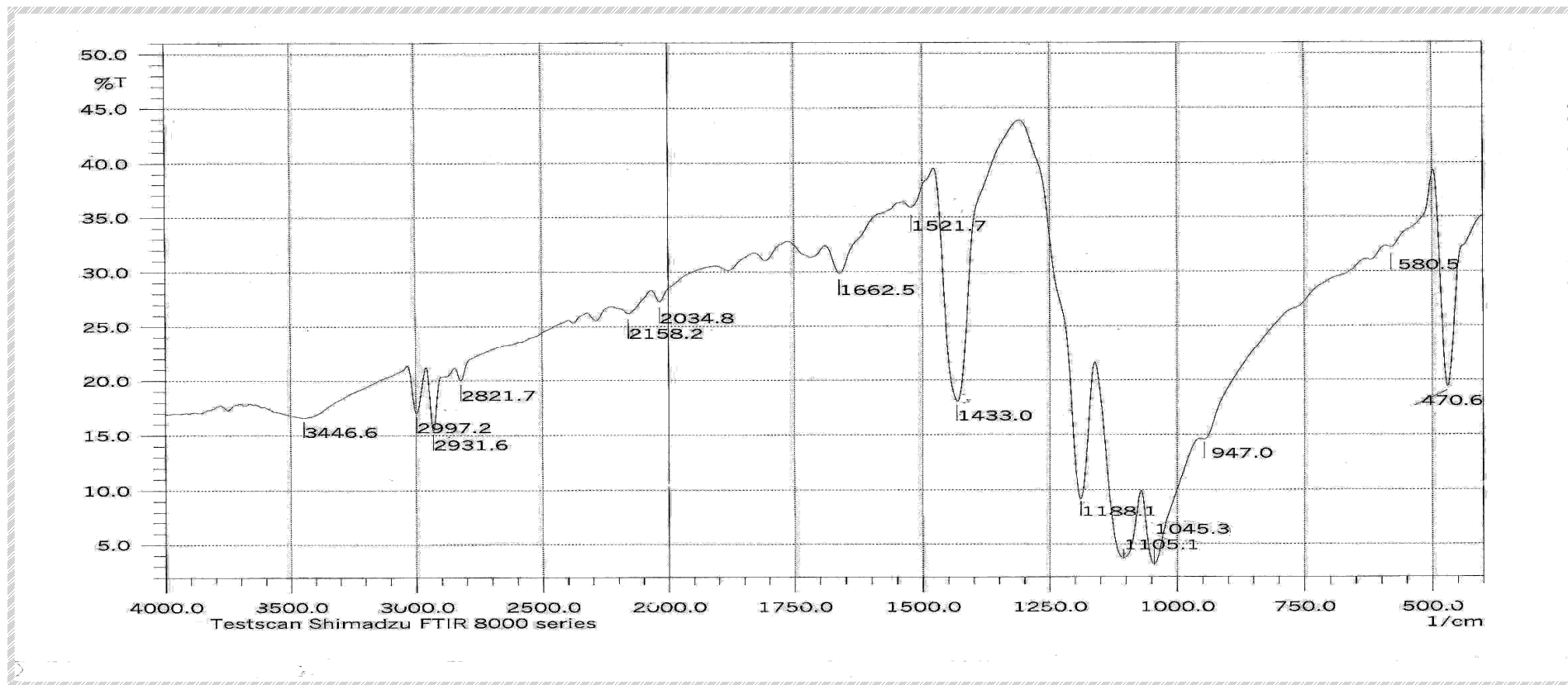


Figure (3.1): FTIR spectrum for potassium methyl xanthate ligand (PMX)

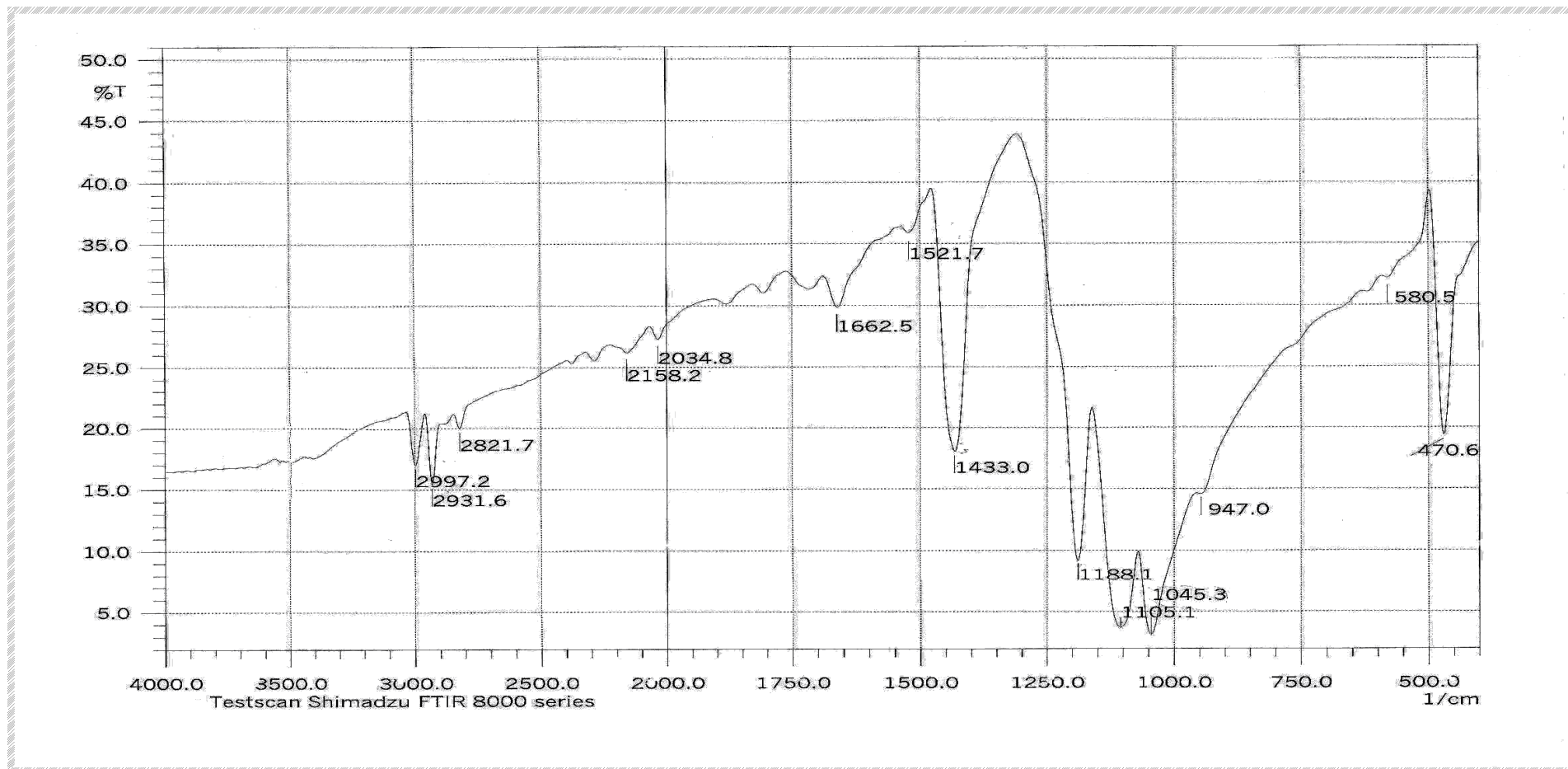


Figure (3.1): FTIR spectrum for potassium methyl xanthate ligand (PMX)

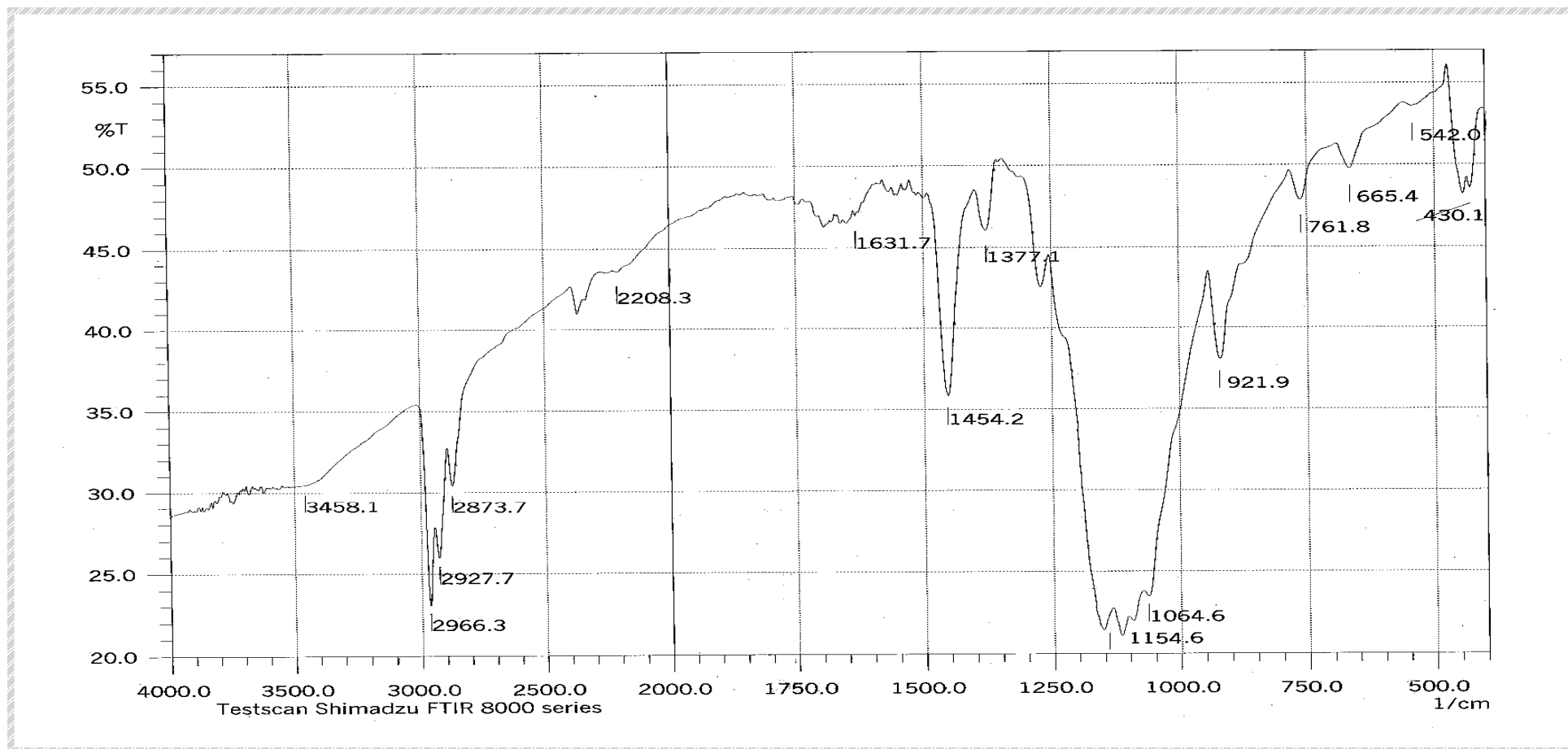


Figure (3.5): FTIR spectrum for potassium propyl xanthate ligand (PPX)

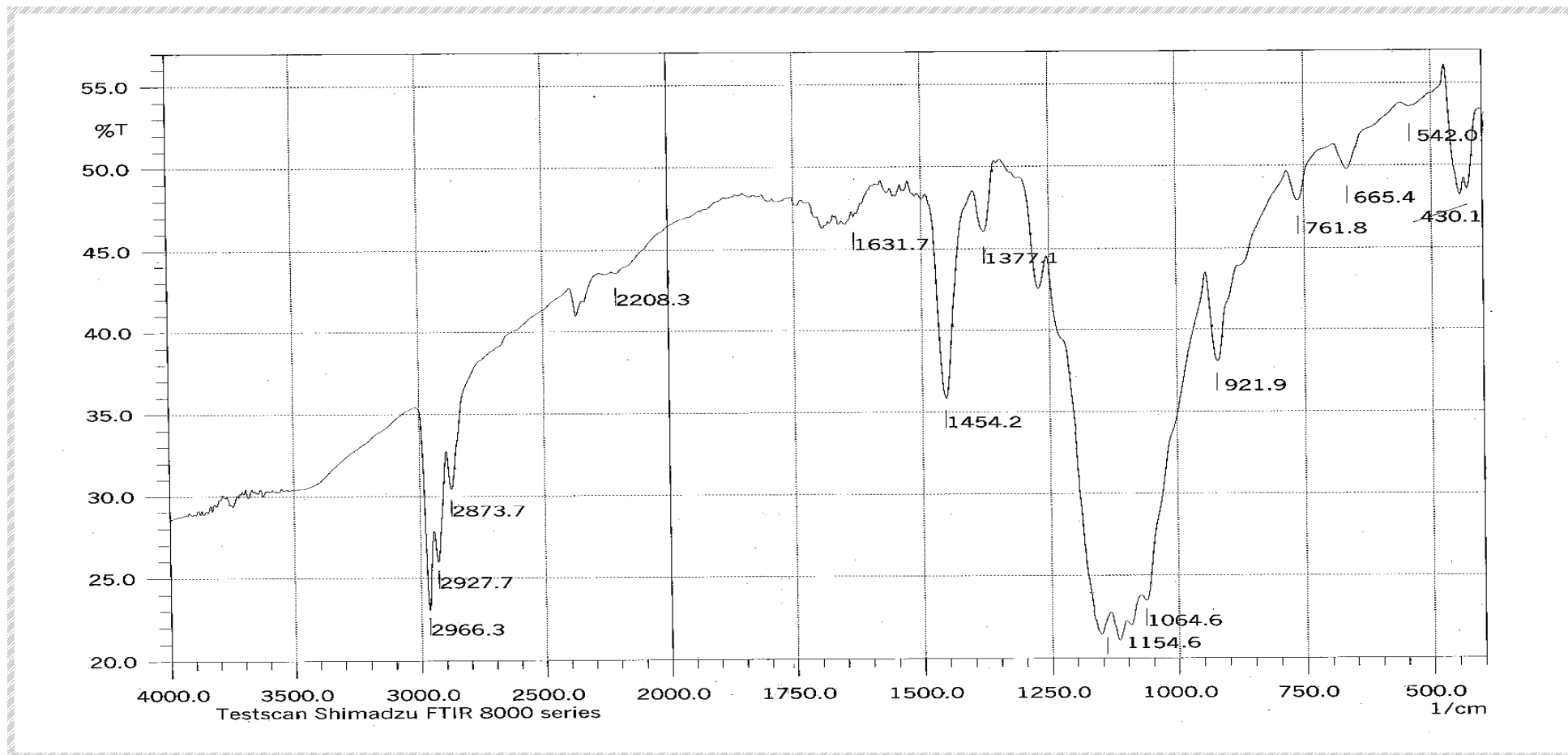


Figure (3.5): FTIR spectrum for potassium propyl xanthate ligand (PPX)